AD-A008 773

THE DYNAMICS OF A GROWING SEPARATED REGION ON AN AIRFOIL

James D. Lang

Frank J. Seiler Research Laboratory
United States Air Force Academy, Colorado

February 1975

UNCLASSIFIED

SECURITY CLASSIFICATION OF THIS PAGE (When Data Entered)

REPORT DOCUMENTATION PAGE

READ INSTRUCTIONS BEFORE COMPLETING FORM

1. REPORT NUMBER: SRL-TR-75-0005	2. GOVT ACCESSION NO.
3. RECIPIENT'S CATALOG NUMBER: AD-A008 773	
4. TITLE (and Subtitle): THE DYNAMICS OF A GROWING SEPARATED REGION ON AN AIRFOIL AD-	5. TYPE OF REPORT & PERIOD COVERED: Scientific Final (Nov 1972 - Feb 1975)
	6. PERFORMING ORG. REPORT NUMBER: 750005
7. AUTHOR(s): James D. Lang, Major, USAF	8. CONTRACT OR GRANT NUMBER(s)
9. PERFORMING ORGANIZATION NAME AND ADDRESS: Department of Aeronautics, USAF Academy, Colorado 80840	10. PROGRAM ELEMENT, PROJECT, TASK AREA & WORK UNIT NUMBERS: DRS 61102F, 7905-01-28
11. CONTROLLING OFFICE NAME AND ADDRESS: Frank J. Seiler Research Laboratory (AFSC), USAF Academy, Colorado 80840	12. REPORT DATE: February 1975
	13. NUMBER OF PAGES: 114
14. MONITORING AGENCY NAME & ADDRESS (if different from Controlling Office)	15. SECURITY CLASS. (of this report): Unclassified
	15a. DECLASSIFICATION/DOWNGRADING SCHEDULE

16. DISTRIBUTION STATEMENT (of this Report)

Approved for public release; distribution unlimited.

17. DISTRIBUTION STATEMENT (of the abstract entered in Block 20, if different from Report)

Same

18. SUPPLEMENTARY NOTES

TECH, OTHER

19. KEY WORDS (Continue on reverse side if necessary and identify by block number)

Control-Surface Buzz
Dynamic Stall
Limit-cycle Behavior
Separated Flow
Separation Bubbles
Unsteady Flow

20. ABSTRACT (Continue on reverse side if necessary and identify by block number)

At present little is known of the dynamics of a separating and reattaching flowfield. This unsteady flow topic relates to a wide range of aerodynamic problems such as dynamic stall and control-surface-buzz.

A theory is developed which models separation bubble dynamics. It includes a quasi-steady model for the external shear-layer, and flow of mass within the bubble at a mean reversed-flow velocity. Pressure perturbations along the bubble are modeled also. The theory is based on experimental results for an airfoil with oscillating spoiler and flap.

DD FORM 1 JAN 73 1473 EDIT

UNCLASSIFIED

SECURITY CLASSIFICATION OF THIS PAGE (When Data Entered)

20. (continued)

The theory is used with the method of Beecham and Titchener in order to predict limit-cycle behavior which was observed on the airfoil model when the spoiler and flap were mechanically coupled and free to oscillate. This behavior is thought to be a subsonic analogy of control-surface-buzz. Good agreement with experimental results is achieved.

The instant of instability and of growth of a laminar separation bubble at the leading-edge of an oscillating airfoil is also investigated theoretically. The beginning of dynamic stall is seen to be related to the dynamics of a separating region and the inviscid flowfield. The theory is applied also to a study of the phenomena of control-surface-buzz, where separation is induced by shock waves.

February 1975

Final Scientific Report

THE DYNAMICS OF A GROWING SEPARATED REGION ON AN AIRFOIL

Nov 1972 - Feb 1975

JAMES D. LANG

USAF Academy, Colorado

This research has been sponsored by the Frank J. Seiler Research Labs (AFSC) with Work Unit No. 7905-01-28 and by the European Office of Aerospace Research and Development (AFSC) under Grant No. 73-2472.

ii

ABSTRACT

At present little is known of the dynamics of a separating and reattaching flowfield. This unsteady flow topic relates to a wide range of aerodynamic problems such as dynamic stall and control-surface-buzz.

A theory is developed which models separation bubble dynamics. It includes a quasi-steady model for the external shear-layer, and flow of mass within the bubble at a mean reversed-flow velocity. Pressure perturbations along the bubble are modeled also. The theory is based on experimental results for an airfoil with oscillating spoiler and flap.

The theory is used with the method of Beecham and Titchener in order to predict limit-cycle behavior which was observed on the airfoil model when the spoiler and flap were mechanically coupled and free to oscillate. This behavior is thought to be a subsonic analogy of control-surface-buzz. Good agreement with experimental results is achieved.

The instant of instability and of growth of a laminar separation bubble at the leading-edge of an oscillating airfoil is also investigated theoretically. The beginning of dynamic stall is seen to be related to the dynamics of a separating region and the inviscid flowfield. The theory is applied also to a study of the phenomena of control-surface-buzz, where separation is induced by shock waves.

TABLE OF CONTENTS

LIST OF ILLUSTRATIONS

LIST OF ABBREVIATIONS AND SYMBOLS

a	a constant, e.g., the slope of a linear velocity profile or a non-dimensional pitch-axis location
a_i	coefficient of a polynomial
a_∞	free-stream speed of sound
A	flap system moment of inertia or separation bubble area or a gain factor
AR	aspect ratio of separation bubble, AR $\equiv \frac{\text{bubble span}}{\text{bubble length}}$
b	airfoil semichord, $b \equiv \frac{c}{2}$
b_f	flap span
b_{sp}	spoiler span
B	flap system mechanical damping
c	airfoil chord or non-dimensional flap hinge location
c_f	flap chord
C	flap system structural stiffness
$C(\nu_a)$	Theodorsen function
C_H	non-dimensional hinge-moment coefficient, $C_H \equiv \frac{H}{q_\infty b_f c_f^2}$
C_p	pressure coefficient, $C_p \equiv \frac{p - p_\infty}{q_\infty}$
C_{H_β}, $C_{H_{\dot\beta}}$, C_{p_α}, $C_{p_{\dot\alpha}}$, C_{p_β}, etc.	non-dimensional derivatives, e.g., $C_{p_{\dot\alpha}} \equiv \frac{\partial C_p}{\partial \alpha'}$, $C_{H_{\dot\beta}} \equiv \frac{\partial C_H}{\partial \beta'}$ (Note: $C_{H_\beta} = -2k_\beta = 2(\frac{c}{c_f})^2 h_\beta$, $C_{H_{\dot\beta}} = -2k_{\dot\beta} = 2(\frac{c}{c_f})^3 h_{\dot\beta}$ where the k's are AGARD notation and the h's are conventional English notation based on airfoil chord)

C_{L_α}	lift-curve slope
ΔC_H	incremental hinge-moment coefficient
ΔC_{H_n}, C_{P_n}	coefficients of Fourier series
$C_{P_{\Gamma_i}}$	pressure coefficient due to circulation effects
d_i	bubble length versus spoiler height curve slope, $d_i \equiv \frac{\partial x_i}{\partial h}$, $i = b,r$
d_R	slope of curve, $d_R = d_r \left(\frac{c}{c_f}\right)$
h_s, h	actual and non-dimensional spoiler height, $h \equiv \frac{h_s}{c_f}$
h_{o_s}, Δh_s, h_o, Δh	actual and non-dimensional spoiler parameters, e.g., $h = h_o + \Delta h \cos \omega t = \frac{h_{o_s}}{c_f} + \frac{\Delta h_s}{c_f} \cos \omega t$
h_{eff}	effective spoiler height
H	hinge-moment or shear-layer shape factor, $H \equiv \frac{\delta^*}{\theta}$
H_β, $H_{\dot\beta}$	dimensional derivatives, e.g., $H_{\dot\beta} = \frac{\partial H}{\partial \dot\beta}$
ΔH	incremental hinge-moment
$H_i^{(2)}$	Hankel function of the second kind of order i
I	integral related to circulation effects
k	a constant, e.g., a coupling parameter
k_i	a constant
ℓ	total separation bubble length or laminar shear layer length
m	turbulent mixing and reattachment region length

M	Mach number or ratio of unsteady and steady flow circulation effects
N_i	describing function coefficients, $i = 1,2$
P, P_o	static and total pressure
P_∞	free-stream static pressure
q_n, q_s	normal and tangential components of velocity at bubble boundary
q_∞	free-stream dynamic pressure, $q_\infty = \frac{1}{2} \rho U_\infty^2$
Q	parameter used to evaluate circulation
Re_x	Reynolds number based on distance x (velocity is either U_s or U_∞)
t	time
u	x-component of velocity
u_B	velocity at bubble dividing streamline at station b
U	x-component of velocity at the edge of a shear layer (also U_e)
U_c	apparent convective velocity
U_o	value of U due to mean airfoil incidence
U_∞	free-stream speed
v_e	entrainment velocity
W	rate of energy dissipation within bubble
x	non-dimensional chordwise distance based on airfoil chord or (in section 4) based on semichord with origin at midchord, i.e., $x = \frac{X}{c}$ or $x = \frac{X}{b} - 1$
x_o	location in wake of vortex element
x_f	flap hinge-line location
x_{sh}	shock-wave location
x_{sp}	spoiler location
X	chordwise distance from airfoil leading-edge or (in part of section 3) from spoiler

y_d, y_e, y_z	distance normal to airfoil surface of dividing streamline, edge of shear-layer, and "zero" streamline
α	airfoil angle-of-attack or a phase angle
α_o	airfoil mean incidence angle
$\Delta\alpha$	amplitude of airfoil oscillation
$\Delta\alpha_s$	stall overshoot angle, $\Delta\alpha_s = \alpha_{\substack{\text{dynamic}\\\text{stall}}} - \alpha_{\substack{\text{static}\\\text{stall}}}$
β	flap deflection angle
β_n	coefficients of Fourier series
$\Delta\beta$	amplitude of flap oscillation
$\Delta\beta_{LC}$	amplitude of limit-cycle oscillation
$\Delta\beta_s$	stall overshoot angle
γ	density of vorticity or gas constant
Γ	circulation
δ	shear-layer thickness
δ^*	shear-layer displacement thickness
δc_p	difference between pressure coefficients in separated and attached flow
ϵ	error parameter
ζ	damping ratio
θ	shear-layer momentum thickness
θ_n	phase angle in Fourier series for pressure
K	a constant, $K \equiv \frac{\rho b_f c_f^4}{2A}$
λ	stability parameter, $\lambda = \frac{\Delta\dot{\beta}}{\Delta\beta}$
μ	viscosity
ν	frequency parameter based on flap chord, $\nu \equiv \frac{\omega c_f}{U_\infty}$

ν_a	frequency parameter based on airfoil semi-chord, $\nu_a \equiv \frac{\omega c}{2 U_\infty} = \frac{\omega b}{U_\infty}$
ξ	non-dimensional chordwise distance, $\xi = \frac{X}{c}$
ρ	free-stream density
σ	pressure recovery coefficient or Crabtree's parameter, $\sigma = \frac{C_p - C_{p_s}}{1 - C_{p_s}}$ or $\sigma = \frac{C_{p_r} - C_{p_s}}{1 - C_{p_s}}$
σ_{CR}	critical value of Crabtree's parameter
τ, τ_a, τ_o, τ_ϵ	non-dimensional time, i.e., $\tau = \frac{U_\infty t}{c_f}$, $\tau_a = \frac{U_\infty t}{b}$, $\tau_o = \frac{\ell_o}{2 \lvert U_c \rvert}$, $\tau_\epsilon = \frac{\ell - X}{\lvert U_c \rvert}$
ϕ	velocity potential or phase angle
ϕ_n	phase angle in Fourier series for flap angle
ψ	phase angle for circulation effects
ψ_n	phase angle in Fourier series for hinge-moment
ω	angular frequency of oscillation
$(\cdot) =$	$\frac{d(\ )}{dt}$
$(') =$	$\frac{d(\ )}{d\tau}$ or $\frac{d(\ )}{d\,\tau_a}$
$<p>$, $<u>$	RMS values of pressure and velocity fluctuations

<u>superscripts</u>

$\tilde{i}$	perturbation quantity
$\hat{i}$	describing functions for transient motion
i'	fluctuating quantity due to turbulence
$\bar{i}$	time average value in turbulent flow

<u>subscripts</u>

a	associated with airfoil dimensions

b	at location where transition and reattachment begins
ℓ	on lower surface
m	at location of maximum velocity
o	mean value
r	at location of reattachment
s	at location of separation
u	on upper surface

I. INTRODUCTION

At present little is known of the dynamics of a separating and reattaching flowfield. This unsteady flow topic relates to a wide range of aerodynamic problems such as control-surface-buzz; dynamic stalling of lifting surfaces or bodies; "wing rock", "departure" and autobuffeting of aircraft; "stall flutter" of helicopter rotor blades, engine compressor blades, and possibly V/STOL aircraft wings and lifting body configurations.[1,2,3]

The above examples of interaction between an oscillating surface (or body) and a separating flow represent significant problems. Unfortunately, there exists a void in knowledge which precludes the development of valid models for the related flowfield. The above examples usually involve low rates of change of properties within the flowfield, thus dynamic viscous effects play an important role. Flutter in one degree of freedom may exist in which there is a mutual interaction between the motion of a body and the separating and reattaching flow. Shock waves may be involved as the mechanisms for inducing flow separation. The topic of flutter in one degree of freedom is discussed by Lambourne in reference 1. Jones, in reference 4, concludes that in this type of flow the flow field is deterministic and the appropriate analytical model is autonomous and nonlinear.

One of the problems associated with these inviscid-viscous flow interactions is that there must be a matching of conditions at the boundaries of the rotational and irrotational flow regions. An iterative process is usually involved. At extremes of this matching problem are cases where either the inviscid or viscous region dominates the other. For example, a thin boundary layer on an airfoil may be neglected completely in many cases of steady and unsteady flow.

In this paper two cases will be investigated which are seen to lie near the above extremes. The first case involves a fence-type spoiler which can be thought of as an overwhelming perturbation and is used to 'control' a sizable separated region on an airfoil. The growth of the separated region is studied. It is found that viscous effects are of primary importance. Near the other extreme is the interaction between a small laminar leading-edge separation bubble and the outer inviscid flow field on an airfoil. Results obtained during these analyses are extended in order to study the complex problem of control-surface-buzz, which lies somewhere between the two extremes of interaction types.

The first part of this paper then deals primarily with a controlled separated region. The purpose is to gain further insight into the dynamics of an unsteady separating flow where the influence of the inviscid flow field is significantly reduced. Reference 5 elaborates on an experiment which was designed to do this. It involves an airfoil with flap and a spoiler which was

mechanically driven in harmonic motion in order to control an unsteady separating flow. The experiment was also designed so that the flap (which was downstream of the spoiler) could be fixed or be allowed to respond freely to the effects of spoiler forcing, or be coupled to the spoiler. The coupled system exhibits limit-cycle oscillations which are thought to be a subsonic analogy of control-surface-buzz.

An excellent survey of work related to separated flows is found in Chang's book (Ref. 6). Other important contributions in the study of steady or quasi-steady separated flows are found, for example: (i) in the analytical work of Crimi and Reeves (Ref. 7) which deals with a separated laminar shear-layer which transitions to a turbulent shear-layer with mixing and reattachment onto a surface, (ii) in the experimental studies of Barnes (Ref. 8) and Newman (Ref. 9) which deal with a separated region aft of a fence-type spoiler, (iii) in the experiment by DeBroderode and Bradshaw (Ref. 10) which deals with a separated region aft of a rearward-facing step and discusses three-dimensional effects and the dependence of bubble length on step height and initial boundary-layer thickness and shape, (iv) in the analysis by Bradshaw and Wong (Ref. 11) which deals with strong and overwhelming perturbations to a shear-layer (caused by steps or spoilers, for example) and the subsequent downstream reattachment and relaxation of the shear-layer, (v) in the analytical work of Norbury and Crabtree (Ref. 12) which deals with the mixing and reattachment region of a separation bubble, and (vi) in the studies by McGregor (Ref. 13), Gaster (Ref. 14), Young and Horton (Ref. 15), Horton (Ref. 16) and more recently Woodward (Ref. 17) which are concerned with growth and bursting of laminar leading-edge separation bubbles.

Trilling (Ref. 18), East and Wilkinson (Ref. 19) and Theisen (Ref. 20) have offered models of a separated region in which unsteady mass flow into the region is considered in order to determine growth characteristics in unsteady flow.

In this paper a mathematical model of a separated region is derived which is used in comparison with the experimental results of reference 5. Further analysis is also offered which extends the analytical model of the experiment to the study of dynamic stall. In particular the stability of a laminar leading-edge separation bubble on an airfoil is studied and when instability is achieved, for example, after an airfoil has pitched upward past the static stall incidence angle, a prediction is made of the instant at which the bubble begins to grow. Subsequent growth and loading due to bubble growth is not analyzed. Also included is an extension of the analysis to include the study of control-surface-buzz.

This report contains part of the material which is presented in reference 21.

II. THEORETICAL PREDICTION OF SPOILER EFFECTS

In reference 5 it was shown that two categories of separation bubbles could be defined. The ratio of spoiler height to boundary-layer thickness (h_s/δ) relates to the strength of the spoiler perturbation and to a resultant bubble type. In the following development only the"long bubble" type, which probably results from an overwhelming perturbation, will be considered. It will be shown that unsteady effects can serve to modify the character of the long bubble in such a way that it may resemble a short bubble.

1. A Simple Steady-Flow Bubble Model

Consider the sketch below, which serves to define several parameters.

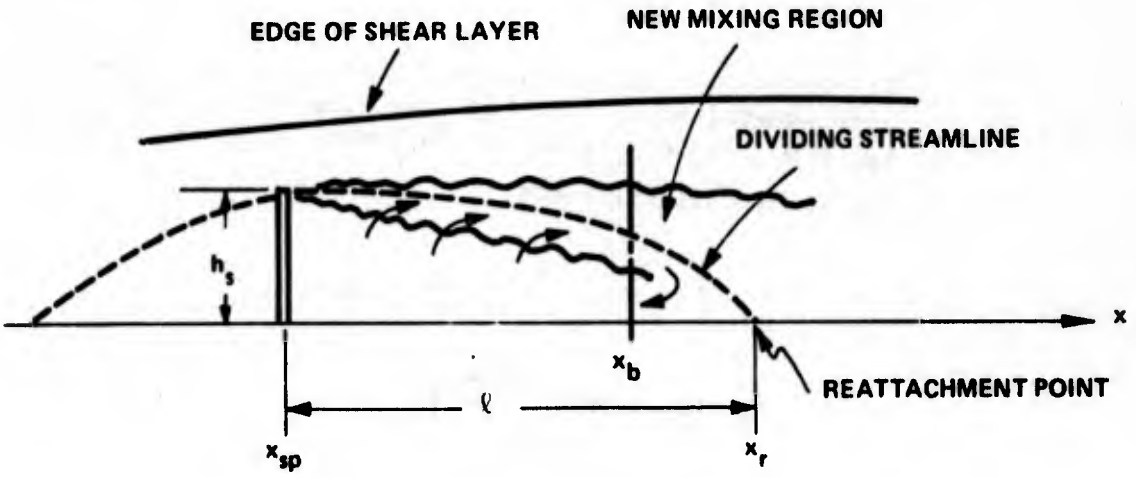

Based on experimental observations and other works (Ref 6) the length of the bubble is represented as a linear function of spoiler height as follows: (See Fig. 13 of reference 5.)

$$\ell = (x_r - x_{sp})\, c = d_r\, (h_s - h_{sc})\, \frac{c}{c_f}$$

or in non-dimensional form as:

$$\frac{\ell}{c_f} \equiv \Delta x_{sp} = (x_r - x_{sp})\, \frac{c}{c_f} = d_r\, \left(\frac{h_s}{c_f} - \frac{h_{sc}}{c_f}\right) \frac{c}{c_f}$$

$$= d_r\, (h - h_c)\, \frac{c}{c_f}$$

or

$$(x_r - x_{sp}) = d_r\ (h - h_c)$$

and

$$x_r = d_r\ (h - h_c) + x_{sp} = d_r h + x_c$$

where

$$x_c = x_{sp} - d_r\ h_c$$

also we have:

$$x_b = d_b h + x_c$$

The chordwise pressure distribution along the surface is approximated by a "roof-top" distribution as shown below, with $C_{p_r} = 0$. (Note: C_p in the following is actual C_p minus C_p due to airfoil thickness.)

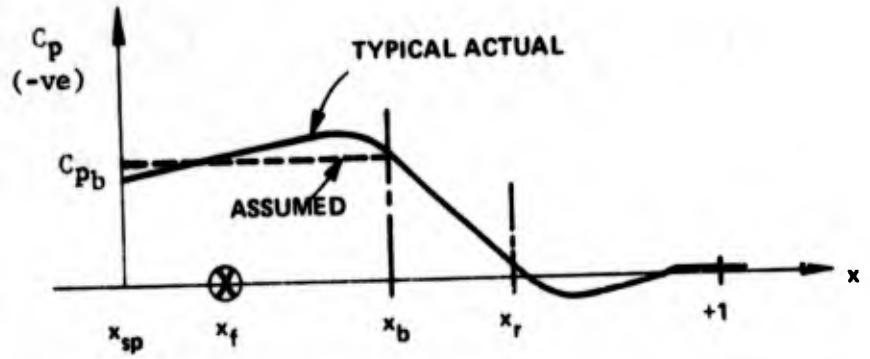

For long bubbles with recompression on the flap surface and pressure divergence at the trailing edge, a linear pressure distribution which recovers to zero at the flap hinge-line is assumed on the lower surface. This simplification is justified by measurements made on the flap lower surface.

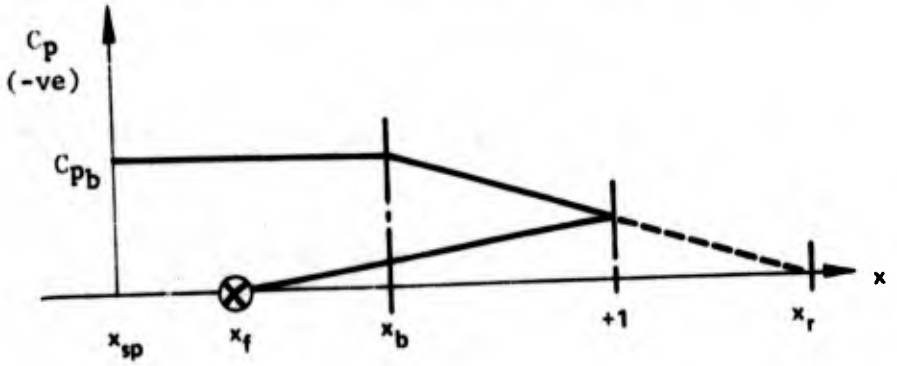

or

$$(x_r - x_{sp}) = d_r\,(h - h_c)$$

and

$$x_r = d_r\,(h - h_c) + x_{sp} = d_r h + x_c$$

where

$$x_c = x_{sp} - d_r\,h_c$$

also we have:

$$x_b = d_b h + x_c$$

The chordwise pressure distribution along the surface is approximated by a "roof-top" distribution as shown below, with $C_{p_r} = 0$. (Note: C_p in the following is actual C_p minus C_p due to airfoil thickness.)

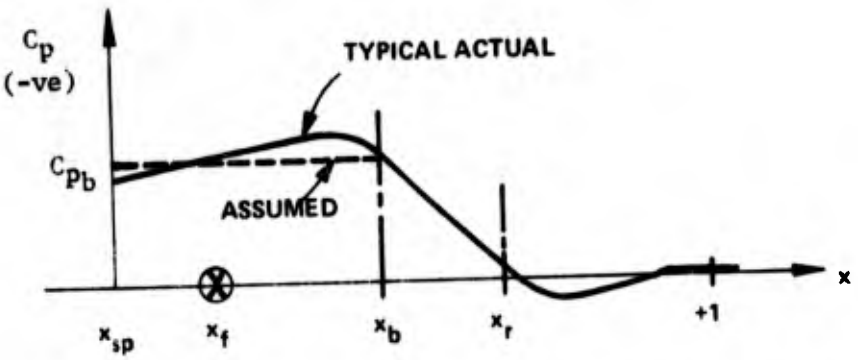

For long bubbles with recompression on the flap surface and pressure divergence at the trailing edge, a linear pressure distribution which recovers to zero at the flap hinge-line is assumed on the lower surface. This simplification is justified by measurements made on the flap lower surface.

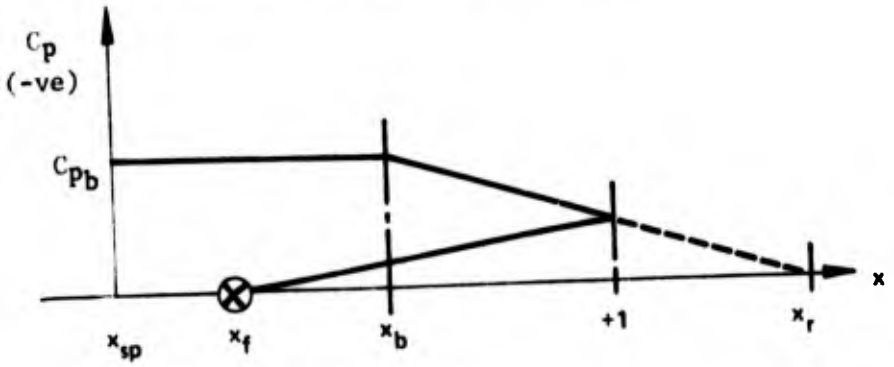

The incremental hinge-moment due to spoiler deflection may be found by integrating pressures over the flap.

$$\Delta C_H \equiv \frac{\Delta H}{q\, b_f\, c_f^2} = -\left(\frac{c}{c_f}\right)^2 \int_{x_f}^{1} (C_{p_\ell} - C_{p_u})(x - x_f)\, dx$$

where pressure coefficients are approximated as discussed above.

We have five cases to consider:

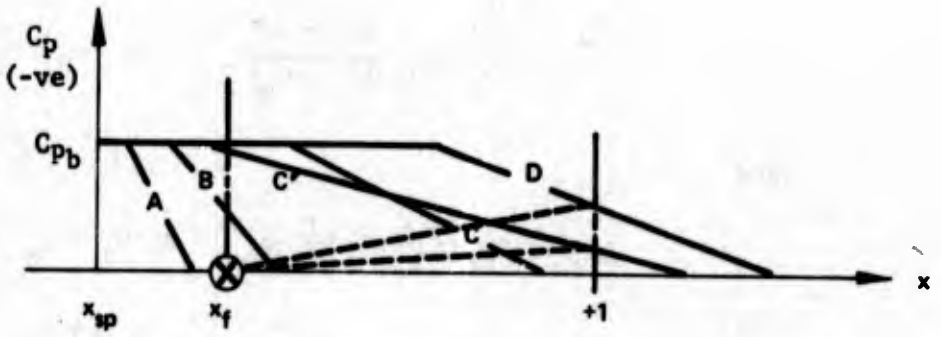

Case A

$$x_r \le x_f \;; \quad \text{i.e.,} \quad h \le \frac{x_f - x_c}{d_r}$$

$$\therefore\; C_{p_\ell} = C_{p_u} = 0 \quad \text{and} \quad \Delta C_H = 0$$

Case B

$$x_b \le x_f \quad \text{and} \quad x_f \le x_r \le 1$$

$$\text{i.e.,} \quad h \le \frac{x_f - x_c}{d_b} \quad \text{and} \quad \frac{x_f - x_c}{d_r} \le h \le \frac{1 - x_c}{d_r}$$

$$\therefore\; C_{p_\ell} = 0 \;; \quad C_{p_u} = C_{p_b} \frac{(x_r - x)}{(x_r - x_b)} \quad \text{for} \quad x_f \le x \le x_r$$

and

$$\Delta C_H = C_{p_b} \frac{\left(\frac{c}{c_f}\right)^2}{(d_r - d_b)} \left[\frac{1}{6} d_r^3\, h^2 + \frac{1}{2} d_r^2\, (x_c - x_f)\, h \right.$$

$$\left. + \frac{1}{2} d_r\, (x_c - x_f)^2 + \frac{1}{6} \frac{(x_c - x_f)^3}{h}\right]$$

Case C

$$x_f \le x_b \quad \text{and} \quad x_r \le 1 \ ;$$

$$\text{i.e.,} \quad \frac{x_f - x_c}{d_b} \le h \quad \text{and} \quad h \le \frac{1 - x_c}{d_r}$$

$$\therefore \ C_{p_\ell} = 0 \ ;$$

$$C_{p_u} = \begin{cases} C_{p_b} & x_f \le x \le x_b \\ C_{p_b} \dfrac{(x_r - x)}{(x_r - x_b)} & x_b \le x \le x_r \end{cases}$$

and

$$\Delta C_H = C_{p_b} \left(\frac{c}{c_f}\right)^2 \left[\frac{1}{6} (d_b^2 + d_b d_r + d_r^2) h^2 + \frac{1}{2} (d_b + d_r)(x_c - x_f) h + \frac{1}{2} (x_c - x_f)^2\right]$$

Case C' (in lieu of Case C)

$$x_b \le x_f \quad \text{and} \quad 1 \le x_r$$

$$\text{i.e.,} \quad h \le \frac{x_f - x_c}{d_b} \quad \text{and} \quad \frac{1 - x_c}{d_r} \le h$$

$$\therefore \ C_{p_\ell} = C_{p_b} \frac{(x_r - 1)(x - x_f)}{(x_r - x_b)(1 - x_f)} \qquad x_f \le x \le 1$$

$$C_{p_u} = C_{p_b} \frac{(x_r - x)}{(x_r - x_b)} \qquad x_f \le x \le 1$$

and

$$\Delta C_H = C_{p_b} \left(\frac{c}{c_f}\right)^2 \frac{(1 - x_f)^2}{6 (d_r - d_b)} \left[d_r + \frac{(x_c - x_f)}{h}\right]$$

Case D

$$x_f \le x_b \le 1 \quad \text{and} \quad 1 \le x_r$$

$$\text{i.e.,} \quad \frac{x_f - x_c}{d_b} \le h \le \frac{1 - x_c}{d_b} \quad \text{and} \quad \frac{1 - x_c}{d_r} \le h$$

$$\therefore \; C_{p_\ell} = C_{p_b} \frac{(x_r - 1)(x - x_f)}{(x_r - x_b)(1 - x_f)} \qquad x_f \le x \le 1$$

$$C_{p_u} = \begin{cases} C_{p_r} & x_f \le x \le x_b \\ C_{p_b} \dfrac{(x_r - x)}{(x_r - x_b)} & x_b \le x \le 1 \end{cases}$$

and

$$\Delta C_H = C_{p_b} \frac{(\frac{c}{c_f})^2}{(d_r - d_b)} \{ -\frac{1}{6} d_b^3 h^2 - \frac{1}{2} d_b^2 (x_c - x_f) h$$

$$+ [\frac{1}{6} d_r (1 - x_f)^2 - \frac{1}{2} d_b (x_c - x_f)^2]$$

$$+ [-\frac{1}{6} (x_c - x_f)^3 + \frac{1}{6} (x_c - x_f)(1 - x_f)^2] \frac{1}{h} \}$$

Experimental data found in Figure 13 of reference 5 yields the following values:

$$d_r = 8.538; \quad d_b = 4.838; \quad x_c = .4167$$

Cases A, B, C' and D are considered with $C_{p_b} = -.4$ (this corresponds to a pressure recovery coefficient value of $\sigma = .286$) and results are plotted in Figure 1. Further approximate results with parameter values of $d_r = 5.50$; $d_b = 3.00$ and $x_c = x_{sp}$ are also shown.

The experimental data is not predicted accurately; however, the non-linear nature of the functional relation $\Delta C_H = f\{h\}$ is firmly established. The above simple model also demonstrates that the hinge-moment functional relation may also be written as $\Delta C_H = C_{p_b} f\{h\}$. Furthermore, we find that for all results $\left|\frac{\partial \Delta C_H}{\partial h}\right|_{max}$ occurs just prior to trailing-edge pressure divergence. For the curve based on experimental data the value of $\frac{\partial \Delta C_H}{\partial h}$ at T.E. pressure divergence (an average since slope is discontinuous there) is -3.548 at $h \cong .068$. This compares fairly well with the experimental value of $\frac{\partial \Delta C_H}{\partial h} = -3.3$ at $h \cong .066$.

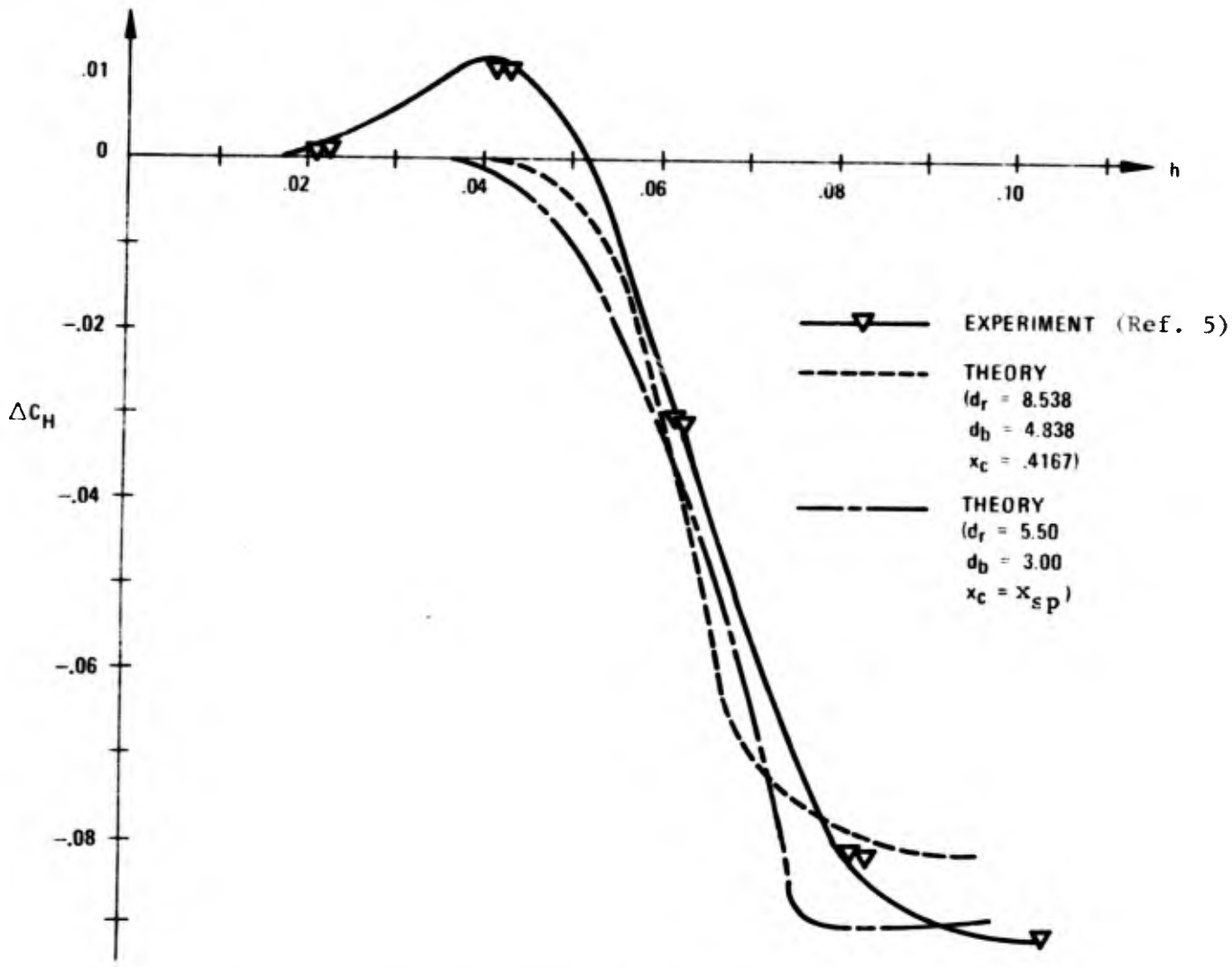

FIG. 1. ACTUAL AND APPROXIMATE HINGE-MOMENT COEFFICIENTS

For quasi-steady spoiler motion of the form $h = h_o + \Delta h \cos \phi$ we find that the above formulation does not properly represent the functional dependence of ΔC_H on h_o and Δh. Accordingly, a polynomial "curve fit" to the experimental data was attempted in order to duplicate the steady-flow functional relation $\Delta C_H = f\{h_o, \Delta h\}$ over a range of h_o and Δh values of interest. A fifth order polynomial in h was needed. This polynomial will be used in the unsteady-flow theory as the steady-flow functional relation.

$$\Delta C_H = a_5 h^5 + a_4 h^4 + a_3 h^3 + a_2 h^2 + a_1 h + a_o$$

The justification for this step lies in the fact that prediction of accurate unsteady effects is based in large part on a good steady-flow model.

Let us now consider the separation bubble in more detail. First we will investigate the pressure rise over the aft portion of the bubble.

A detailed view of the aft portion of the bubble, to include mean velocity profiles, is shown below.

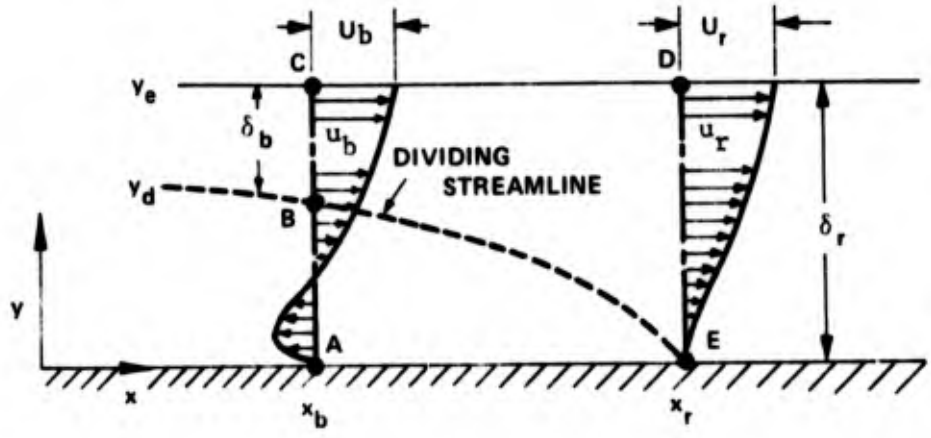

Norbury and Crabtree (Ref 12) have represented the turbulent mixing, and reattachment region on a separation bubble as above. They derived an expression for the pressure recovery coefficient by assuming that the principal mixing process and corresponding pressure rise occur in the region BCDE as shown on the sketch. The pressures across ABC and DE are assumed uniform and equal to p_b and p_r. The portion of the bubble to the left of station x_b is assumed to be a region of constant pressure "dead air" with pressure p_b. Further assumptions are that: CD is a streamline parallel to AE, no fluid enters or leaves AB on the average, and that curvature of the surface AE may be neglected.

p_b and p_r are related to U_b and U_r by Bernoulli's equation:

$$p_b + \frac{1}{2} \rho U_b^2 = p_r + \frac{1}{2} \rho U_r^2$$

By use of the steady flow momentum equation applied to the control volume ABCDE, the following expression is derived for the pressure difference $(p_r - p_b)$.

$$(p_r - p_b) = \frac{\rho}{\delta_r} \left[\int_{y_d}^{y_e} u_b^2 \, dy - \int_0^{\delta_r} u_r^2 \, dy \right]$$

Viscous and turbulent stresses are neglected in this development as they were in reference 12, thus an error is introduced with an effect that cannot be determined. However, it appears reasonable to postulate that pressure effects dominate the process of momentum transfer in the x-direction in the shear layer. Assuming a linear velocity profile across BC of the form:

$$\frac{u_b}{U_b} = a + (1 - a) \frac{y - y_d}{\delta_b}$$

At the dividing streamline $(y = y_d)$ and

$$u_b = a U_b \equiv u_B$$

so we have:

$$(p_r - p_b) = \frac{\rho}{\delta_r} \left[\frac{1}{3} u_B^2 \, \delta_b \left(1 + \frac{1}{a} + \frac{1}{a^2}\right) + U_r^2 \left(\theta_r + \delta_r^* - \delta_r\right) \right] \qquad (1)$$

where θ_r and δ_r^* are the momentum and displacement thicknesses of the shear layer at reattachment.

The steady flow continuity equation is:

$$\int_{y_d}^{y_e} u_b \, dy = \int_0^{\delta_r} u_r \, dy$$

or

$$\frac{1}{2} u_B \delta_b \left(1 + \frac{1}{a}\right) = U_r \left(\delta_r - \delta_r^*\right) \qquad (2)$$

Norbury and Crabtree proceeded to develop an expression for the pressure recovery coefficient, σ, where:

$$\sigma \equiv \frac{p_r - p_b}{\frac{1}{2}\rho U_b^2} = \frac{C_{p_r} - C_{p_b}}{1 - C_{p_b}}$$

This parameter will be discussed in detail in section III. For now we assume that σ remains constant as spoiler height varies in steady flow. Actually the bubble parameters d_r, d_b and σ are expected to be functions of $R_{e_\delta}*$ as discussed in reference 22, but for an overwhelming spoiler perturbation we expect the Reynolds Number dependence to be minimal.

The pressure rise in the reattachment region has also been modeled by many authors with the assumption of isentropic recompression along the dividing streamline (Ref 6). This approach will not be attempted here.

Now consider the steady flow continuity equation applied to the interior of the separation bubble, i.e., the so-called "dead air" region. (See also Ref 19). We have $\dot{m}_{in} = \dot{m}_{out}$. At the dividing streamline on the average $\dot{m}_{in} = \dot{m}_{out} \cong 0$, but now consider the region near reattachment.

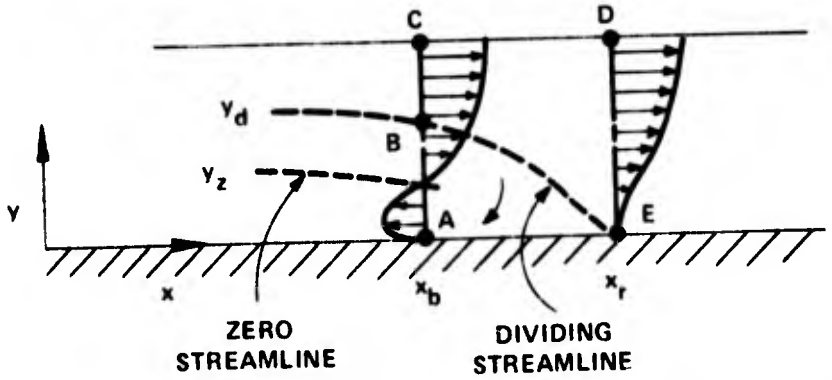

In the region ABE we have $\dot{m}_{in} = \dot{m}_{out}$ and the mass flux per unit span is:

$$\dot{m}_{out} = -\rho \int_0^{y_z} u \, dy$$

and

$$\dot{m}_{in} = \rho \int_{y_z}^{y_d} u \, dy = \dot{m}_{out}$$

Fluid to the left of region ABE is entrained from under the zero streamline into the new mixing layer such that:

$$\dot{m}_{out} = \rho c \int_{x_{sp}}^{x=x_b} v_e \, dx = \rho \int_{y_z}^{y_d} u \, dy$$

where v_e is the entrainment velocity of fluid into the mixing region. Vasilu (in Ref. 6) assumes $\frac{v_e}{U_e}$ = const. where U_e is the velocity at the edge of the shear layer along the bubble.

Since C_p is assumed constant over much of the bubble we have $\frac{U_e}{U_\infty}$ = const and

$$\dot{m}_{out} = \rho c \, v_e \int_{x_{sp}}^{x_b} dx \cong \rho \, v_e \ell \qquad \text{since } v_e \to 0 \text{ as } x \to x_r$$

Fluid recirculated into the dead air region from the region near reattachment can be represented as:

$$\dot{m}_{in} = \rho \int_{y_z}^{y_d} u \, dy = \rho \, u_B \, \delta_o$$

where u_B is the velocity along the dividing streamline and δ_o is a resultant length. (For a linear velocity profile from y_z to y_d, $\delta_o = \frac{y_d - y_z}{2}$.)

And for the separated region we have:

$$\rho \, u_B \, \delta_o = \rho \, v_e \ell$$

and

$$\delta_o = \frac{v_e}{u_B} \ell$$

i.e., bubble length parameters scale to ℓ in steady flow.

Also within the bubble at any station x we find that mass flux recirculated into the region bounded by the spoiler, station x and the zero streamline is:

$$\dot{m}_{in}(x) = \dot{m}_{out}(x) = \rho c \int_{x_{sp}}^{x} v_e \, dx$$

$$= \rho c \, v_e \, (x - x_{sp})$$

$$= \rho c \, v_e \ell \frac{(x - x_{sp})}{\ell} = \dot{m}_{in} \, (x_r) \frac{(x - x_{sp})c}{\ell}$$

These and previous equations describe approximate steady-flow bubble behavior. In the following pages, an attempt is made to account for the effect of harmonic oscillations of the spoiler about a mean position which involves a long bubble type of separation.

2. Unsteady Flow Modifications

a. Unsteady Bubble Growth

Spoiler motion of the form $h = h_o + \Delta h \cos \omega t$ will be considered. Use of a reduced frequency parameter ν results in:

$$h = h_o + \Delta h \cos \nu \tau$$

Consider now the "quasi-steady" assumption that separation bubble growth is in phase with spoiler height. The bubble growth relation would be:

$$\rho \frac{d}{dt} (A) = \dot{m}_{in}(t) - \dot{m}_{out}(t)$$

where we approximate:

$$A \cong \frac{1}{2} h_s \ell$$

and

$$\rho \frac{d}{dt} (A) \cong \frac{\rho}{2} (h_s \dot{\ell} + \dot{h}_s \ell)$$

but in the quasi-steady assumption:

$$\ell = d_r \frac{c}{c_f} (h_s - h_{sc}) \cong d_r \frac{c}{c_f} h_s$$

and

$$\dot{\ell} = d_r \frac{c}{c_f} \dot{h}_s$$

$$\therefore \rho \frac{d}{dt} (A) \cong \rho\, d_r \frac{c}{c_f} h_s \dot{h}_s = \rho\, d_r\, cc_f\, h\dot{h}$$

Define this as the quasi steady mass flux $\dot{m}_\epsilon$ so that

$$\rho \frac{d}{dt} (A) = \dot{m}_\epsilon (t) = \rho\, d_r\, cc_f\, h\dot{h} \tag{3}$$

In reference 19, East and Wilkinson postulate that a similar mass flux may result when a new filament line is "selected" at the spoiler tip. Piston theory is used in their hypersonic flow problem in order to account for the unsteady effect.

In the quasi-steady model we also assume that $\dot{m}_{out_{QS}} = \dot{m}_{out_{SS}}$ where the "steady-state" mass flux is as before:

$$\dot{m}_{out_{SS}} \cong \rho\, v_e \ell$$

And that $\dot{m}_{in_{QS}} = \dot{m}_{in_{SS}} + \dot{m}_\epsilon$ where $\dot{m}_{in_{SS}} = \rho\, u_B\, \delta_o$ and where modifications to u_B and δ_o account for the quantity $\dot{m}_\epsilon$ in quasi-steady flow. That is, in the assumed model $\dot{m}_\epsilon$ is a mass flux that is forced into or out of the bubble in the reattachment region. Later it will be shown how this may be achieved.

As done for the steady flow quantity $\dot{m}_{in}(x)$ we assume in the quasi-steady case

$$\dot{m}_\epsilon (x) = \dot{m}_\epsilon (x_r) \frac{(x - x_{sp})\, c}{\ell}$$

The above quasi-steady result involves a bubble that grows in phase with spoiler motion. Since this is at odds with experimental data we are led to the conclusion that a quasi-steady model is not appropriate. In reference 18, for example, it is argued that since a characteristic time for the outer shear layer is δ/U_∞ as compared to $\ell/|U_c|$ for the separated flow (where U_c is the mean reversed flow velocity), an appropriate assumption would be that the outer layer reacts instantaneously to spoiler motion; i.e., the return mass flow is $\dot{m}_\epsilon$ from the quasi-steady assumption.

Now consider an elemental area, δA, within the bubble where we make the unsteady-flow assumption (as in reference 18) that the backflow mass fluctuations, $\dot{m}_\epsilon$, travel upstream at a mean

flow velocity, U_c. That is, $\dot{m}_\epsilon(X) = \dot{m}_\epsilon(X, t - \tau_\epsilon) = \dot{m}_\epsilon\left(X, t - \frac{\ell - X}{|U_c|}\right)$ where now X is a distance measured aft from the spoiler. Then

$$\rho \frac{d}{dt}[\delta A(X,t)] = \dot{m}_{in_\epsilon} - \dot{m}_{out_\epsilon}$$

$$= \dot{m}_\epsilon\left(X + dX, t - \frac{\ell - (X + dX)}{|U_c|}\right)$$

$$- \dot{m}_\epsilon\left(X, t - \frac{\ell - X}{|U_c|}\right)$$

For long wavelength (i.e., $\frac{\omega \ell}{|U_c|} \ll 2\pi$) we find from a Taylor series expansion that

$$\rho \frac{d}{dt}(\delta A) \cong \frac{\partial}{\partial X} \dot{m}_\epsilon (X, t - \tau_\epsilon)\, dX$$

$$\cong \frac{\partial}{\partial X} \dot{m}_\epsilon (\ell, t - \tau_\epsilon) \frac{X}{\ell}\, dX$$

$$\cong \dot{m}_\epsilon (\ell, t - \tau_\epsilon) \frac{dX}{\ell}$$

Now we integrate over the bubble area

$$\rho \int_{\text{bubble}} \frac{d}{dt}(\delta A) = \rho \frac{d}{dt}(A) = \frac{1}{\ell} \int_0^\ell \dot{m}_\epsilon \left(\ell, t - \frac{\ell - X}{|U_c|}\right) dX$$

where $\dot{m}_\epsilon(\ell, t - \tau_\epsilon) = \rho\, d_r\, cc_f\, h(t - \tau_\epsilon)\, \dot{h}(t - \tau_\epsilon)$. For $h = h_o + \Delta h \cos \omega t$; $\dot{h} = -\omega \Delta h \sin \omega t$ we find:

$$\frac{d}{dt}(A) = -\frac{|U_c|\, d_r cc_f}{\ell} \left[2h_o \Delta h \sin \omega\left(t - \frac{\ell}{2|U_c|}\right)\right.$$

$$\left. \sin \omega \frac{\ell}{2|U_c|} + \frac{\Delta h^2}{2} \sin 2\omega\left(t - \frac{\ell}{2|U_c|}\right) \sin \omega \frac{\ell}{|U_c|}\right]$$

Consider now small perturbations so that $h = h_o + \tilde{h}$; $\ell = \ell_o + \tilde{\ell}$ where $\tilde{h} = \Delta h \cos \omega t$ and $|\tilde{h}| \ll h_o$ & $|\tilde{\ell}| \ll \ell_o$.

We have:

$$\frac{d}{dt}(A) \cong \frac{2\,|U_c|\,d_r c c_f}{\ell_o \omega} h_o \sin\left(\omega \frac{\ell_o}{2|U_c|}\right)$$

$$\left[-\omega \Delta h \sin \omega\left(t - \frac{\ell_o}{2|U_c|}\right)\right]$$

but $d_r\, c\, h_o = \ell_o$

$$\therefore \frac{d}{dt}(A) \cong \frac{2|U_c|c_f}{\omega} \sin\left(\frac{\omega \ell_o}{2|U_c|}\right) \dot{\tilde{h}}\left(t - \frac{\ell_o}{2|U_c|}\right)$$

But since the area is $A \cong \frac{1}{2} h_s\, \ell = \frac{1}{2} h \ell\, c_f$ then $\frac{d}{dt}(A) \cong \frac{1}{2}\left[\dot{\tilde{h}}\, \ell_o + \dot{\tilde{\ell}}\, h_o\right] c_f$ and we find the unsteady flow result:

$$\dot{\tilde{\ell}} \cong \frac{\ell_o}{h_o}\left[\frac{2}{\omega \tau_o} \sin \omega \tau_o\, \dot{\tilde{h}}\,(t - \tau_o) - \dot{\tilde{h}}\right]$$

where $\tau_o \equiv \frac{\ell_o}{2|U_c|}$. For $\tilde{h} = \Delta h \cos \omega t$ we find:

$$\dot{\tilde{\ell}} \cong \frac{\ell_o}{h_o}\left[(k \cos \omega \tau_o - 1)\, \dot{\tilde{h}} + (k\, \omega \sin \omega \tau_o)\, \tilde{h}\right]$$

where

$$k = \frac{4|U_c|}{\ell_o \omega} \sin \omega \frac{\ell_o}{2|U_c|} = \frac{2}{\omega \tau_o} \sin \omega \tau_o$$

Integrating to find $\tilde{\ell}(t)$ we have:

$$\tilde{\ell}(t) - \tilde{\ell}(o) = \frac{\ell_o}{h_o}\left[(k \cos \omega \tau_o - 1)\, \Delta h\, (\cos \omega t - 1)\right.$$

$$\left. + (k \sin \omega \tau_o)\, \Delta h \sin \omega t\right]$$

Assume that over a cycle the average length perturbation is zero so that

$$\tilde{\ell}(o) = \frac{\ell_o}{h_o}(k \cos \omega \tau_o - 1)\, \Delta h$$

and

$$\tilde{\ell}(t) = \frac{\ell_o}{h_o} [(k \cos \omega \tau_o - 1) \Delta h \cos \omega t + (k \sin \omega \tau_o) \Delta h \sin \omega t]$$

This can be written as:

$$\tilde{\ell}(t) = \frac{\ell_o}{h_o} A \Delta h \cos (\omega t - \alpha) = d_r c A \Delta h \cos (\omega t - \alpha)$$

where

$$A = (k^2 - 2 k \cos \omega \tau_o + 1)^{\frac{1}{2}}$$

and

$$A \geq 0$$

also

$$\alpha = \tan^{-1} \left[\frac{\sin \omega \tau_o}{\cos \omega \tau_o - \frac{1}{k}} \right]$$

$$\alpha \geq 0$$

Now:

$$\omega \tau_o = \omega \frac{\ell_o}{2|U_c|} = \frac{\omega c_f}{U_\infty} \left| \frac{U_\infty}{U_c} \right| \frac{d_r c}{2 c_f} h_o = 2 \nu h_o \frac{d_r}{\left| \frac{U_c}{U_\infty} \right|}$$

Note that for quasi-steady bubble growth:

$$\tilde{\ell}(t) = \frac{\ell_o}{h_o} \tilde{h}(t) = d_r c \Delta h \cos \omega t$$

so that the unsteady result above involves an effective spoiler height perturbation that is amplitude and phase dependent on a time lag, τ_o, where

$$\tau_o = \frac{\ell_o}{2|U_c|}$$

That is,

$$\tilde{h}_{eff} = A\,\Delta h \cos(\omega t - \alpha)$$

This result can be achieved by alternative assumptions about the mechanisms of unsteady bubble growth. Inherent in the present result is a model for unsteady entrainment of fluid from the bubble into the outer shear layer. For small perturbations the present model is expected to be correct to first order.

Let us investigate this linear time lag model in detail. First consider small bubbles at low frequency with

$$\omega \tau_o \ll 1 \quad \left(\text{where } |U_c| \sim 0\ \left(\frac{U_\infty}{3}\right)\right)$$

We find

$$k = \frac{2}{\omega \tau_o} \sin \omega \tau_o \cong 2$$

and

$$A \cong 1$$

$$\alpha \cong \tan^{-1}(2\,\omega \tau_o) = \tan^{-1}\left(\omega \frac{\ell_o}{|U_c|}\right)$$

Therefore, the length perturbation is:

$$\tilde{\ell}(t) \cong d_r\, c\, \Delta h \cos \omega \left(t - \frac{\ell_o}{|U_c|}\right)$$

That is, the length lags its quasi-steady location by a time lag which is the "bubble characteristic time."

Now consider a larger bubble and higher frequency where the relation is more complex. For example, consider the following values:

$$\nu = .12; \quad \ell_o = 6"; \quad \left|\frac{U_c}{U_\infty}\right| = \frac{1}{3}$$

then $\omega \tau_o = .18$ rad; $k \cong 1.99$; $A \cong 1.02$ and $\alpha \cong 20.3^\circ = .354$ rad

$$\therefore\ \tilde{\ell}(t) = d_r\, c\, \Delta h\,(1.02) \cos(\omega t - 20.3^\circ)$$

The linear approximation yields:

$$\tilde{\ell}(t) \cong d_r \, c \, \Delta h \cos(\omega t - 19.8^o)$$

The unsteady bubble growth relation also shows that the region of the bubble near reattachment grows in phase with spoiler motion.

b. The Pressure Rise Near Reattachment

The mass flux term, $\dot{m}_\epsilon$, which is included in the unsteady flow model can be represented as

$$\dot{m}_\epsilon = - \rho \, u_B \, \tilde{\delta}_b$$

that is, a perturbation near x_b at the "dividing streamline" results in the additional mass flux. If we assume that conditions at reattachment are unaffected then from the continuity equation (2) we find:

$$\frac{1}{2} u_B \delta_b \left(1 + \frac{1}{a}\right) = \frac{1}{2} (u_B + \tilde{u}_B)(\delta_b + \tilde{\delta}_b)\left(1 + \frac{1}{a}\right)$$

$$= U_r \, (\delta_r - \delta_r^*)$$

and

$$\tilde{u}_B \, \delta_b \cong - u_B \, \tilde{\delta}_b$$

That is, a perturbation of δ_b results in a proportional change to u_B.

The momentum equation (1) yields an appropriate perturbation to p_b.

$$- \tilde{p_b} \delta_r \cong \rho \left[\frac{2}{3} u \, \tilde{u}_B \, \delta_b \left(1 + \frac{1}{a} + \frac{1}{a^2}\right)\right.$$

$$\left. + \frac{1}{3} u_B^2 \, \tilde{\delta_b} \left(1 + \frac{1}{a} + \frac{1}{a^2}\right)\right] + \dot{m}_\epsilon u_B$$

$$= \rho \left[- \frac{1}{3} u_B^2 \, \tilde{\delta_b} \left(1 + \frac{1}{a} + \frac{1}{a^2}\right)\right] - \rho \, u_B^2 \, \tilde{\delta_b}$$

or

$$\tilde{p_b} = \rho \, u_B^2 \, \frac{\tilde{\delta_b}}{\delta_r} \left[\frac{1}{3} \left(4 + \frac{1}{a} + \frac{1}{a^2}\right)\right]$$

and in coefficient form:

$$\tilde{C}_{p_b} \equiv \frac{\tilde{p}_b}{\frac{1}{2}\rho U_\infty^2} = -\left[\frac{1}{3}\left(4 + \frac{1}{a} + \frac{1}{a^2}\right)\right] \frac{\dot{m}_\epsilon u_B}{\frac{1}{2}\rho U_\infty^2 \delta_r}$$

Now $\delta_r = 0\ (h_s)$ and continuing the assumption that conditions at reattachment are unaffected by small perturbations to h we have:

$$\delta_r = \delta_{r_o} \cong k_1\ d_r\ c\ h_o$$

From the quasi-steady equation for mass flux (3) we have:

$$\dot{m}_\epsilon \cong \rho\ d_r\ cc_f\ h_o\ \tilde{\dot{h}}$$

Therefore, the pressure perturbation can be written as:

$$\tilde{C}_{p_b} = -\left[\frac{1}{3}\left(4 + \frac{1}{a} + \frac{1}{a^2}\right)\right] \frac{2\ c_f\ u_B}{k_1\ U_\infty^2}\ \tilde{\dot{h}}$$

or if we assume a constant relation

$$k_2 = \frac{u_B}{|U_c|}$$

then, since $\tilde{\dot{h}} = -\omega\ \Delta h\ \sin \omega t$,

$$\tilde{C}_{p_b} = +\left[\frac{1}{3}\left(4 + \frac{1}{a} + \frac{1}{a^2}\right)\right] 2\ \frac{k_2}{k_1}\left(\frac{\omega\ c_f}{U_\infty}\right)\left|\frac{U_c}{U_\infty}\right| \Delta h \sin \omega t$$

$$= k_3\ \nu \left|\frac{U_c}{U_\infty}\right| \Delta h \sin \omega t$$

where

$$k_3 = \left[\frac{2}{3}\left(4 + \frac{1}{a} + \frac{1}{a^2}\right)\right] \frac{d_r\ c\ h_o\ u_B}{\delta_{r_o}\ |U_c|}$$

Thus, we see that the pressure perturbation depends on spoiler rate and a shear-layer parameter, k_3. This corresponds to a perturbation to the pressure recovery coefficient, σ, and indicates that the normally constant value of σ for a reattaching shear-layer may be modified in unsteady flow.

In order to gain insight into the mechanisms involved in these unsteady flow perturbations, let us consider and extend a treatment of vorticity within the separation bubble.

McGregor (Ref 13) investigated the conditions necessary for equilibrium of the separation bubble in steady-flow. Constancy of circulation and the maintenance of kinetic energy are required.

Circulation around the bubble is

$$\Gamma = \iint_{\text{bubble}} \gamma \, dx \, dy = \oint_{c} q_s \, ds$$

where γ is the vorticity $(\frac{\partial v}{\partial x} - \frac{\partial u}{\partial y})$ and C is a curve, described in the counterclockwise sense, which encloses the bubble. It coincides with the dividing streamline, spoiler aft face and airfoil surface, in steady flow. q_s is the tangential velocity component around the dividing streamline.

If we consider turbulent flow so that u, v and γ consist of mean values $\bar{u}$, $\bar{v}$, and $\bar{\gamma}$ on which are superimposed random fluctuating components u', v' and γ' due to turbulence and whose time average values are zero then we find (Ref 13):

$$\frac{d\Gamma}{dt} - \oint \bar{\gamma} \, \bar{q}_n \, ds = - \nu \oint \frac{\partial \bar{\gamma}}{\partial n} \, ds + \oint \overline{\gamma' q_n'} \, ds \qquad (4)$$

In steady flow the terms on the L.H.S. are zero since $\bar{q}_n = 0$ on the bubble boundary. Then we have:

$$\nu \oint \frac{\partial \bar{\gamma}}{\partial n} \, ds = \oint \overline{\gamma' q_n'} \, ds$$

On the surface of the model $q_n' = 0$ and we may write

$$\nu \int_{\text{sepn}}^{\text{reatt}} \frac{\partial \bar{\gamma}}{\partial y} \, dx_{\text{surf}} + \left[\int_{\text{reatt}}^{\text{sepn}} (\nu \frac{\partial \bar{\gamma}}{\partial n} - \overline{\gamma' q_n'}) \, ds \right] = 0$$

The first term is related to the pressure distribution and the first part of the second term may be neglected so that:

$$\frac{1}{\rho} (p_{\text{sepn}} - p_{\text{reatt}}) \cong \int_{\text{sepn}}^{\text{reatt}} \overline{\gamma' q_n'} \, ds$$

This gives the relation between the fluctuating vorticity and normal velocity at the bubble boundary and the pressure

rise.[13] The rate of transfer of vorticity is very high in the reattachment region since the pressure rise occurs primarily there.

Consider now an unsteady flow assumption that involves the LHS of equation (4). Assume that the sum of the terms is zero, as in steady flow, but in unsteady flow we have:

$$\frac{d\Gamma}{dt} = \oint \bar{\gamma}\, \bar{q}_n \, ds$$

where $\oint \bar{\gamma}\, \bar{q}_n \, ds = \bar{\gamma}_{avg} \frac{d}{dt} (A_{bubble})$ with $\bar{\gamma}_{avg}$ an average value of vorticity along the dividing streamline.

Previous experiments have shown that for low spoiler heights (roughly for $h_s \leq .015\ c$) airfoil lift is relatively unaffected by spoiler projection.[9,23,24] This is thought to be associated with shear layer reattachment on the airfoil surface for low spoiler heights.

It appears reasonable to postulate, therefore, that for low spoiler heights (which do not involve T.E. pressure divergence) total airfoil circulation remains constant so that

$$\Gamma_{airfoil} = \Gamma_{\substack{wetted \\ surface}} + \Gamma_{bubble} = \Gamma_o$$

Now Wood's theory (Ref 25) predicts that lift generated by the wetted surface varies in direct proportion to spoiler height, so that

$$\Gamma_{\substack{wetted \\ surface}} \cong \Gamma_o + k_4 h$$

where $k_4 > 0$. This results in:

$$\Gamma_{bubble} \cong - k_4 h$$

and

$$\frac{d\Gamma_{bubble}}{dt} \cong - k_4 \dot{h}$$

Also we have

$$\frac{d\Gamma_{bubble}}{dt} = \oint \bar{\gamma}\, \bar{q}_n \, ds \cong \bar{\gamma}_{avg} \frac{d}{dt} (A_{bubble})$$

If we neglect phase lags then both $\bar{q}_n$ and A are proportional to $\dot{h}$ and $\bar{\gamma}(s) < 0$, which is to be expected. Thus, on the spoiler upstroke ($\dot{h} > 0$), we find that vorticity of clockwise sense is added to the bubble interior, and conversely on the downstroke, vorticity of clockwise sense is removed from the bubble interior.

If we consider now the maintenance of kinetic energy of the bubble, as in Ref 13, we may look at the steady flow equilibrium relation:

$$W = +\mu \oint \overline{\gamma\, q_s}\, ds + \oint \overline{q_n' p'}\, ds - \oint \bar{q}_s\, (-\rho\, \overline{q_s' q_n'})\, ds \qquad (5)$$

where W is the rate of dissipation of energy due to viscosity and

$$W \cong \mu \iint \bar{\gamma}^2\, dx\, dy$$

The terms on the RHS of equation (5) represent, in turn, the rate at which work is done: on the bubble by the viscous stresses, on the turbulent motion by the pressure fluctuations, and on the bubble by the turbulent shearing stress tangential to the bubble boundary. All but the last term may be neglected as an approximation.

$$\therefore\ W \cong \mu \iint \bar{\gamma}^2\, dx\, dy \cong -\oint \bar{q}_s\, (-\rho\, \overline{q_s' q_n'})\, ds$$

as the energy equilibrium relation for the bubble.[13]

Note that the bubble contains both positive and negative vorticity. The negative vorticity largely diffuses into the bubble in steady flow and the positive vorticity is created at the surface. The rate of dissipation, W, is least for any given circulation, Γ_{bubble}, when the vorticity is all of the same sign.

In unsteady flow where we have found that negative vorticity (of clockwise sense) is either transferred into or out of the bubble we expect the following:

$$\frac{dW}{W} < \frac{d\Gamma}{\Gamma} \quad \text{for } \dot{h} > 0$$

and

$$\frac{dW}{W} > \frac{d\Gamma}{\Gamma} \quad \text{for } \dot{h} < 0$$

That is, the energy dissipation increases less rapidly than circulation on the upstroke and more rapidly than circulation on the downstroke. Thus, on the upstroke an increased pressure rise across the bubble, with corresponding increase in energy dissipation, can be maintained. The increased magnitude of circulation on the upstroke is associated with this pressure rise.

Other qualitative judgements can be made. On the upstroke, an increased pressure rise and increased magnitude of circulation are expected to result in a more highly curved reattachment "streamline." On the other hand, our quasi-steady mass flux model results in near quasi-steady growth for the region of the bubble near to reattachment, thus we expect that the height of this region increases faster than its length, on the upstroke. This deformation to bubble shape is also compatible with increased inviscid external flow velocities and decreased pressures near the point of maximum bubble thickness, that is, probably near x_b.

One factor has not been considered yet. That is, on the spoiler upstroke when vorticity is transferred to the bubble and circulation magnitude increases, there is likely to be an additional integral effect on circulation. This follows if energy is being added to the bubble faster than it is dissipated. A more comprehensive unsteady flow model would probably yield this result.

The previous discussion of bubble vorticity is not offered as a rigorous study of actual conditions. The quasi-steady and unsteady flow assumptions are not well supported in general; however, the qualitative results appear to explain much of the observed behavior. Further testing is absolutely necessary in order to justify and/or refine these assumptions.

3. Unsteady Flow Model

Two significant unsteady flow effects will be included in the steady flow equation for ΔC_H. A polynomial approximation is used for the steady flow relation and modified to account for unsteady pressure perturbations, which are taken to act over the dead air region. An effective spoiler height is used, which lags actual spoiler motion.

Thus, the steady-flow relation:

$$\Delta C_H = a_5 h^5 + a_4 h^4 + a_3 h^3 + a_2 h^2 + a_1 h + a_o$$

is modified to the unsteady flow approximation for $h = h_o + \Delta h \cos \omega t$:

$$\Delta C_H(t) \cong \left[1 + \frac{\tilde{C}_{p_b}}{C_{p_{b_o}}}\right] \left[a_5 h_{eff}^5 + a_4 h_{eff}^4 + a_3 h_{eff}^3 + a_2 h_{eff}^2 + a_1 h_{eff} + a_o\right] \quad (6)$$

where $C_{p_{b_o}}$ is the steady flow value of C_{p_b}

$$\tilde{C}_{p_b} = k_3 \nu \left|\frac{U_c}{U_\infty}\right| \Delta h \sin \omega t$$

and

$$h_{eff} = h_o + A \Delta h \cos (\omega t - \alpha)$$

The following parameter values are chosen based on experimental observations and other results.[6]

$$C_{p_{b_o}} \cong -.4$$

which yields

$$\frac{u_B}{U_b} \cong .535 = a$$

Also, we have

$$\frac{U_c}{U_\infty} \cong \frac{1}{3}$$

so that

$$\frac{u_B}{|U_c|} \cong 2.0$$

But,

$$k_3 = \left[\frac{2}{3}\left(4 + \frac{1}{a} + \frac{1}{a^2}\right)\right] \frac{d_r c h_o}{\delta_{r_o}} \frac{u_B}{|U_c|}$$

$$\therefore \; k_3 \cong 12.0 \frac{d_r c h_o}{\delta_{r_o}}$$

Now, based on boundary layer measurements,[5] assume $3\, h_o\, c_f \cong \delta_{r_o}$ so that

$$k_3 \cong 4.0 \frac{d_r c}{c_f} \cong 16.0\, d_r = 88$$

where $d_r = 5.5$ and $x_r = d_r h + x_{sp}$. A best steady-flow curve fit yields:

$$a_5 = -4 \times 10^5; \; a_4 = 1.3 \times 10^5; \; a_3 = -1.48 \times 10^4;$$

$$a_2 = 689 \quad ; \; a_1 = -12.38375; \; a_o = .06190375$$

Figure 2 shows a comparison of the unsteady prediction and experiment (reconstructed curves) for the following three cases:

Case	h_o	Δh
B	.053	.026
C	.076	.027
E	.062	.040

$\nu = .12$ for all curves.

Also shown on Figure 2 are unsteady predictions which include an empirical modification to allow for the integral circulation effect mentioned previously.

The unsteady "dead-air" pressure perturbations, $\tilde{C}_{p_b}$, are integrated from the start of the spoiler upstroke, multiplied by a factor of ½ (to approximately allow for dissipation of energy due to viscous and turbulent stresses) and superimposed on the quasi-steady value of $\tilde{C}_{p_b}$; that is,

$$(\tilde{C}_{p_b})_{mod} = k_3 \nu \left|\frac{U_c}{U_\infty}\right| \Delta h \left[\sin \omega t - \frac{1}{2}(1 + \cos \omega t)\right]$$

This empirical modification improves the otherwise fair agreement which is demonstrated in Figure 2; however, it is

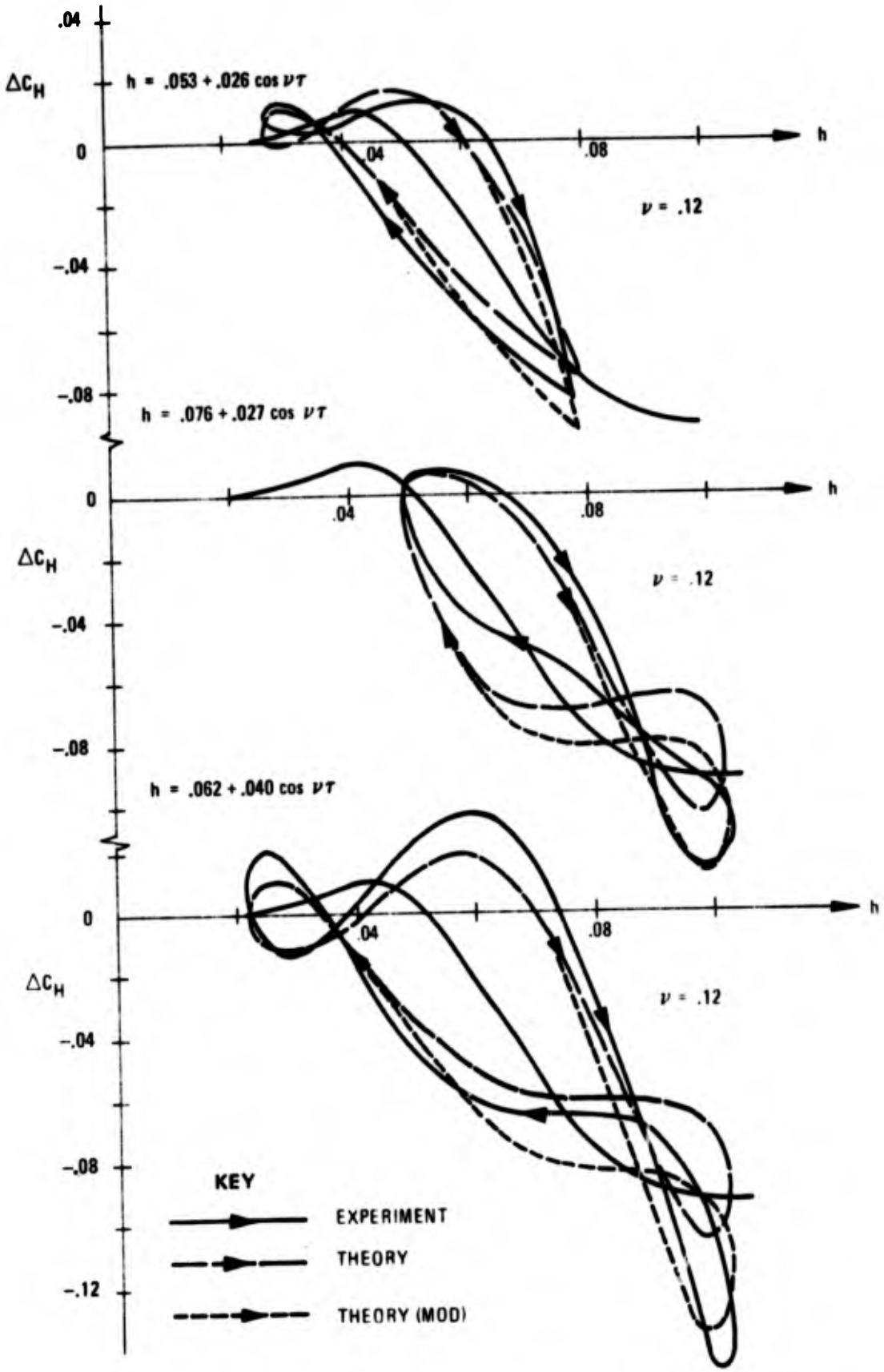

FIG. 2. DYNAMIC HINGE-MOMENT VARIATIONS, EXPERIMENT AND THEORY

not used in further analysis since it is a rather speculative addition to the unsteady theory.

The present theory cannot be compared with other flap-fixed, spoiler-forced results for two reasons:

1. The steady-flow curve fit is only valid for $.03 \leq h \leq .10$.

2. For large bubbles which involve recompression on the flap surface and "reattachment" at a point (line in 3-D flow) of confluence in the wake, the mass flux relations are no longer valid for the bubble.

However, it will be seen that the theory can be used in order to predict limit-cycle behavior of the coupled flap/spoiler system.

4. The Describing Functions

For spoiler motion of the form $h = h_o + \Delta h \cos \nu\tau$, with h_o, Δh and ν constant, the resultant incremental hinge-moment coefficient may be represented in Fourier series form as:

$$\Delta C_H = \Delta C_{H_o} \{h_o, \Delta h, \nu\} + \sum_{n=1}^{\infty} \Delta C_{H_n} \{h_o, \Delta h, \nu\}$$

$$\cos [n\omega t + \psi_n \{h_o, \Delta h, \nu\}]$$

Results obtained from the unsteady relation (equation 6) are as follows:

$$\Delta C_{H_o} = \frac{1}{2\pi} \int_o^{2\pi} \Delta C_H \{h_o + \Delta h \cos \omega t, -\omega \Delta h \sin \omega t\} \, d(\omega t)$$

Thus:

$$\Delta C_{H_o} = [(a_5 h_o^5 + a_4 h_o^4 + a_3 h_o^3 + a_2 h_o^2 + a_1 h_o + a_o)$$

$$+ \frac{1}{2} (10a_5 h_o^3 + 6a_4 h_o^2 + 3a_3 h_o + a_2) \Delta h^2 A^2$$

$$+ \frac{3}{8} (5a_5 h_o + a_4) \Delta h^4 A^4] + \frac{k_3 \nu \, |U_c/U_\infty|}{2 \, C_{p_{b_o}}} \Delta h \sin \alpha$$

$$[(5a_5 h_o^4 + 4a_4 h_o^3 + 3a_3 h_o^2 + 2a_2 h_o + a_1) \Delta h A$$

$$+ \frac{3}{4} (10a_5 h_o^2 + 4a_4 h_o + a_3) \Delta h^3 A^3 + \frac{5}{8} (a_5) \Delta h^5 A^5] \qquad (7)$$

Now define the describing function $\frac{\Delta C_{H_1}}{\Delta h}$,

$$\frac{\Delta C_{H_1}}{\Delta h} \equiv N_1 + i\, N_2$$

where

$$\begin{bmatrix} N_1 \\ \\ N_2 \end{bmatrix} = \frac{1}{\pi \Delta h} \int_0^{2\pi} \Delta C_H \{h_o + \Delta h \cos \omega t, -\omega \Delta h \sin \omega t\} \begin{bmatrix} \cos \omega t \\ \\ \sin \omega t \end{bmatrix} d(\omega t)$$

We find:

$$N_1 = [(5a_5 h_o^4 + 4a_4 h_o^3 + 3a_3 h_o^2 + 2a_2 h_o + a_1) + \frac{3}{4}(10a_5 h_o^2 + 4a_4 h_o + a_3)\Delta h^2 A^2 + \frac{5}{8}(a_5)\Delta h^4 A^4]$$
$$A \cos \alpha + \frac{k_3 \nu \, |U_c/U_\infty|}{2\, C_{p_{b_o}}} \sin 2\alpha \left[\frac{1}{2}(10a_5 h_o^3 + 6a_4 h_o^2 + 3a_3 h_o + a_2)\Delta h^2 A^2 + \frac{1}{2}(5a_5 h_o + a_4)\Delta h^4 A^4\right] \tag{8}$$

and

$$N_2 = [(5a_5 h_o^4 + 4a_4 h_o^3 + 3a_3 h_o^2 + 2a_2 h_o + a_1) + \frac{3}{4}(10a_5 h_o^2 + 4a_4 h_o + a_3)\Delta h^2 A^2 + \frac{5}{8}(a_5)\Delta h^4 A^4]$$
$$(-A \sin \alpha) + \frac{k_3 \nu \, |U_c/U_\infty|}{2\, C_{p_{b_o}}} \cos 2\alpha \left[\frac{1}{2}(10a_5 h_o^3 + 6a_4 h_o^2 + 3a_3 h_o + a_2)\Delta h^2 A^2 + \frac{1}{2}(5a_5 h_o + a_4)\Delta h^4 A^4\right]$$
$$- \frac{k_3 \nu |U_c/U_\infty|}{C_{p_{b_o}}} [(a_5 h_o^5 + a_4 h_o^4 + a_3 h_o^3 + a_2 h_o^2 + a_1 h_o$$

$$+ a_o) + \frac{1}{2}(10a_5 h_o^3 + 6a_4 h_o^2 + 3a_3 h_o + a_2)\Delta h^2 A^2$$

$$+ \frac{3}{8}(5a_5 h_o + a_4)\Delta h^4 A^4] \qquad (9)$$

Also we find:

$$\left|\frac{\Delta C_{H_1}}{\Delta h}\right| = (N_1^2 + N_2^2)^{\frac{1}{2}}$$

and

$$\psi_1 = 180^o + \tan^{-1}\frac{N_2}{N_1}$$

Thus, the first two terms of the Fourier series representation are:

$$\Delta C_H \cong \Delta C_{H_o} + \Delta C_{H_1} \cos(\omega t + \psi_1)$$

or

$$\Delta C_H \cong \Delta C_{H_o} + N_1 \Delta h \cos \omega t + \frac{N_2}{\omega}(-\omega \Delta h \sin \omega t)$$

Plots of ΔC_{H_o}, $\frac{\Delta C_{H_1}}{\Delta h}$ and ψ_1, N_1 and N_2 are shown in Figures 3 to 5 and may be compared to the experimental steady flow results, which are also shown.

Unsteady predictions for ΔC_{H_o} are generally confirmed by experimental results. (See data in references 5 and 21.) Frequency effect is clearly duplicated; that is, there is a reduction in magnitude of ΔC_{H_o} as frequency increases. Existing discrepancies, which are minor, can be attributed primarily to the approximate fifth order polynomial curve fit for steady flow.

Predictions of the describing function, $\frac{\Delta C_{H_1}}{\Delta h}$, are also dependent on the goodness of fit of the polynomial. For high values of h_o there is obvious discrepancy and the complicated dependency of $\frac{\Delta C_{H_1}}{\Delta h}$ on Δh is not reproduced. Furthermore, frequency effect on magnitude is not accurately predicted for high h_o, and phase shift ψ_1 is not predicted well over some of the h_o range. Several reasons exist for these discrepancies:

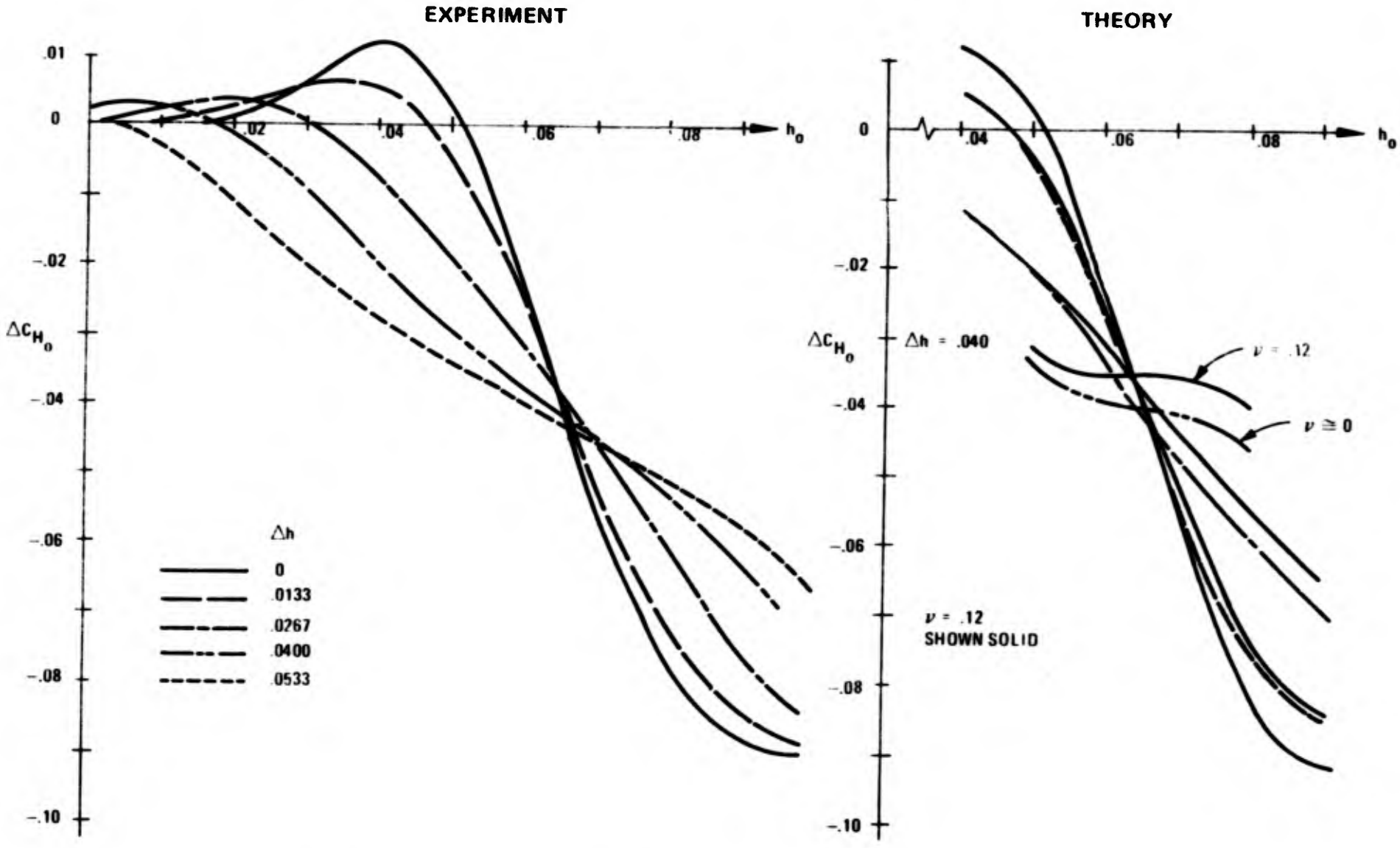

FIG. 3. VARIATION OF ΔC_{H_o} WITH h_o, Δh AND ν

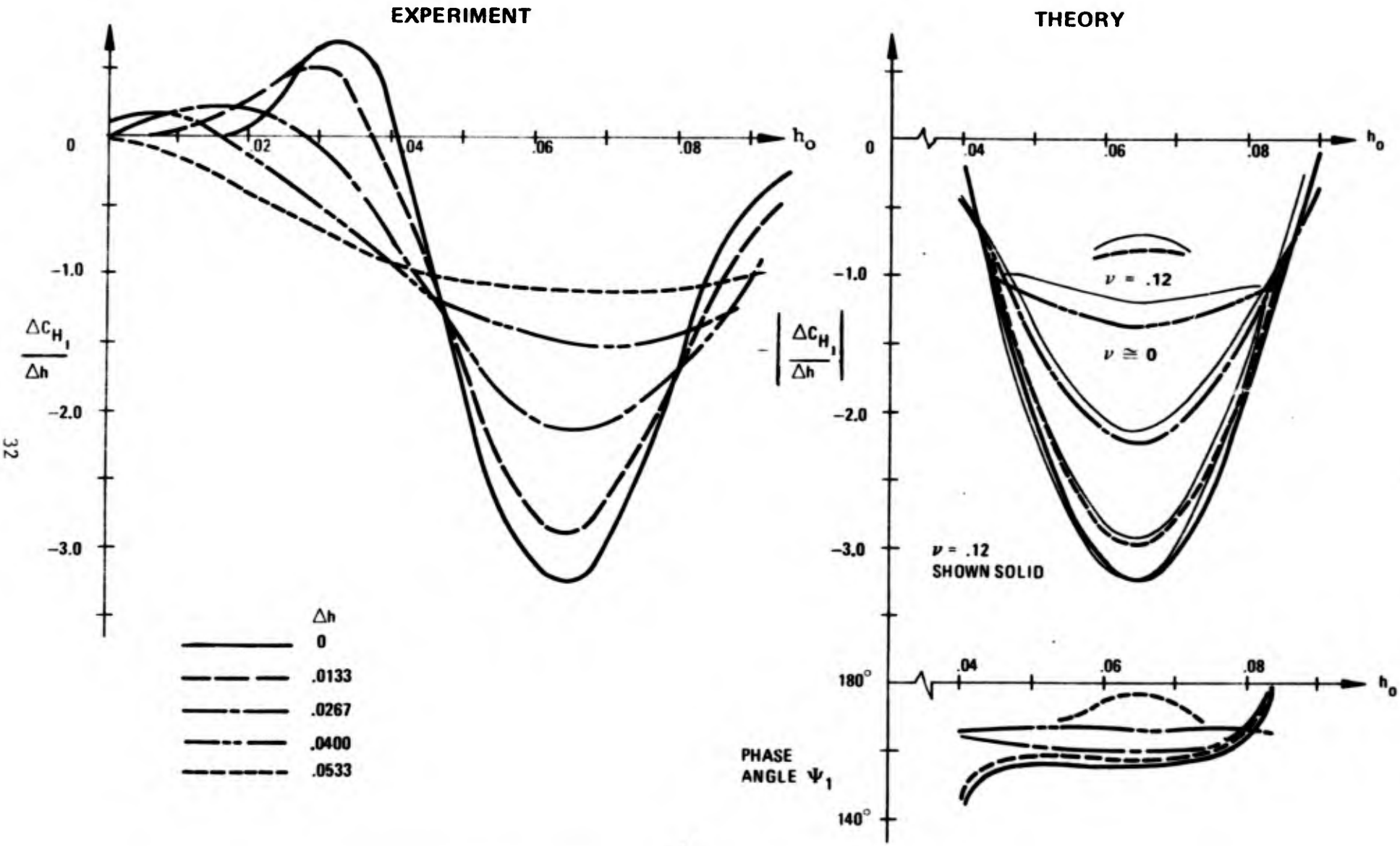

FIG. 4. VARIATION OF DESCRIBING FUNCTION, $\frac{\Delta C_{H_1}}{\Delta h}$

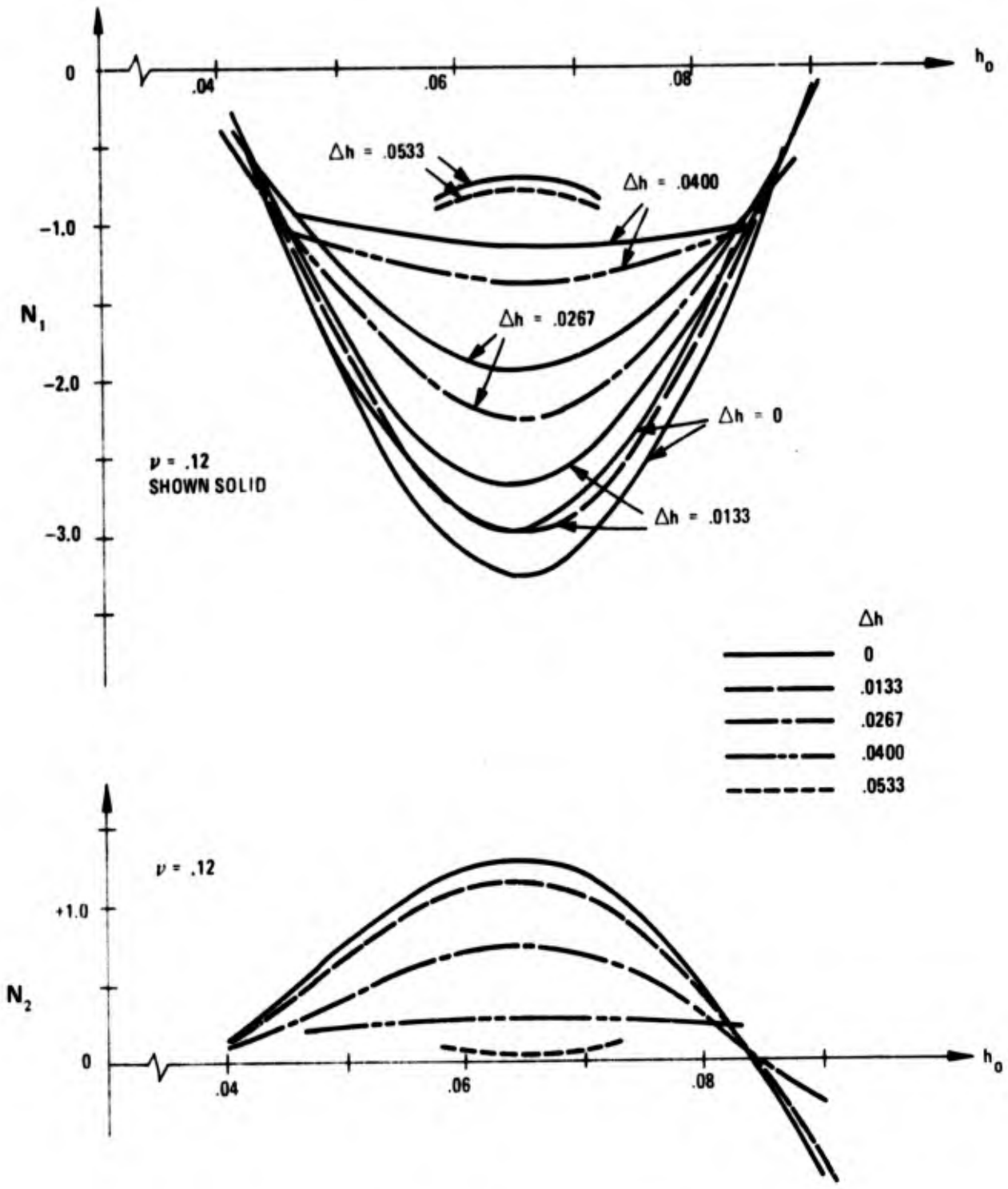

FIG. 5. DESCRIBING FUNCTION COEFFICIENTS

1. The experimental results reflect the integral effect on circulation, which would tend to increase $\frac{\Delta C_{H_1}}{\Delta h}$ as frequency and h_o increase.

2. For spoiler motion which involves very low spoiler heights during part of the cycle, the short bubble type is formed at the onset of the upstroke. Pressure recovery to high values aft of reattachment can influence the hinge-moment greatly. This, plus the low pressures in the bubble near reattachment (which relate to large negative incremental moments) combine to increase $\left|\frac{\Delta C_{H_1}}{\Delta h}\right|$ as frequency increases.

3. The theory does not allow for large bubbles where reattachment, hence mixing and additional mass flux, occurs in the wake.

4. In the limit at very high frequencies, the bubble is washed off the airfoil into the wake. It does not dissipate as in our model. The effect of bubble "wash off" is that a large region of high suction is able to affect hinge-moment greatly.

Although there appear to be large discrepancies in the unsteady describing function in general, it appears that the functional relation is in fair, if not good, agreement in the region near $h_o = .065$; that is, for small perturbations with reattachment near the T.E. This region is of prime interest as will be shown when coupled system behavior is considered.

Before leaving this topic, it is necessary to consider the evaluation of describing functions which can be used when spoiler motion is of the form:

$$h = h_o(t) + \Delta h\,(t)\,\cos\,\omega(t)\,t$$

That is, for transient motion, where h_o, Δh and ω are assumed to vary slowly and can be averaged over a cycle of motion. We have: $\dot{h} \cong \dot{\Delta h} \cos \omega t - \omega\,\Delta h \sin \omega t$ and now proceed to form an expression for $\Delta C_H(t)$ which includes the first "damped harmonic."[26] The following expressions are evaluated:

$$\Delta\hat{C}_{H_o} = \frac{1}{2\pi}\int_0^{2\pi} \Delta C_H \{h_o + \Delta h \cos \omega t,\ \dot{\Delta h} \cos \omega t$$

$$- \omega\,\Delta h \sin \omega t\}\, d(\omega t)$$

$$\begin{bmatrix} \hat{N}_1 \\ \hat{N}_2 \end{bmatrix} = \frac{1}{\pi \Delta h} \int_0^{2\pi} \Delta C_H \{h_o + \Delta h \cos \omega t, \dot{\Delta h} \cos \omega t - \omega \Delta h \sin \omega t\} \begin{bmatrix} \cos \omega t \\ \sin \omega t \end{bmatrix} d(\omega t)$$

And we find:

$$\Delta \hat{C}_{H_o} = \Delta C_{H_o} - \frac{k_3 \, c_f \, |U_c|}{C_{p_{b_o}} \, U_\infty^2} \dot{\Delta h} \left[\frac{1}{2} (5a_5 h_o^4 + 4a_4 h_o^3 + 3a_3 h_o^2 + 2a_2 h_o) \Delta hA + \frac{3}{8} (10a_5 h_o^2 + 4a_4 h_o + a_3) \Delta h^3 A^3 + \frac{5}{16} (a_5) \Delta h^5 A^5 \right] \cos \alpha \qquad (10)$$

where ΔC_{H_o} is given in equation (7).

$$\hat{N}_1 = N_1 - \frac{k_3 \, c_f \, |U_c|}{C_{p_{b_o}} \, U_\infty^2} \frac{\dot{\Delta h}}{\Delta h} \{[(a_5 h_o^5 + a_4 h_o^4 + a_3 h_o^3 + a_2 h_o^2 + a_1 h_o + a_o) + \frac{1}{2} (10a_5 h_o^3 + 6a_4 h_o^2 + 3a_3 h_o + a_2) \Delta h^2 A^2 + \frac{3}{8} (5a_5 h_o + a_4) \Delta h^4 A^4] + [\frac{1}{4} (10a_5 h_o^3 + 6a_4 h_o^2 + 3a_3 h_o + a_2) \Delta h^2 A^2 + \frac{1}{4} (5a_5 h_o + a_4) \Delta h^4 A^4] \cos 2\alpha \} \qquad (11)$$

where N_1 is given in equation (8), and

$$\hat{N}_2 = N_2 + \frac{k_3 \, c_f \, |U_c|}{C_{p_{b_o}} \, U_\infty^2} \frac{\dot{\Delta h}}{\omega \Delta h} [\frac{1}{4} (10a_5 h_o^3 + 6a_4 h_o^2 + 3a_3 h_o + a_2) \Delta h^2 A^2 + \frac{1}{4} (5a_5 h_o + a_4) \Delta h^4 A^4] \sin 2\alpha \qquad (12)$$

where N_2 is given in equation (9).

The above relations will be used in order to investigate system stability and transient behavior for the coupled flap/spoiler system. The first terms in the Fourier series representation for ΔC_H would be:[26]

$$\Delta C_H \cong \Delta\hat{C}_{H_o} + \hat{N}_1 \Delta h \cos \omega t + \frac{\hat{N}_2}{\omega} (\dot{\Delta h} \cos \omega t - \omega \Delta h \sin \omega t)$$

$$\cong \Delta\hat{C}_{H_o} + [\hat{N}_1 + \frac{\hat{N}_2}{\omega} \frac{\dot{\Delta h}}{\Delta h}] \Delta h \cos \omega t + \frac{\hat{N}_2}{\omega} (-\omega \Delta h \sin \omega t)$$

5. Prediction of Coupled System Behavior

When the spoiler and flap are mechanically coupled we expect, in some cases, that self-excited oscillations may occur which lead to stable limit cycle motion.

Consider now the linear coupling relation:

$$h = h_{o_1} + k\beta \tag{13}$$

which involves the coupling parameters h_{o_1} and k. We seek to investigate the dependence of system stability on these parameters.

The system equation of motion is of the form:

$$A\ddot{\beta} + B\dot{\beta} + C\beta = H$$

where

$$H = H_{\dot{\beta}}\dot{\beta} + H_{\beta}\beta + \Delta H$$

This form of the equation has been justified by experimental results. (See references 5 and 21.) So we have:

$$\ddot{\beta} + \frac{(B - H_{\dot{\beta}})}{A}\dot{\beta} + \frac{(C - H_{\beta})}{A}\beta = \frac{\Delta H}{A} \tag{14}$$

In the flap-free case ΔH, the forcing function, was due solely to spoiler motion, but now it is a function of flap motion through the coupling relation (13). We have:

$$\frac{\Delta H}{A} = \frac{\Delta C_H q_\infty b_f c_f^2}{A} \tag{15}$$

where $\Delta C_H = f\{\beta_o, \beta_1, \omega\}$ for spoiler motion of the form $\beta \cong \beta_o + \beta_1 \cos \omega t$.

This form of motion is assumed since the LHS of equation (14) relates to a system with low-pass filter characteristics. That is, higher harmonic content of β (t) may be neglected. Therefore, it is appropriate to represent $\Delta C_H(t)$, in order to determine system stability, as:

$$\Delta C_H \cong \Delta \hat{C}_{H_o} + [\hat{N}_1 + \frac{\hat{N}_2}{\omega} \frac{\dot{\beta}_1}{\beta_1}] k \beta_1 \cos \omega t$$

$$+ \frac{\hat{N}_2}{\omega} (-\omega k \beta_1 \sin \omega t)$$

since

$$\Delta h = k \beta_1$$

But now $\Delta \hat{C}_{H_o}$, $\hat{N}_1$ and $\hat{N}_2$ are functions of the assumed slowly varying parameters β_o, β_1 and ω.

In order to study sustained (limit-cycle) oscillations we represent ΔC_H as:

$$\Delta C_H \cong \Delta C_{H_o} + N_1 k \beta_1 \cos \omega t + \frac{N_2}{\omega} (-\omega k \beta_1 \sin \omega t)$$

A direct solution of equation (14) is not attempted, instead (as in references 27 and 28) we consider an approximate method of solving non-linear differential equations.

First define $\lambda \equiv \frac{\dot{\beta}_1}{\beta_1} = \frac{\dot{\Delta h}}{\Delta h}$.

Then from equations (14) and (15) we find the following approximate relations for β_o, λ and ω^2: [27]

$$\beta_o \cong \frac{\Delta \hat{C}_{H_o} q_\infty b_f c_f^2}{(C - H_{\dot{\beta}})} = \frac{\Delta \hat{C}_{H_o}}{(\frac{C}{q_\infty b_f c_f^2} - C_{H_{\dot{\beta}}})} \qquad (16)$$

$$\lambda \cong - \frac{(B - H_{\dot{\beta}}) - \frac{\hat{N}_2}{\omega} k q_\infty b_f c_f^2)}{2A}$$

$$= \frac{1}{2A} [(\frac{c_f}{U_\infty} C_{H_{\dot{\beta}}} + k \frac{\hat{N}_2}{\omega}) q_\infty b_f c_f^2 - B] \qquad (17)$$

$$\omega^2 \cong -\lambda^2 + \left[\frac{(C - H_\beta) - k\,\hat{N}_1\, q_\infty\, b_f\, c_f^2}{A}\right]$$

$$= -\lambda^2 + \left[\frac{C - (C_{H_\beta} + k\,\hat{N}_1)\, q_\infty\, b_f\, c_f^2}{A}\right] \qquad (18)$$

where $h_o = h_{o_1} + k\,\beta_o$; $\Delta h = k\,\beta_1$ and $\nu \equiv \frac{\omega\, c_f}{U_\infty}$.

Note that an equivalent linear equation may be used to represent equation (14) as:

$$\ddot{\beta} - 2\lambda\dot{\beta} + \omega_n^2\,\beta = 0$$

where $\omega_n^2 = \omega^2 + \lambda^2$ and $-\lambda = \zeta\omega_n$.

The set of equations (16) to (18) was evaluated for an "ideal" coupled system. (That is, dry friction was not included.) The system is taken to be initially at rest at the steady-flow "equilibrium" position. Initially then $\beta_1 = \Delta h = 0$. Parameter values matched the experimental configuration with a few minor exceptions. Moment of inertia, A, was taken as constant for the coupled system. It is actually a weak function of the coupling parameter k. Also mechanical damping was taken as constant. It is also a weak function of k. Values of C_{H_β} and $C_{H_{\dot\beta}}$ result from the series of flap-forced testing with zero spoiler height. The parameter values are:

$$A = .0099 \text{ sl-ft}^2;\quad B = .0115\ \frac{\text{ft-lb-sec}}{\text{rad}}$$

$$C = .477\ \frac{\text{ft-lb}}{\text{rad}};\quad C_{H_\beta} = -.518$$

$$C_{H_{\dot\beta}} = -1.29;\quad q_\infty\, b_f\, c_f^2 = 10.20 \text{ ft-lb}$$

$$\left(\text{i.e., } U_\infty = 150\ \frac{\text{ft}}{\text{sec}}\right)$$

Figure 6 presents the system stability parameters over a wide range of coupling parameters. The lines of constant β_o are seen to be straight, which is to be expected since $h_{o_1} = h_o - k\,\beta_o$. The curve of $\lambda = 0$ defines the system stability boundary. Regions in the upper right side are most unstable, while the stable region is confined roughly to the lower left. We find too that at $\beta_o \cong -4^o$, which corresponds to $h_o \cong .065$, the system is most unstable for any given k. This coincides with the peak value of $\hat{N}_2$. The constant frequency curves nearly follow the curves of constant λ due primarily to the similarity

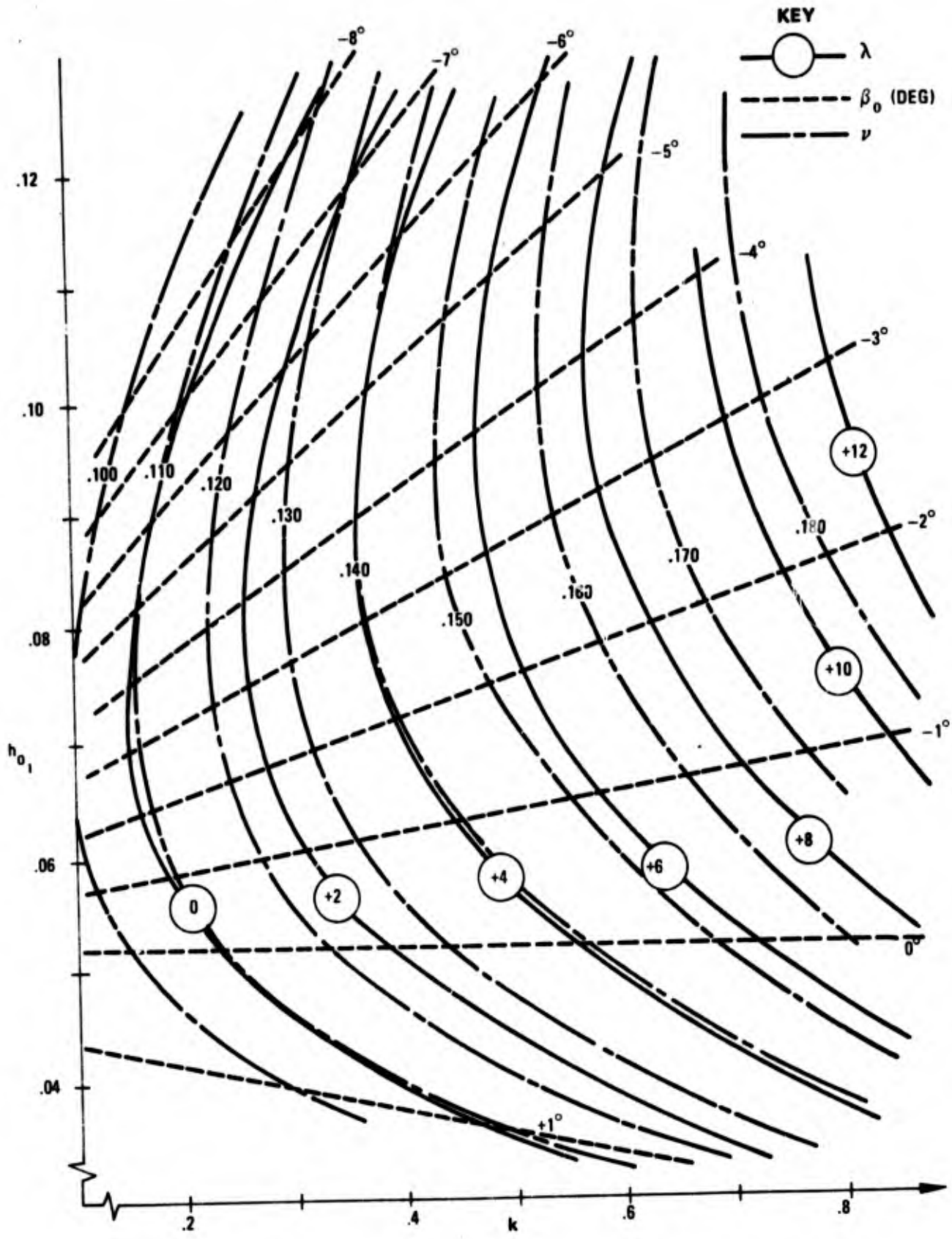

FIG. 6. SYSTEM STABILITY PARAMETERS

in h_o dependence of $|N_1|$ and N_2. An equivalent damping ratio, ζ, takes on a value of approximately -.07 at $h_{o_1} = .08$; $k = .3$. For $h_{o_1} = .10$; $k = .6$, then $\zeta \cong -.21$.

It is found that unstable combinations of coupling parameters will lead to sustained oscillations, or limit-cycle behavior. The system of equations (16) to (18) was included in an algorithm which searched through permissible values of β_o, β_1 and ω in order to satisfy the set of equations with $\lambda = 0$. A high-speed digital computer was used. At the limit cycle we have:

$$\Delta\hat{C}_{H_o} = \Delta C_{H_o}\ ;\quad \hat{N}_1 = N_1 \quad \text{and} \quad \hat{N}_2 = N_2$$

and

$$\Delta C_H \cong \Delta C_{H_o} + N_1\ k\ \beta_1 \cos \omega t + \frac{N_2}{\omega}\ (-\omega k\ \beta_1 \sin \omega t)$$

Figure 7 contains curves of constant parameter values; β_o, β_1 and ν. Note that there is evidence of the "rectification" effect on ΔC_{H_o}. A comparison of Figures 3, 6 and 7 shows that the $\beta_o \cong -4^o$ curve is relatively unaffected, which follows from the unsteady theory (see Figure 3). For low values of h_{o_1} (hence, low values of h_o) we find that $\beta_{o_{LC}} < \beta_{o_{ss}}$; where LC and SS stand for limit-cycle and steady-state "equilibrium," respectively. Conversely, for high values of h_o; $\beta_{o_{LC}} > \beta_{o_{ss}}$. This effect is more pronounced for large β_1. Limit-cycle frequencies are less than for $\beta_1 \cong 0$. This is due to reduced magnitudes of N_1 as β_1 goes from zero to limit-cycle amplitude. The frequency change is more pronounced for large β_1. Maximum limit-cycle amplitudes occur near $h_{o_1} = .08$; $k = .26$. This corresponds to $h_o \cong .065$ as expected. Limit-cycle amplitude decreases as k increases past about .26 because of the combined frequency effect and the nonlinear dependence of N_2 on Δh. Also, $\beta_1 = \frac{\Delta h}{k}$. Note also that for low values of h_{o_1} and k, limit-cycle behavior is predicted even though the system is predicted to be stable at "equilibrium." This apparent anomaly is due to the rectification effect on ΔC_{H_o}, hence β_o. In this case "hard oscillator" behavior exists; that is, the system needs an initial disturbance of sufficient magnitude to provoke limit-cycle behavior. Limitations of the present model could also account for this phenomenon.

The theory was modified to allow for the presence of dry friction since it was discovered that this was a significant damping contribution to the actual coupled system. Several tests were performed in order to verify that dry friction was, in fact, present and to measure its contribution. An equivalent linear representation was calculated and is included in the

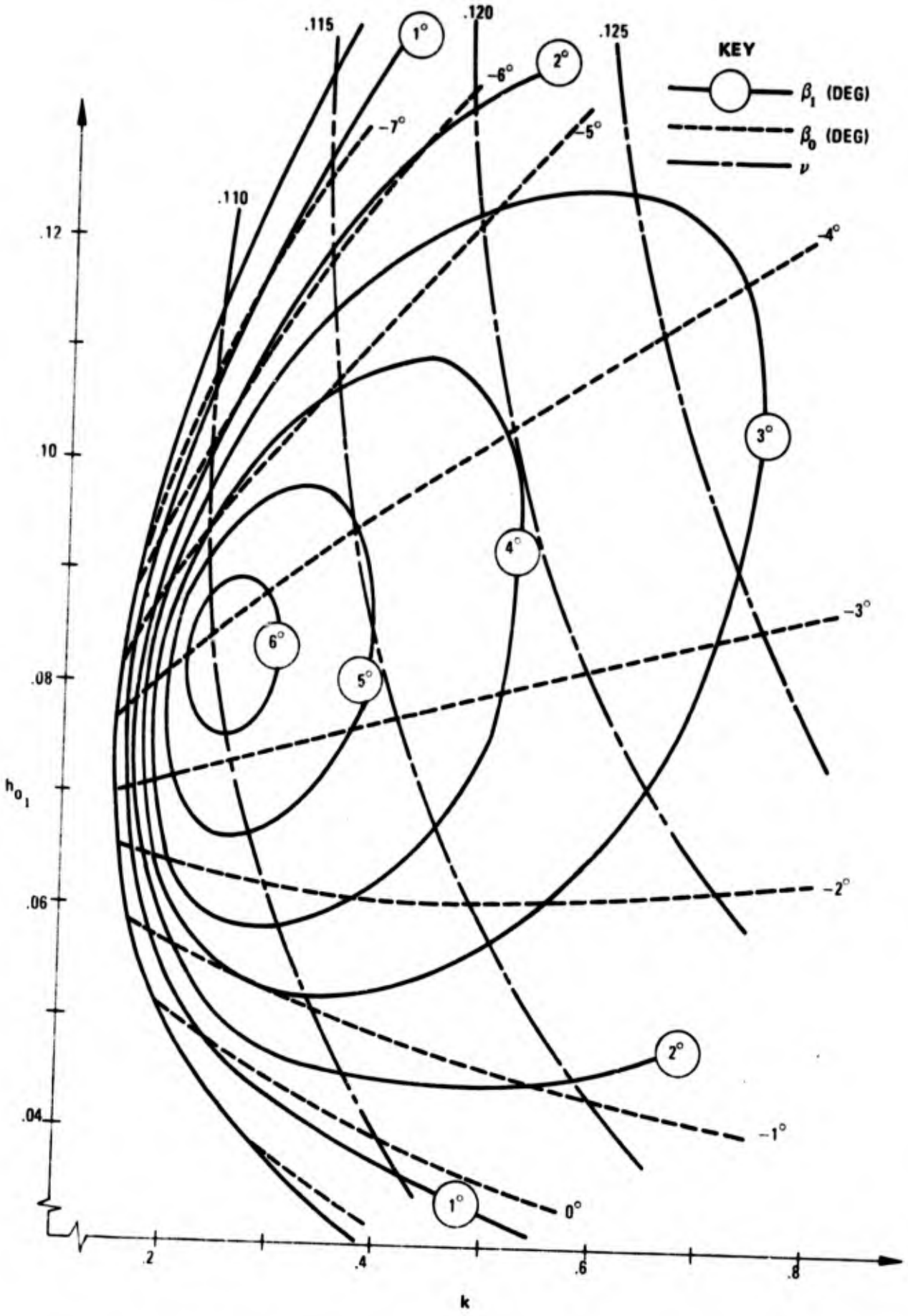

FIG. 7. LIMIT-CYCLE PARAMETERS (IDEAL COUPLING)

system equation of motion as an additional damping term of the form:

$$B' = k_5 \; k^2 \; \frac{h_o}{\Delta h \, \omega} \; q_\infty \; b_f \; c_f^2$$

The dependence on $h_o \; q_\infty \; b_f$ occurs because the normal force on the spoiler face is a function of dynamic pressure and spoiler wetted area. The k^2 dependence represents the effect of gear ratio on moment and provides a best fit to the test data. The constant value is $k_5 \cong .232$.

Thus, at the limit-cycle, equation (17) becomes:

$$B = \left[\frac{c_f}{U_\infty} \, C_{H\dot{\beta}} + k \, \frac{N_2}{\omega} - k_5 \; k^2 \; \frac{h_o}{\Delta h \, \omega}\right] q_\infty \; b_f \; c_f^2$$

Once again a search algorithm was run and results are shown in Figure 8. In this case, however, computer data was considered unreliable in the region shown. Suitable convergence in the shaded region could not be achieved unless parameter increments were made small at the cost of large amounts of computer time. The presence of dry friction, which is inversely proportional to Δh, precludes self-excited oscillations as verified in the experiment; however, stable limit-cycle behavior is predicted as was observed. The effect of dry friction is not extremely significant except that lower amplitude limit-cycles are reached, with the maximum occurring near $h_{o_1} = .073$ and $k = .25$. The contours of constant β_1 are shifted downward and to the left due to dependence of dry friction on h_o and k. The curves of constant β_o are not significantly altered; however, frequencies are uniformly increased due to the fact that the lower amplitudes, β_1, relate to lower values of Δh at limit-cycle, hence to higher values of $|N_1|$ and frequency.

Finally, in Figure 9 data points taken from several coupled system tests are shown. Curves of constant frequency, β_o and β_1 are shown interpolated between the points. In all cases amplitude data was within 20% of the final results shown. Frequency results are within 10%. Only data taken for a free-stream speed of $U_\infty = 150$ ft/sec was used. Some of the tests at extreme values of h_{o_1} did not demonstrate long-term sustained limit-cycle behavior. It is probable that three-dimensional effects could account for this. Although the range of parameter variations was small for the series of tests (due primarily to model limitations) the agreement between experiment and theory is surprisingly good. Frequencies, amplitudes and mean values of flap angle appear to be well predicted. Note that largest amplitudes occur near $\beta_o = -3^o$ which corresponds to $h_o \cong .06$. This is the region where the unsteady theory is expected to be most accurate.

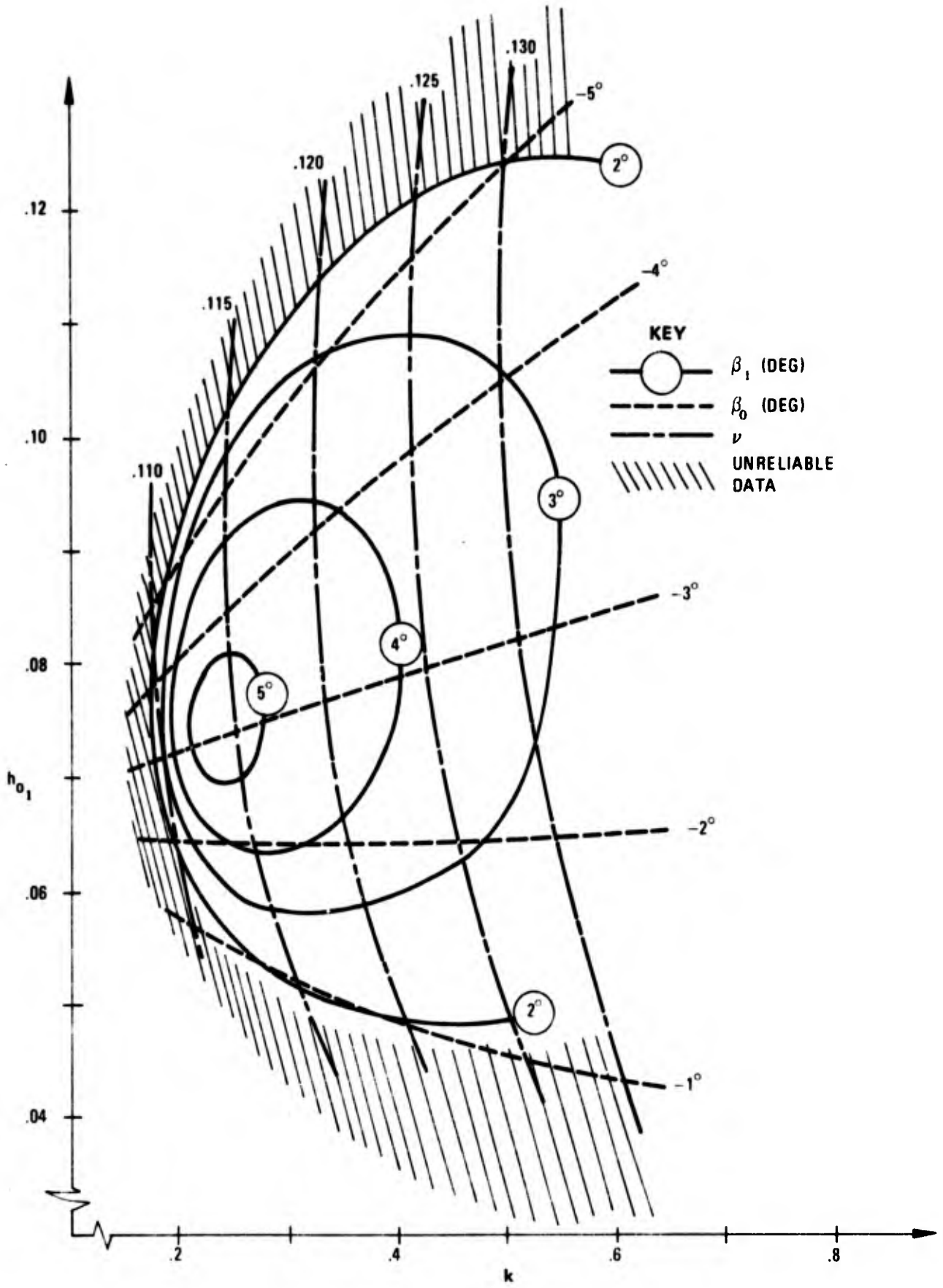

FIG. 8. **LIMIT-CYCLE PARAMETERS (ACTUAL COUPLING, INCLUDES DRY FRICTION)**

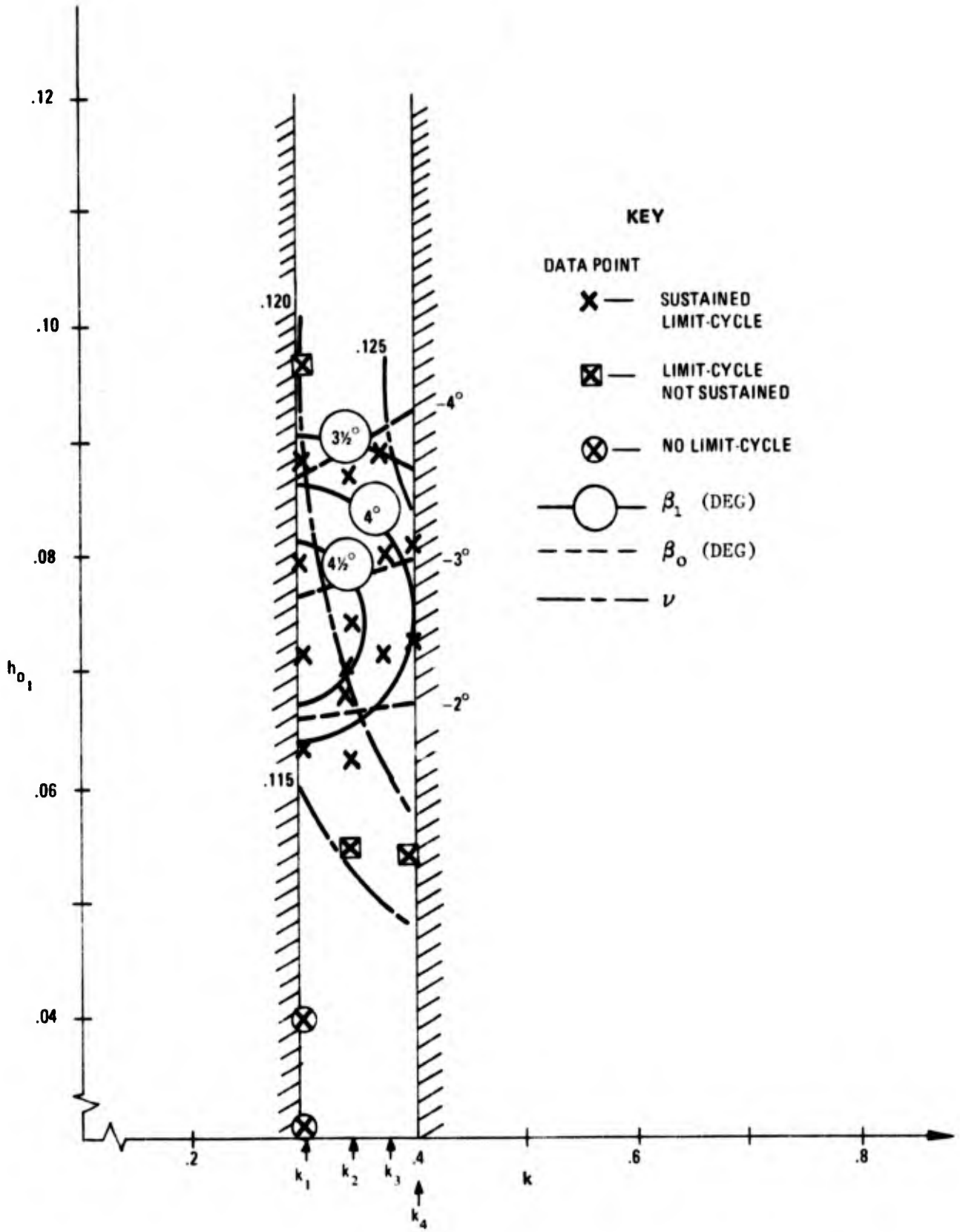

FIG. 9. **EXPERIMENTAL RESULTS LIMIT-CYCLE PARAMETERS**

The concept of relative stability of the limit-cycle oscillations is worthy of mention. Consider the function λ,

$$\lambda = f\{h_o, \Delta h, \nu\}$$

and its total derivative:

$$d\lambda = \frac{\partial \lambda}{\partial h_o} dh_o + \frac{\partial \lambda}{\partial \Delta h} d\Delta h + \frac{\partial \lambda}{\partial \nu} d\nu \qquad (19)$$

The value of $\frac{d\lambda}{d\Delta h}$ can be taken as a measure of the relative stability of sustained nonlinear oscillations. Also we can evaluate sensitivities; e.g.,

$$\frac{\partial \lambda}{\partial h_o} \; ; \; \frac{\partial \lambda}{\partial \Delta h} \quad \text{and} \quad \frac{\partial \lambda}{\partial \nu}$$

The relative stability can be investigated approximately by reference to equations (16) to (18) and Figures 3 and 5. From Figure 5 and equation (17) we have:

$$\frac{\partial \lambda}{\partial \Delta h} < 0 \quad \text{for} \quad .045 < h_o < .085$$

and

$$\frac{\partial \lambda}{\partial h_o} \text{ is } \begin{cases} > 0 \text{ for } h_o < .065 \\ < 0 \text{ for } h_o > .065 \end{cases}$$

also,

$$\frac{\partial \lambda}{\partial \nu} > 0$$

We also find from Figure 3, equation (16) and the relation $h_o = h_{o_1} + k\,\beta_o$:

$$\frac{\partial h_o}{\partial \Delta h} \text{ is } \begin{cases} < 0 \text{ for } h_o < .065 \\ > 0 \text{ for } h_o > .065 \end{cases}$$

and from equation (18) and Figure 5

$$\frac{\partial \nu}{\partial \Delta h} < 0 \quad \text{(approximately)}$$

Equation (19) is approximately:

$$\frac{d\lambda}{d\Delta h} \cong \left[\frac{\partial \lambda}{\partial h_o}\frac{\partial h_o}{\partial \Delta h} + \frac{\partial \lambda}{\partial \Delta h} + \frac{\partial \lambda}{\partial \nu}\frac{\partial \nu}{\partial \Delta h}\right] < 0$$

for $.045 < h_o < .085$. Thus, relative stability of the limit-cycle oscillations in Figures 7 and 8 is predicted. A more rigorous demonstration of stability will not be attempted here.

In conclusion, it has been shown via small perturbation analysis, that significant unsteady effects alter the steady-flow bubble growth relations. Of course, a complete solution of the problem must involve a matching of the bubble dynamics to those of the external, inviscid flow field. The significant dynamic effects, however, are shown to primarily involve the viscous bubble region. The unsteady mass flux and continuity relation applied to the bubble and the momentum relations that are assumed to prevail near reattachment yield a dynamic behavior that has the following characteristics:

1. Bubble length lags spoiler motion due to mass flux which is convected into the bubble near reattachment and which is assumed to travel upstream at a mean backflow velocity.

2. The pressure rise to reattachment, hence pressure in the dead-air region, is altered in the unsteady case in order to satisfy momentum relations.

3. The combined effect of 1 and 2 above results in dynamic bubble behavior that is in good qualitative and fair quantitative agreement with experimental observations.

4. Negative damping, for small amplitudes of oscillation, and subsequent limit-cycle behavior is predicted for the coupled system. This predicted behavior is confirmed by experimental observations.

The unsteady bubble model is expected to be valid when reattachment occurs on the flap surface. For larger bubbles, the model must be modified in order to account for mass flux from the shear layer on the flap lower surface. Further experimental and analytical work is needed in order to properly model large bubble dynamics. Also, the unsteady energy relation within the bubble needs to be better understood. It is probable that additional integral effects exist and they are expected to be highly dependent on the frequency of spoiler motion. Also, three-dimensional effects are not included. Theisen (Ref 20) is one among many who recognize that spanwise flow in the bubble can alter the dynamics of the separated region. The present model, however, contains two important dynamic effects which have not previously been modeled. This is thought to be the

most significant analytical result of the investigation, although some of the important assumptions must be regarded as somewhat speculative at present.

It will be shown that these methods may be applied to other similar problems in order to obtain useful results.

III. FURTHER ANALYSIS OF RELATED PROBLEMS

In the study of interactions between an oscillating body and a separating flow it is not always possible to consider the separating region as in the previous section. For a type of flow perturbation such as a spoiler, it is expected that in some important cases the perturbation may be considered overwhelming and consequent analysis may neglect, as a first approximation, the influence of the external flow field. In the case of a laminar separation bubble at the leading-edge of an airfoil, for example, it has been demonstrated (Ref. 29 and 30) that the external inviscid flow field may dominate the behavior of the separated region. It will be shown, however, that results of the previous section are useful.

1. Initiation of Dynamic Stall

As an airfoil pitches upward through its static stall angle it is known that an "overshoot" of this stall angle usually occurs. At a higher incidence "dynamic stall" is initiated with resulting forces and moments that differ in character and intensity from the steady flow stall case.[31,32] Similarly, on the downstroke, reattachment may be delayed; or in other words, the static reattachment angle is "undershot." Even if hysteresis in separation and reattachment did not exist in steady flow, the overshoot and undershoot phenomena result in apparent hysteresis in all cases of unsteady flow.

For an airfoil that is free to oscillate in pitch, the loading due to dynamic stall can lead to a self-excited oscillation that builds in amplitude until a limit-cycle is reached. Such a motion is termed "stall flutter" and is known to be applicable to helicopter rotor blades, engine compressor blades, space shuttle (and lifting body) configurations, certain V/STOL aircraft types, and to the study of aircraft response to severe gusts.

Motion of a control-surface can also initiate dynamic stall.[2,33] Furthermore, "stall flutter" of a flap-type control-surface has been observed on an airfoil at incidence.[34] This type of instability involved the single-degree-of-freedom of rotation of the flap about the hinge-line.

This section is concerned with the prediction of the overshoot and undershoot angles of dynamic stall and it deals with the type of dynamic stall that involves a leading-edge separation bubble. Pertinent elements of the flow field are modeled so that their interactions in unsteady flow can be studied. It is found that the resulting model for flow over an airfoil is useful for predicting when the leading-edge bubble bursts (hence initiating dynamic stall) and for studying the conditions necessary for flow to reattach. The following development is, in part, a summary of material contained in reference 22.

a. Flow Elements

When flow is attached to an airfoil that is oscillating about a moderate value of mean incidence, or for an airfoil at moderate incidence with an oscillating flap, the flow elements are taken to be:[7]

1. A potential flow field that acts over the surface of airfoil with mean properties that are related to the airfoil at its mean incidence.

2. The effects of airfoil or flap motion on the potential flow field to include the effect of vorticity which is shed into the wake.

3. A laminar boundary layer from the leading-edge stagnation point to the point of laminar separation on the upper surface.

4. A constant pressure laminar shear layer to the transition point.

5. The turbulent mixing and reattachment region.

6. The turbulent shear layer from the reattachment point to the trailing edge.

These elements are associated with a leading-edge separation bubble, and are only considered during the portion(s) of a cycle of motion when a bubble exists. The laminar separation and turbulent reattachment points define the fore and aft limits of the bubble which is shown schematically in Figure 10.

The effect of the turbulent shear layer aft of reattachment will be neglected in this section, thus precluding the influence of trailing-edge separation.

Airfoil or flap motion is prescribed. We consider two cases of forced motion, with reference to the diagram below.

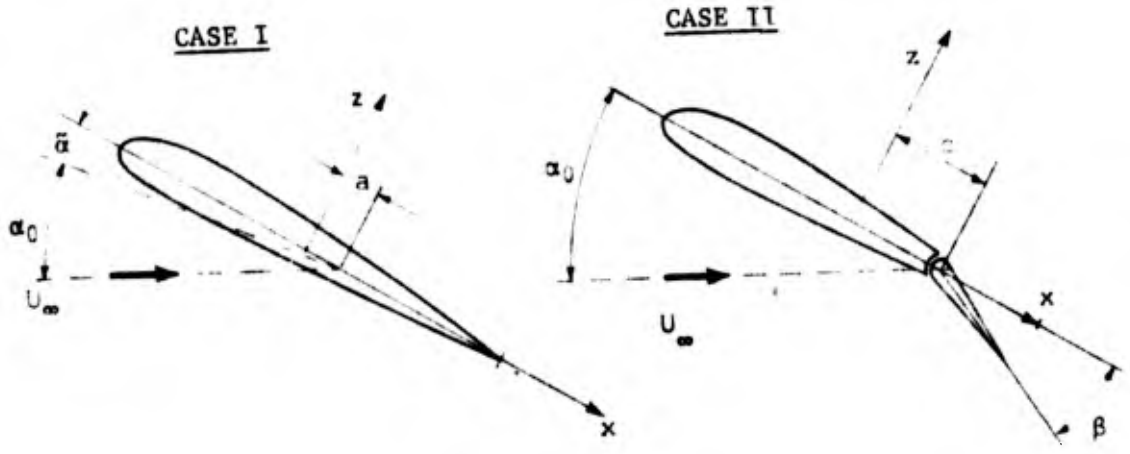

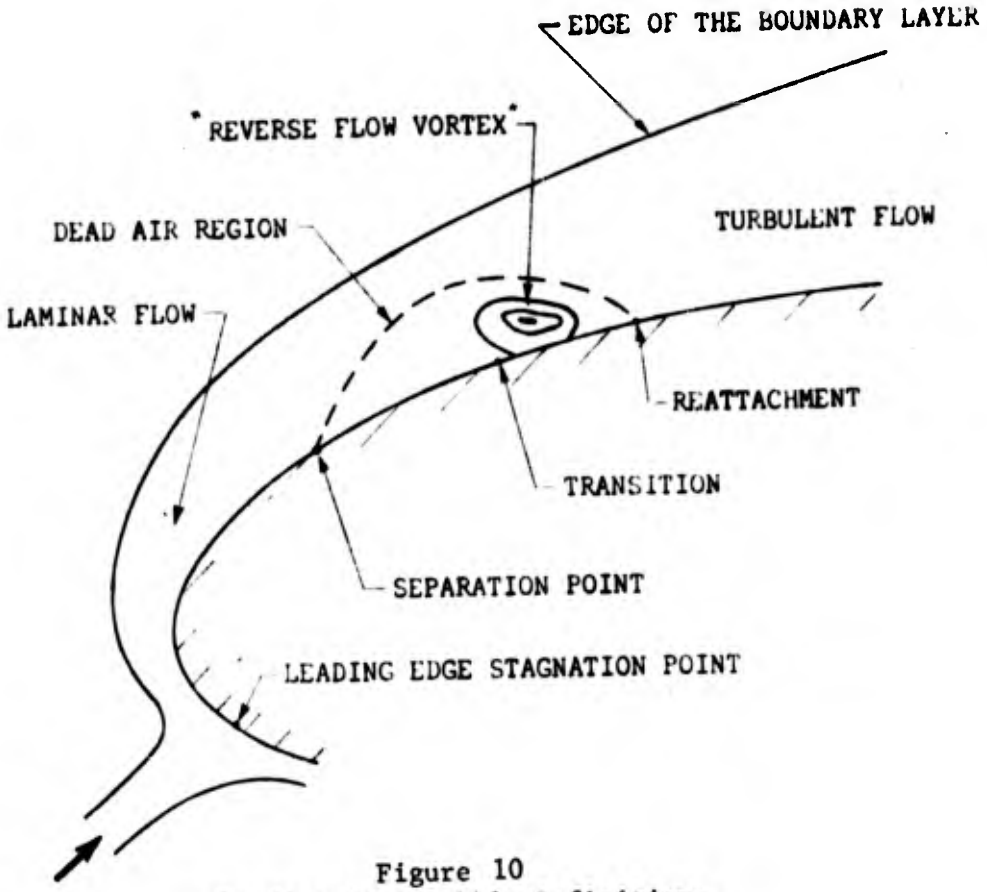

Figure 10
Leading-Edge Bubble Definitions

CASE I. The airfoil, at a mean incidence α_o, is forced to pitch about an axis x = a, with amplitude $\Delta\alpha$ such that

$$\alpha(t) = \alpha_o + \tilde{\alpha} = \alpha_o + \Delta\alpha \cos \omega t$$

where α_o, $\Delta\alpha$ and ω are constant prescribed values.

CASE II. The airfoil is fixed at an incidence α_o, and the flap is forced to oscillate with amplitude $\Delta\beta$. The flap is a plain flap with hinge-line at x = c.

$$\alpha = \alpha_o$$

$$\beta(t) = \Delta\beta \cos \omega t$$

We now define non-dimensional time and reduced frequency parameters.

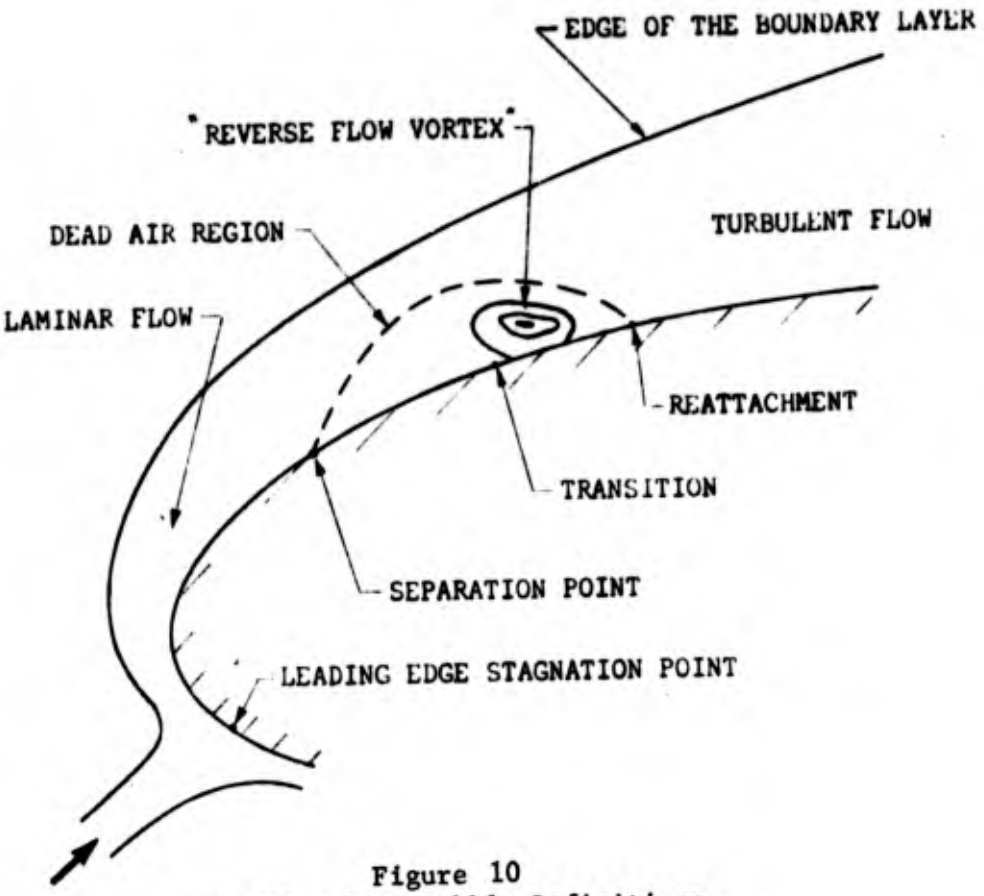

Figure 10
Leading-Edge Bubble Definitions

CASE I. The airfoil, at a mean incidence α_o, is forced to pitch about an axis x = a, with amplitude $\Delta\alpha$ such that

$$\alpha(t) = \alpha_o + \tilde{\alpha} = \alpha_o + \Delta\alpha \cos \omega t$$

where α_o, $\Delta\alpha$ and ω are constant prescribed values.

CASE II. The airfoil is fixed at an incidence α_o, and the flap is forced to oscillate with amplitude $\Delta\beta$. The flap is a plain flap with hinge-line at x = c.

$$\alpha = \alpha_o$$

$$\beta(t) = \Delta\beta \cos \omega t$$

We now define non-dimensional time and reduced frequency parameters.

CASE I

$$\tau_a \equiv \frac{U_\infty t}{b} \quad \text{and} \quad \nu_a \equiv \frac{\omega b}{U_\infty}$$

also

$$\alpha' \equiv \frac{d\alpha}{d\tau_a} = \left(\frac{b}{U_\infty}\right) \dot{\alpha} \quad \text{and} \quad \alpha'' = \left(\frac{b}{U_\infty}\right)^2 \ddot{\alpha}$$

where b is airfoil semi-chord.

CASE II

$$\tau \equiv \frac{U_\infty t}{c_f} \quad \text{and} \quad \nu \equiv \frac{\omega c_f}{U_\infty}$$

so that

$$\beta' \equiv \frac{d\beta}{d\tau} = \left(\frac{c_f}{U_\infty}\right) \frac{d\beta}{dt}, \text{ etc.}$$

also we have

$$\frac{c_f}{b} = (1 - c)$$

so that

$$\nu = (1 - c)\, \nu_a$$

Also, we have a non-dimensional chordwise distance x based on b with origin at mid-chord:

$$x \equiv \frac{X}{b} - 1$$

Pressures and velocities at the edge of the boundary and shear layers are found by considering an appropriate potential flow model. The model used here involves a non-linear pressure-velocity relation and considers the instantaneous value of velocity to be a superposition of a mean, steady flow value and a time varying perturbation. McCroskey (Ref. 30) recently and independently considered a similar inviscid flow field.

We consider the non-linear Bernoulli equation for unsteady flow.

$$C_p \equiv \frac{P - P_\infty}{\frac{1}{2}\rho U_\infty^2} = 1 - \left(\frac{U}{U_\infty}\right)^2 - \frac{2}{U_\infty^2} \frac{\partial \phi}{\partial t} \qquad (20)$$

with U, the velocity evaluated at the airfoil surface from the potential flow solution, assumed equal to the velocity at the edge of the boundary layer in attached flow.

Now

$$\frac{U}{U_\infty} = \frac{U_o}{U_\infty} + \frac{\tilde{u}}{U_\infty} \quad ; \quad \phi = \phi_o + \tilde{\phi} \tag{21}$$

and

$$\frac{\partial \phi}{\partial t} = \frac{\partial \tilde{\phi}}{\partial t}$$

U_o/U_∞ will be found from the NACA method and $\tilde{u}/U_\infty$ will be found from "classical" unsteady thin airfoil theory.

The unsteady thin airfoil results are found to contain the usual singular terms with corresponding infinite velocities at the leading edge and flap hinge-line. Since the leading edge region is critical in this analysis we chose to correct the unsteady results by employing Lighthill's correction factor, which is applicable to the thin airfoil approximation. The factor makes the first order thin airfoil solution valid over the entire airfoil surface. (See reference 22.)

Thus, in equation (21) where U_o/U_∞ is known from the NACA method, we find $\tilde{u}/U_\infty$ from:

$$\frac{\tilde{u}}{U_\infty}(x,t) = \left(\frac{1+x}{1+x+\rho_N}\right)^{\frac{1}{2}} \left(\frac{\tilde{u}}{U_\infty}\right)_{th} \tag{22}$$

where

$$\left(\frac{\tilde{u}}{U_\infty}\right)_{th}$$

is the thin airfoil result and the correction factor;

$$\left(\frac{1+x}{1+x+\rho_N}\right)^{\frac{1}{2}}$$

due to Lighthill includes the parameter ρ_N which is the non-dimensional leading-edge radius based on chord length, i.e.,

$$\rho_N = .0158$$

for a NACA 0012 profile.

$(\frac{\tilde{u}}{u_\infty})_{th}$ is found, as explained in reference 22, from the relation:

$$(\frac{\tilde{u}}{U_\infty})_{th} = -\frac{1}{2}\left(\tilde{C}_{p_u} + \frac{2}{U_\infty^2}\frac{\partial \tilde{\phi}}{\partial t}\right) \tag{23}$$

where

$$\tilde{C}_{p_u} = \begin{cases} C_{p_\alpha}\tilde{\alpha} + C_{p_{\dot\alpha}}\tilde{\alpha}' + C_{p_{\ddot\alpha}}\tilde{\alpha}' + C_{p_{\Gamma(\alpha)}} & \text{CASE I} \\ C_{p_\beta}\beta + C_{p_{\dot\beta}}\beta' + C_{p_{\ddot\beta}}\beta'' + C_{p_{\Gamma(\beta)}} & \text{CASE II} \end{cases}$$

The non-dimensional derivatives are for Case I:

$$C_{p_\alpha} = 0$$

$$C_{p_{\dot\alpha}} = -\left[(1 + 2x)\sqrt{\frac{1 - x}{1 + x}} + 2\sqrt{1 - x^2}\right]$$

$$C_{p_{\ddot\alpha}} = (2a - x)\sqrt{1 - x^2}$$

and for Case II:

$$C_{p_\beta} = \frac{2}{\pi}\left[\ell n|N| + \sqrt{1 - c^2}\sqrt{\frac{1 - x}{1 + x}}\right]$$

$$C_{p_{\dot\beta}} = \frac{-2}{\pi(1 - c)}\left\{\cos^{-1} c\sqrt{1 - x^2} - 2(x - c)\ell n|N| + \frac{1}{2}\left[\cos^{-1} c\,(1 + 2x) + c\sqrt{1 - c^2}\right]\sqrt{\frac{1 - x}{1 + x}}\right\}$$

$$C_{p_{\ddot\beta}} = \frac{-1}{\pi(1 - c)^2}\left\{\left[\sqrt{1 - c^2} + (x - 2c)\cos^{-1} c\right]\sqrt{1 - x^2} - (x - c)^2\,\ell n|N|\right\}$$

where

$$N = \frac{(1 - cx - \sqrt{1 - c^2}\sqrt{1 - x^2})}{(x - c)}$$

The above derivatives are valid for attached flow and general motion, but with the Kutta condition satisfied.

$(\frac{\tilde{u}}{u_\infty})_{th}$ is found, as explained in reference 22, from the relation:

$$(\frac{\tilde{u}}{U_\infty})_{th} = -\frac{1}{2}\left(\tilde{C}_{p_u} + \frac{2}{U_\infty^2}\frac{\partial \tilde{\phi}}{\partial t}\right) \tag{23}$$

where

$$\tilde{C}_{p_u} = \begin{cases} C_{p_\alpha}\tilde{\alpha} + C_{p_{\dot{\alpha}}}\tilde{\alpha}' + C_{p_{\ddot{\alpha}}}\tilde{\alpha}' + C_{p_{\Gamma_{(\alpha)}}} & \text{CASE I} \\ C_{p_\beta}\beta + C_{p_{\dot{\beta}}}\beta' + C_{p_{\ddot{\beta}}}\beta'' + C_{p_{\Gamma_{(\beta)}}} & \text{CASE II} \end{cases}$$

The non-dimensional derivatives are for Case I:

$$C_{p_\alpha} = 0$$

$$C_{p_{\dot{\alpha}}} = -\left[(1 + 2x)\sqrt{\frac{1 - x}{1 + x}} + 2\sqrt{1 - x^2}\right]$$

$$C_{p_{\ddot{\alpha}}} = (2a - x)\sqrt{1 - x^2}$$

and for Case II:

$$C_{p_\beta} = \frac{2}{\pi}\left[\ell n|N| + \sqrt{1 - c^2}\sqrt{\frac{1 - x}{1 + x}}\right]$$

$$C_{p_{\dot{\beta}}} = \frac{-2}{\pi(1 - c)}\left\{\cos^{-1} c\sqrt{1 - x^2} - 2(x - c)\ell n|N| + \frac{1}{2}\left[\cos^{-1} c\,(1 + 2x) + c\sqrt{1 - c^2}\right]\sqrt{\frac{1 - x}{1 + x}}\right\}$$

$$C_{p_{\ddot{\beta}}} = \frac{-1}{\pi(1 - c)^2}\left\{\left[\sqrt{1 - c^2} + (x - 2c)\cos^{-1} c\right]\sqrt{1 - x^2} - (x - c)^2\ell n|N|\right\}$$

where

$$N = \frac{(1 - cx - \sqrt{1 - c^2}\sqrt{1 - x^2})}{(x - c)}$$

The above derivatives are valid for attached flow and general motion, but with the Kutta condition satisfied.

The perturbation quantities $C_{p_{\Gamma_{(\alpha)}}}$ and $C_{p_{\Gamma_{(\beta)}}}$ are sensitive to the distribution of shed vorticity in the wake, and we have the approximations:

$$C_{p_{\Gamma_{(\alpha)}}} = -\frac{2}{U_\infty} C \cdot Q_{(\alpha)} \quad \text{and} \quad C_{p_{\Gamma_{(\beta)}}} = -\frac{2}{U_\infty} C \cdot Q_{(\beta)}$$

where

$C \cong C(\nu_a)$; the Theodorsen Function

and Q is found from the Kutta condition to be:

$$Q \equiv \frac{1}{2\pi} \int_1^\infty \frac{x_o + 1}{\sqrt{x_o^2 - 1}} \gamma(x_o, t)\, dx_o$$

$$= \begin{cases} U_\infty \left[\tilde{\alpha} + \left(\frac{1}{2} - a\right) \tilde{\alpha}'\right] & \text{CASE I} \\ \frac{U_\infty}{\pi} \left[T_{10}\beta + \frac{T_{11}}{2(1 - c)} \beta'\right] & \text{CASE II} \end{cases}$$

where

$$T_{10} = \sqrt{1 - c^2} + \cos^{-1} c$$

$$T_{11} = \cos^{-1} c\,(1 - 2c) + \sqrt{1 - c^2}\,(2 - c)$$

It can be seen that dynamic effects modify the magnitude and phase relation of pressures due to circulation. The relation:

$$M = M_o e^{-i\psi} \equiv \frac{C_{p_{\Gamma_{unsteady}}}}{C_{p_{\Gamma_{steady}}}}$$

is plotted in Figure 11 and shows the dependence of circulation effects on frequency and pitch-axis location. A combination of high frequency and aft location of the pitch axis contributes to reduced circulation effects that lag airfoil or flap motion. At low frequencies, pitch axis location is of lesser importance. This "circulation lag" effect due to shed vorticity has been referred to by Ericsson and Reding[35] as a significant factor in stall overshoot. Flap effects are given by the dashed curves.

Figures 12 and 13 indicate the chordwise distribution of the components of pressure coefficient. Note that the "apparent

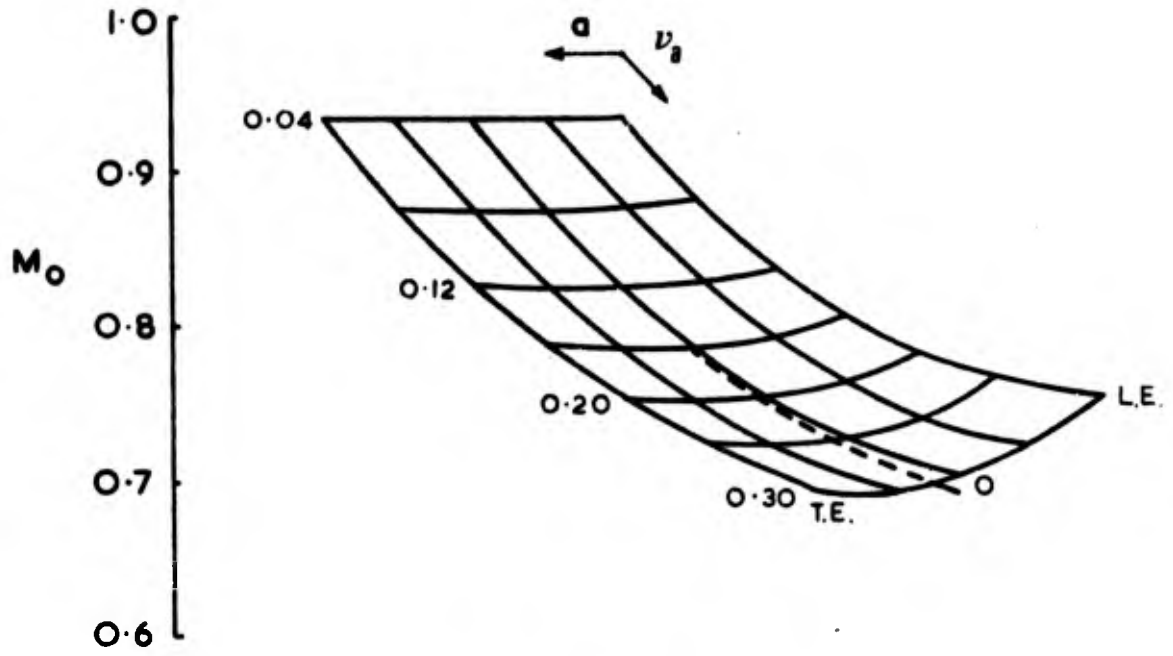

$$M_o e^{-i\psi} = \frac{C_{p_\Gamma \text{ UNSTEADY}}}{C_{p_\Gamma \text{ STEADY}}}$$

——— AIRFOIL MOTION
- - - - FLAP MOTION

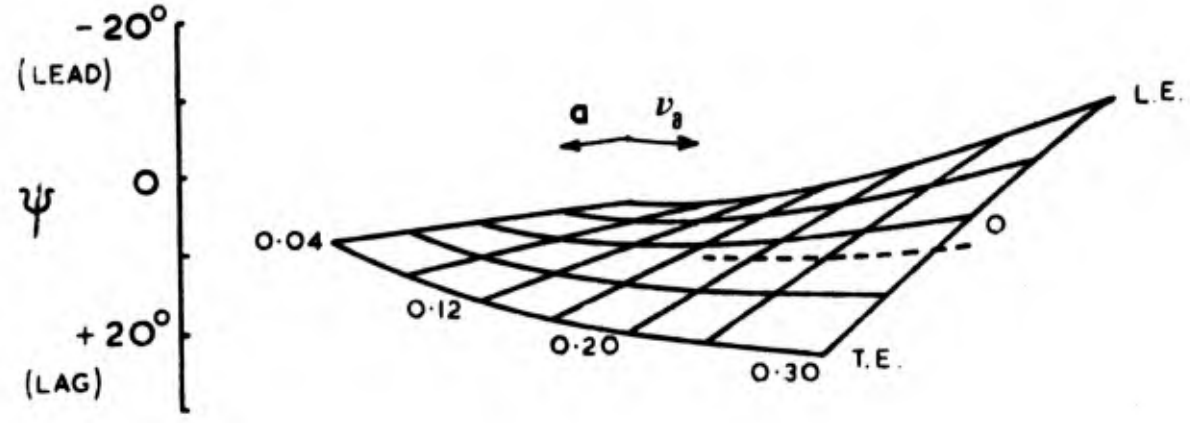

FIG. 11. EFFECT OF PITCH AXIS AND FREQUENCY ON CIRCULATION.

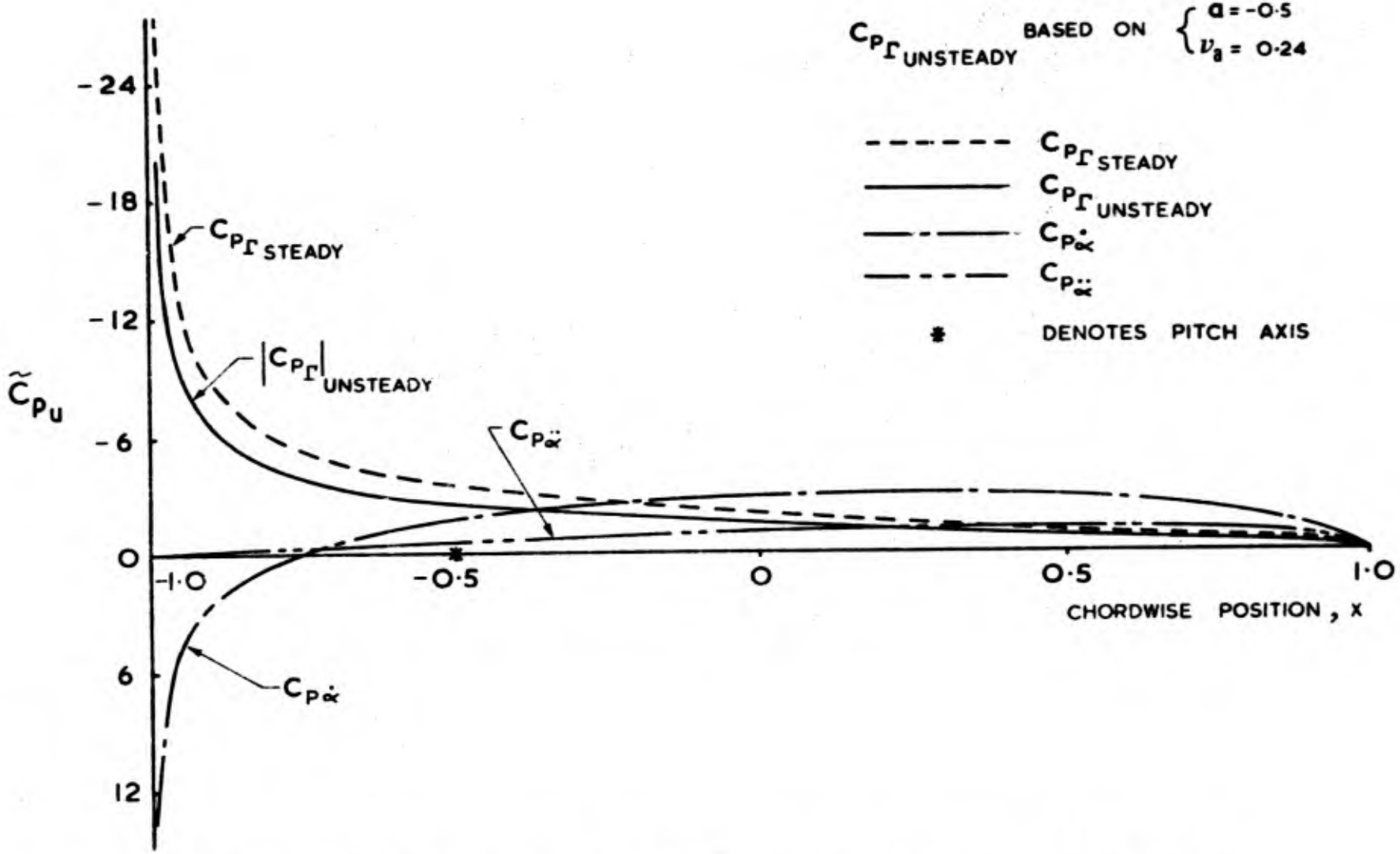

FIG. 12. COMPONENT PARTS OF $\tilde{C}_{P_U}$ DUE TO AIRFOIL MOTION.

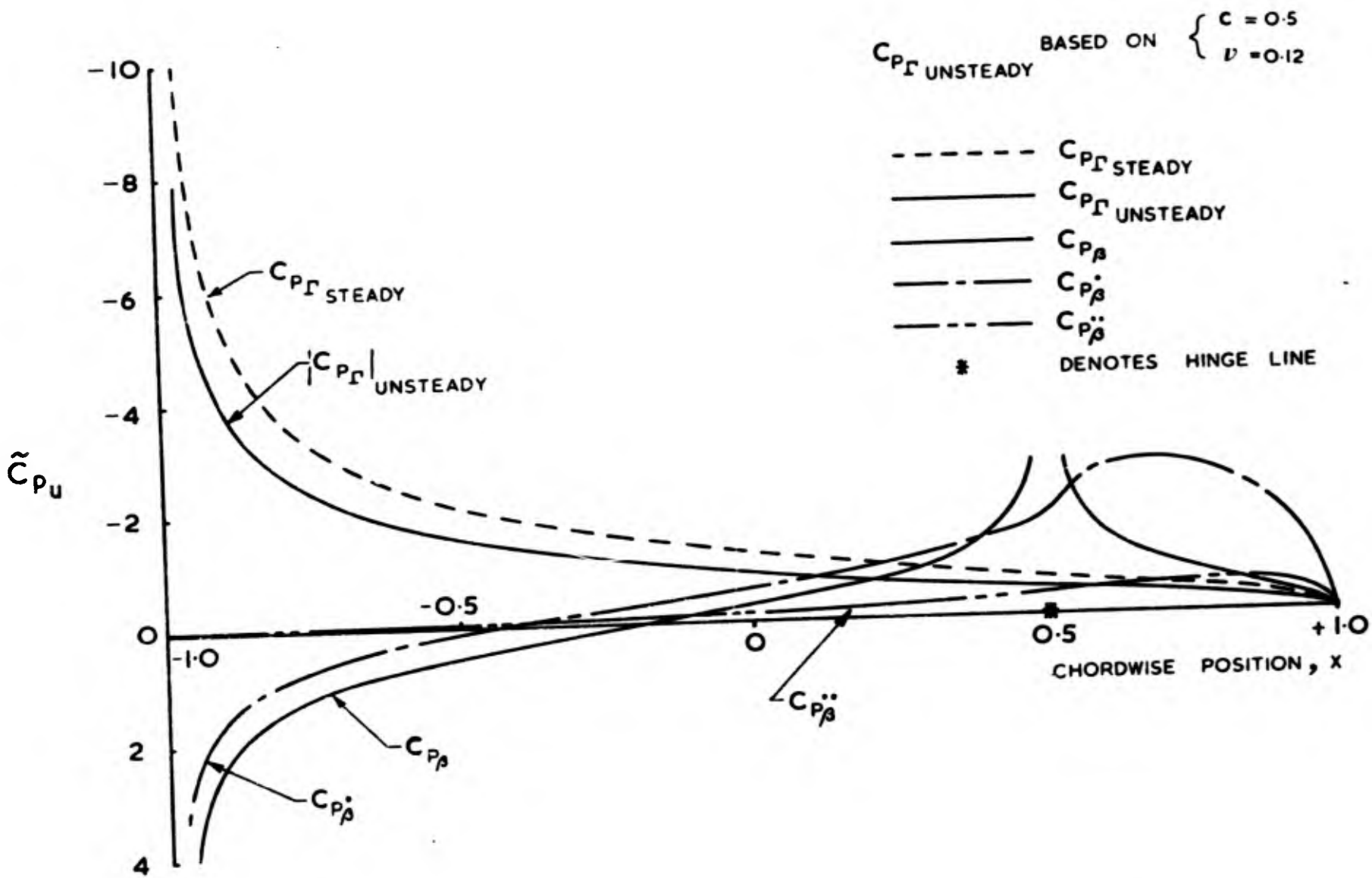

FIG. 13. COMPONENT PARTS OF $\tilde{C}_{Pu}$ DUE TO FLAP MOTION.

mass" terms $C_{p\ddot{\alpha}}$ and $C_{p\ddot{\beta}}$ are small. Their overall contributions ($C_{p\ddot{\alpha}}\,\tilde{\alpha}''$ and $C_{p\ddot{\beta}}\,\beta''$) are usually small except for high frequencies. The $C_{p\ddot{\alpha}}$ term is highly dependent upon pitch axis location. The damping terms $C_{p\dot{\alpha}}\,\tilde{\alpha}'$ and $C_{p\dot{\beta}}\,\beta'$ are definitely significant, especially near the leading edge. The curves of Figures 12 and 13 do not include the influence of the correction factor due to Lighthill (equation 22) which is significant near the leading edge. The correction factor, however, would not cause a noticeable modification to the curves due to the scale of the x axis. The circulation dependent components, $C_{p\Gamma}$, in the figures are based on unit values of $\tilde{\alpha}$ and β, and are dependent on frequency and pitch axis location.

The combined effect of pressure components is shown in Figures 14 and 15. In Figure 14 we see a comparison between steady flow and unsteady flow perturbations. The motion involved is represented by:

$$\tilde{\alpha} = 5^{\circ} \cos\,(0.16\,\tau_a)$$

and the five pictures represent the instantaneous pressure distributions at time intervals that are equally spaced on the airfoil upstroke (i.e., $\dot{\alpha} > 0$). This type of representation (again excluding Lighthill's leading-edge correction) has been offered by Carta[29] as indicative of the important role unsteady flow effects play in dynamic stall. This additional, unsteady distribution involves favorable pressure gradients along the entire airfoil chord as the airfoil pitches upward past $\tilde{\alpha} = 0$. This effect helps not only in a delay of bubble bursting, but in a "suppression" of trailing-edge stall as well. See reference 22 for more details on this.

Figure 15 involves motion of the form:

$$\beta = 5.73^{\circ} \cos\,(0.12\tau)$$

and indicates trends, near the leading-edge especially, that are qualitatively similar to those for airfoil pitching.

Let us now solve for the unsteady velocity perturbations. We may represent the last term in equation (23) as:

$$\frac{2}{U_\infty^2}\,\frac{\partial \tilde{\phi}}{\partial t} = \frac{2}{U_\infty^2}\left[\frac{\partial \tilde{\phi}_\epsilon}{\partial t} + \frac{\partial \tilde{\phi}_\Gamma}{\partial t}\right]$$

where:

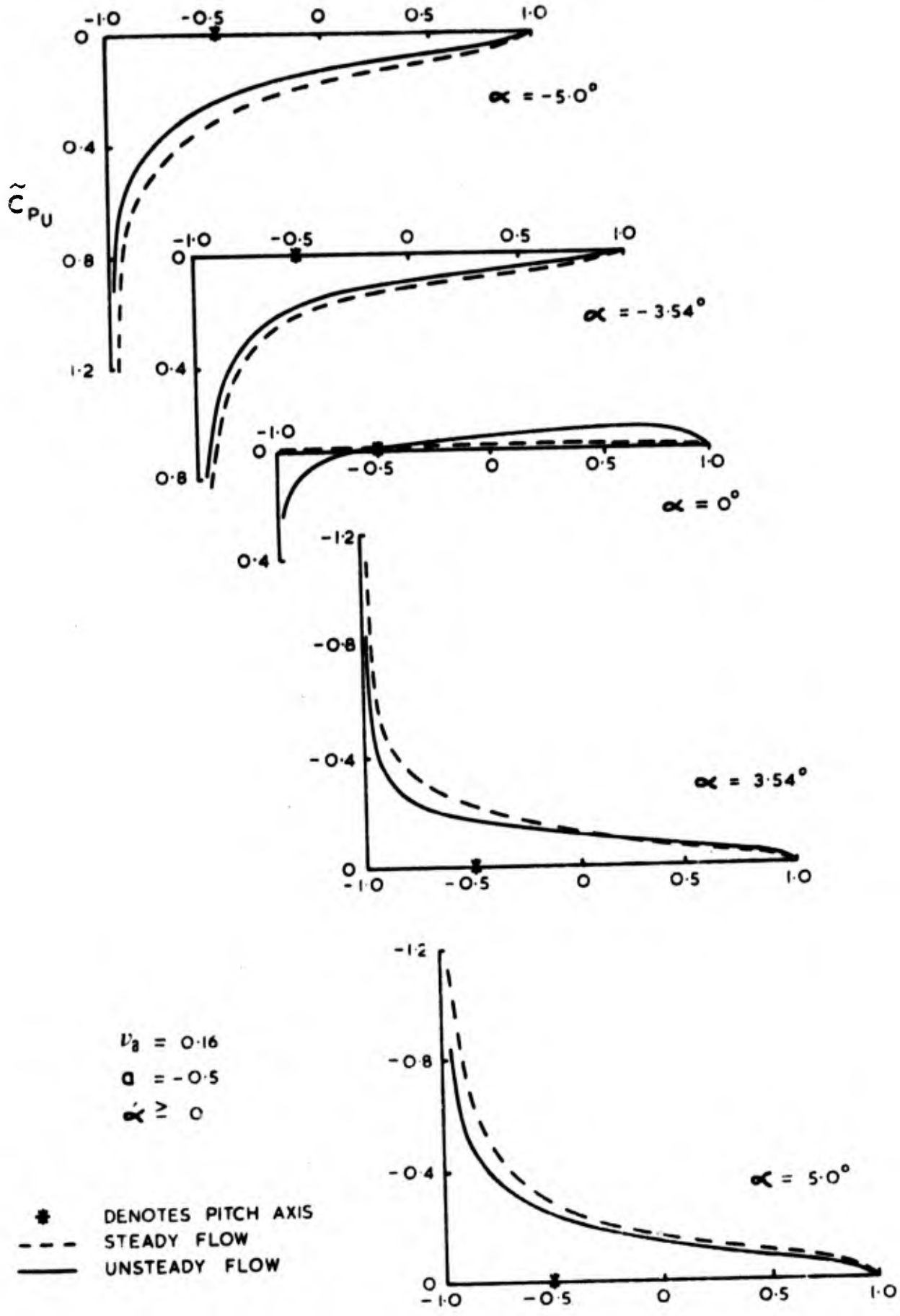

FIG. 14. INSTANTANEOUS PRESSURE DISTRIBUTION DUE TO AIRFOIL MOTION.

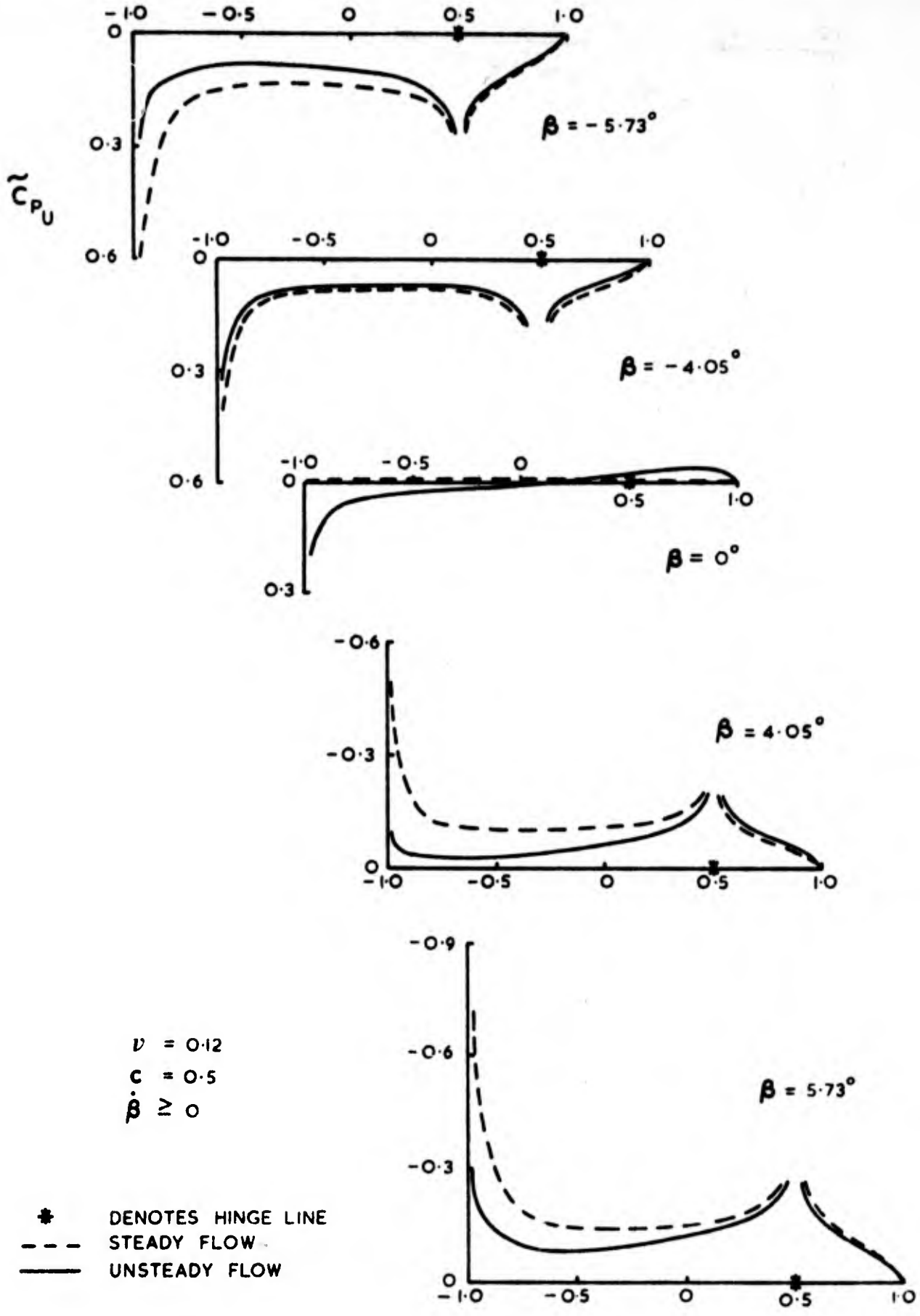

FIG. 15. INSTANTANEOUS PRESSURE DISTRIBUTION DUE TO FLAP MOTION.

$$\frac{2}{U_\infty}\frac{\partial \tilde{\phi}_\epsilon}{\partial t} = \begin{cases} 2\sqrt{1-x^2}\,\tilde{\zeta}' + (x-2a)\sqrt{1-x^2}\,\tilde{\alpha}' & \text{CASE I} \\ \frac{2}{\pi(1-c)}\left[\cos^{-1} c\sqrt{1-x^2} - (x-c)\,\ell n|N|\right]\beta' & \\ + \frac{1}{\pi(1-c)^2}\left[\sqrt{1-c^2}\sqrt{1-x^2} + \cos^{-1} c\cdot\right. & \\ \left.(x-2c)\sqrt{1-x^2} - (x-c)^2\,\ell n|N|\right]\beta'' & \text{CASE II} \end{cases}$$

and

$$\frac{2}{U_\infty^2}\frac{\partial \tilde{\phi}_\Gamma}{\partial t} = -\frac{4}{\pi U_\infty}\sqrt{1-x^2}\,\frac{I(\nu_a,x)}{\left[H_1^{(2)}(\nu_a) + i\,H_0^{(2)}(\nu_a)\right]}\cdot Q$$

where

$$I(\nu_a,x) \equiv \int_1^\infty \frac{e^{-i\nu_a x_o}\,dx_o}{\sqrt{x_o^2-1}\,(x_o - x)}$$

and I is evaluated numerically.

In Figures 16 and 17 we see the difference in the unsteady quantities:

$$\tilde{C}_{p_u} \quad \text{and} \quad -2\frac{\tilde{u}}{U_\infty}$$

It is apparent that for either airfoil or flap motion, these two quantities differ in magnitude and phase by very small amounts near the leading edge. The largest magnitude discrepancy occurs near mid-chord and the largest phase difference occurs at the trailing-edge. In all cases, as one would expect, the velocity perturbations $-\tilde{u}/U_\infty$ lag the pressure perturbations $\tilde{C}_{p_u}$. These magnitude and phase relations are very much frequency and pitch axis location dependent, and the curves of Figures 16 and 17 must be treated as such.

The laminar boundary layer, separation point and shear layer are approximately accounted for by the quasi-steady assumption that they react instantaneously to changes in the outer flow. This assumption has been justified for example in references 22 and 30. Figure 18 will serve to define some parameters in the assumed bubble model.

The laminar separation point is found by use of an empirical result found by Owen and Klanfer, Gault and Györgyfalvy,[6] that is,

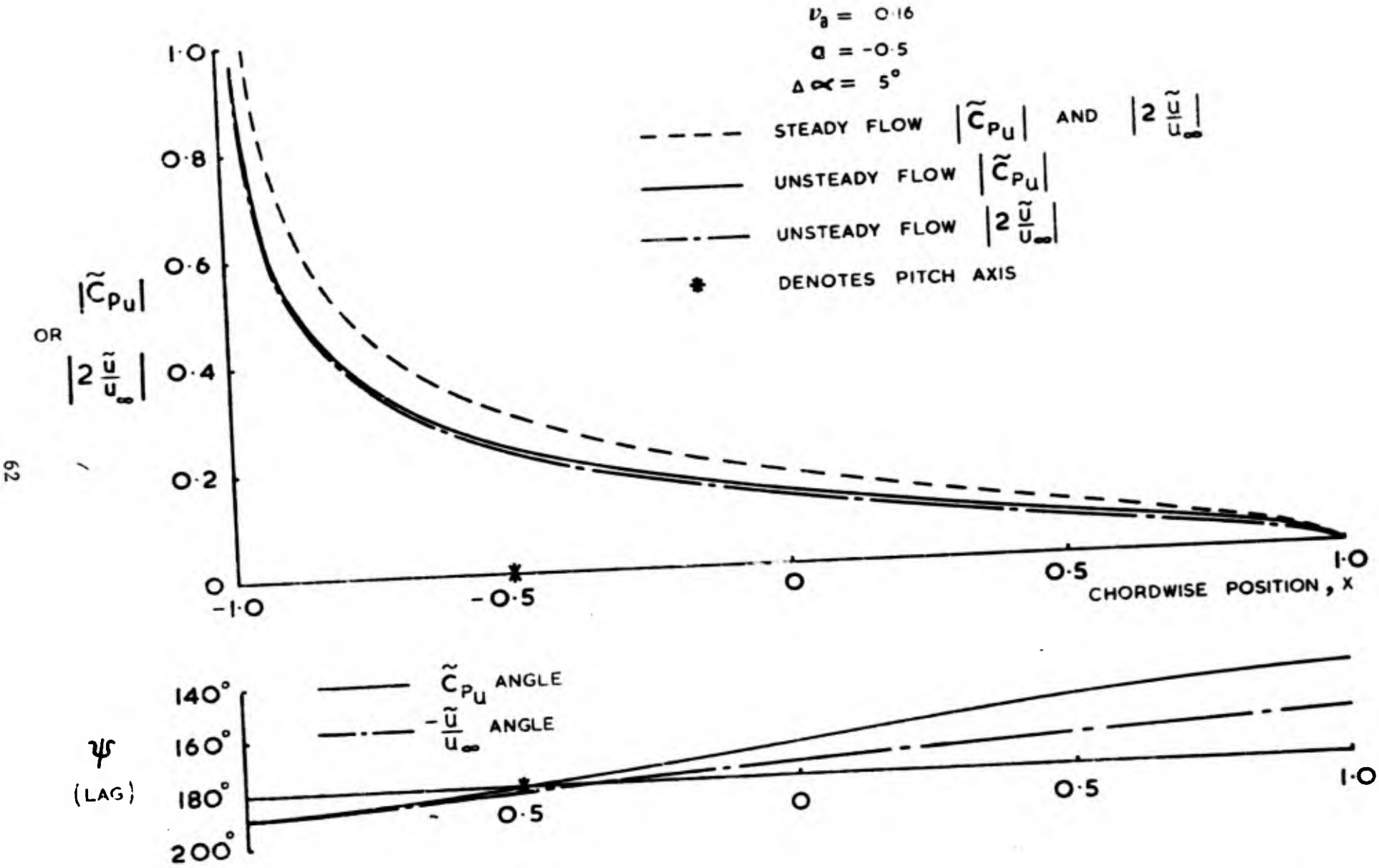

FIG. 16. MAGNITUDE AND PHASE OF $\tilde{C}_{Pu}$ AND $\frac{\tilde{u}}{u_\infty}$ FOR AIRFOIL MOTION.

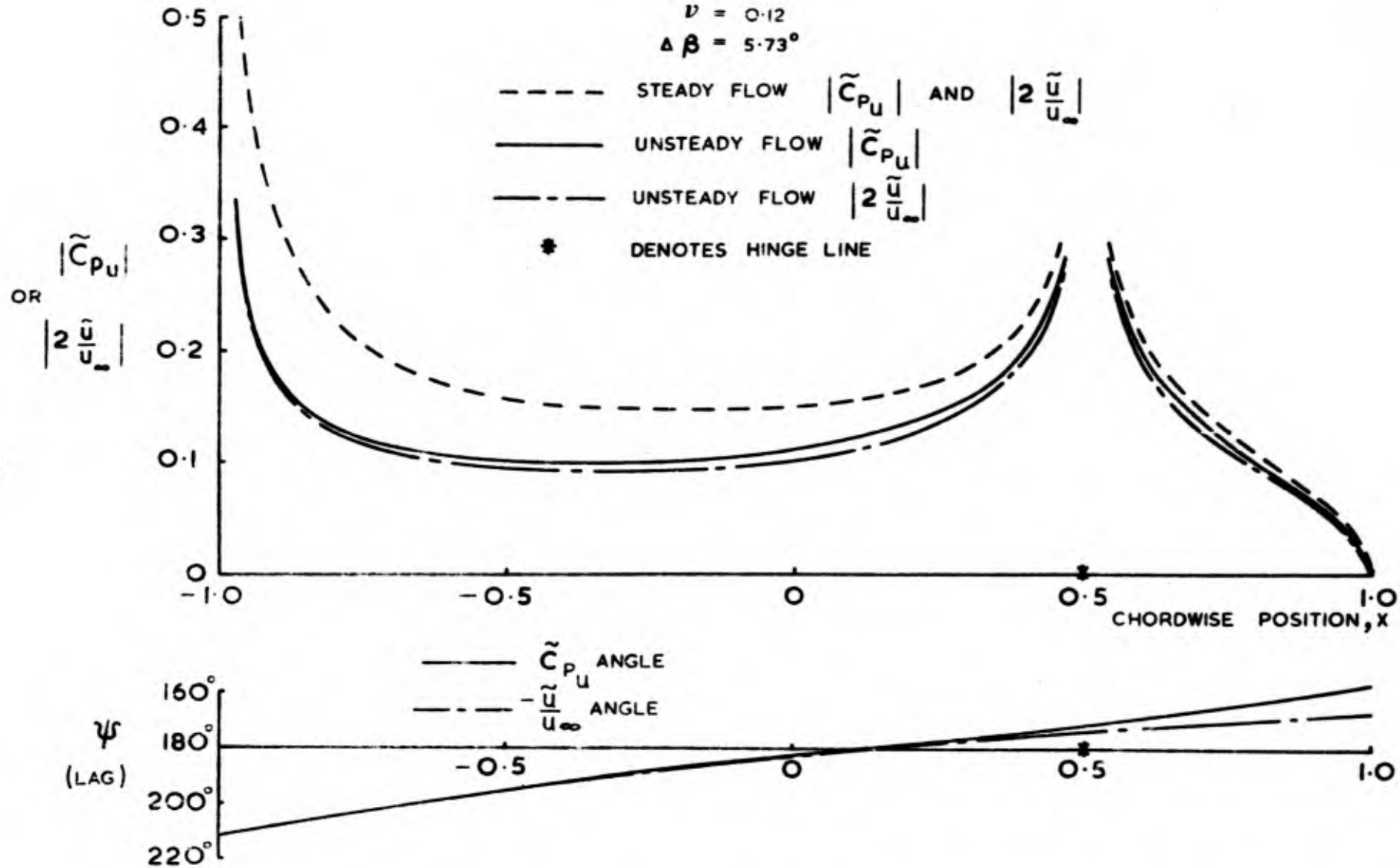

FIG. 17. MAGNITUDE AND PHASE OF $\tilde{C}_{p_u}$ AND $\frac{\tilde{u}}{u_\infty}$ FOR FLAP MOTION.

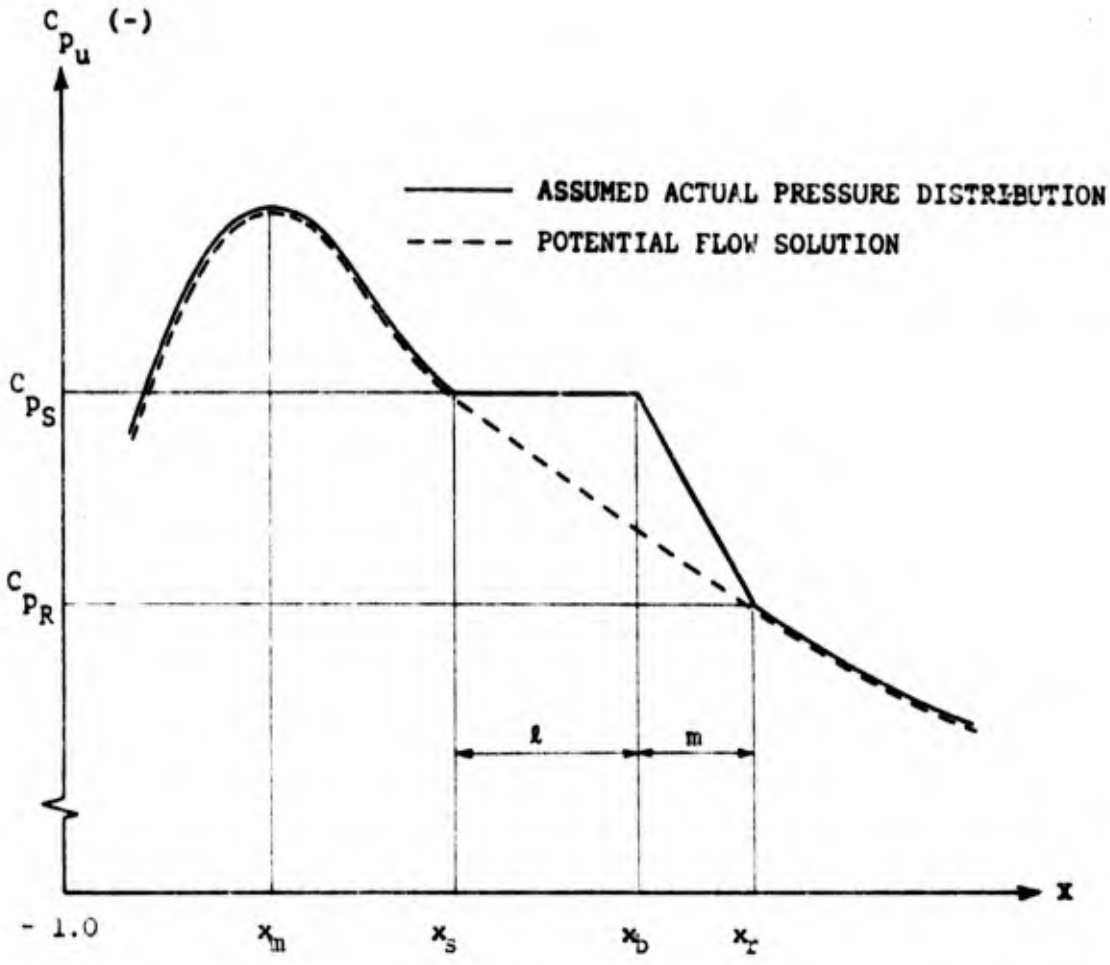

Figure 18
Leading-Edge Bubble Parameters

$$\frac{U_s}{U_\infty} \cong .95 \frac{U_m}{U_\infty}$$

where U_s/U_∞ and U_m/U_∞ are velocity ratios at separation and the point of maximum velocity.

If we consider the mean steady flow then from the NACA method:

$$\frac{U_o}{U_\infty} = \frac{U_1}{U_\infty} + \frac{U_2}{U_\infty} C_{L_\alpha} \cdot \alpha_o$$

$$= \frac{U_1}{U_\infty}(x) + \frac{U_2}{U_\infty}(x)\, C_{L_\alpha} \cdot \alpha_o$$

and we find

$$\frac{U_m}{U_\infty} = \left(\frac{U_o}{U_\infty}\right)_{max}$$

from:

$$\frac{\partial \left(\frac{U_1}{U_\infty}\right)}{\partial x} + \frac{\partial \left(\frac{U_2}{U_\infty}\right)}{\partial x} C_{L_\alpha} \cdot \alpha_o = 0$$

which yields the magnitude and location of

$$\left(\frac{U_o}{U_\infty}\right)_{max}$$

as a function of α_o.

From the above relations we find the predicted separation point.

Velocity perturbations are accounted for by considering the following:

$$x_s = x_{so} + \Delta x_s = x_{so} + \frac{\partial x_s}{\partial \left(\frac{U}{U_\infty}\right)} \cdot \frac{\tilde{u}}{U_\infty}$$

where x_{so} is the predicted steady flow value of x_s, the laminar separation point. Although

$$\left|\frac{\Delta x_s}{x_{so}}\right| \ll 1$$

this perturbation quantity is found to yield a significant effect.

The quantity $\partial x_s / \partial (U/U_\infty)$ is evaluated for $x_s = x_{so}$; $\tilde{u}/U_\infty = 0$, as discussed in reference 22.

The relation which is used to determine the instantaneous location of the laminar separation point is then:

$$x_s(t) = x_{so}(\alpha_o) + \left[\frac{\partial x_s}{\partial \left(\frac{U}{U_\infty}\right)}\right]_{\substack{\alpha = \alpha_o \\ x_s = x_{so}}} \cdot \frac{\tilde{u}}{U_\infty}(t)$$

On Figure 18 the locations x_m and x_s refer to maximum velocity and separation points. x_r is the point of turbulent reattachment. Distance ℓ defines the laminar shear layer length and m defines the turbulent mixing and reattachment region. Note that transition and the beginning of reattachment are taken to coincide at a point (x_b). Also note that at separation and reattachment, pressures (and velocities) are assumed equal to their potential flow values at the same point. These assumptions have been shown to be reasonably accurate.

Now we are interested in finding the lengths ℓ and m so that we can determine the pressure (or velocity) rise across the assumed bubble.

At present no analytical solution or numerical method is found to be adequate in predicting the length ℓ. Even with knowledge of the laminar boundary layer parameters at separation, free-stream turbulence level, surface roughness and Reynolds No., there is no known method that allows for a determination of transition point in a laminar shear layer that is also influenced by unsteady pressures, velocities and surface curvature.

We, therefore, choose to fall back on an empirical model that is due to Von Doenhoff.[6] The Von Doenhoff model is:

$$R_{e_{x_b}} \equiv \frac{\rho U_s (x_b - x_s) b}{\mu} = \frac{\rho U_s \ell b}{\mu} \cong 5 \times 10^4$$

where U_s is the velocity at the edge of the boundary layer at the separation point, x_s. Therefore, we have:

$$\ell(t) \cong \frac{5 \times 10^4 \mu}{U_s(t)\, b\, \rho}$$

It is shown in reference 22 that an appropriate quasi-steady flow model for the turbulent mixing and reattachment region is:

$$m(t) \cong \frac{k_1 \mu}{U_s(t)\, b\, \rho}$$

where k_1 is a function of $R_{e_{\delta_s^*}}$; that is, the Reynolds number based on shear-layer displacement thickness at separation.

Based on experimental results, the relations above are combined and a constant added so that we have approximately:

$$\ell(t) + m(t) = \frac{k_2}{U_s(t)} + k_3$$

Thus, the bubble length parameters can be found for quasi-steady bubble growth. Since the potential flow solution is known for all time, the pressures and velocities at separation and reattachment can also be found.

An example of steady flow predictions for the location of separation, transition and reattachment points is shown in Figure 19 for the NACA 0012 airfoil. Parameter values are found in reference 22.

The separation point results for the NACA 0012 are in good agreement with values that were interpolated from NACA 0010 (mod) and NACA 66_3 - 018 experimental measurements for R_{e_c} = 2 x 10^6 which were taken from reference 36. Results for bubble length at $\alpha = 14^o$ which are found in reference 37 are in very good agreement with present results; however, data from reference 36 indicates that the laminar shear layer length of the model is consistently overestimated by about 0.75% of chord, and the turbulent region length is overestimated by about 0.5% chord. The rates of movement of these points as incidence is varied are found to be in good agreement with experiment. It must be noted, however, that the present model provides solutions at incidence above the static stall so the high incidence values found in Figure 19 should not be taken to imply that bubble bursting is not achieved. In the case of the NACA 0012 (for $R_{e_c} = 2 \times 10^6$) it appears that static stall is achieved when the leading-edge bubble bursts at an incidence of around 13^o-16^o.

The pressure recovery coefficient, σ, or Crabtree's parameter can be evaluated also. It is defined:

$$\sigma \equiv \frac{C_{p_r} - C_{p_s}}{1 - C_{p_s}}$$

It has been evaluated in steady-flow for the NACA 0012 and results are plotted in Figures 20 and 21.

Figure 20 involves the NACA 0012 with various combinations of α_o and $\tilde{\alpha}$. The trends appear at least qualitatively correct except that most combinations of $\alpha_o + \tilde{\alpha}$ do not yield exactly the same result for an equivalent "non-perturbed" incidence. For example, for $\alpha_o = 14^o$, $\tilde{\alpha} = 0^o$ we have $\sigma = .273$ whereas for $\alpha_o = 10^o$; $\tilde{\alpha} = 4^o$ we have $\sigma = .276$. This discrepancy is expected, however, and thought to be acceptable in light of the fact that the pressure distribution imposed by perturbations, α, is of the thin airfoil form (i.e., $\sim \sqrt{(1 - x)/(1 + x)}$) and includes Lighthill's correction factor. Similarly, the results of Figure 21 show the same effect. The irregular curvature to the $\alpha = 0$ curve at high incidence is related to the assumed polynomial representation of velocity ratios from the NACA method and to the limitations of the NACA method.

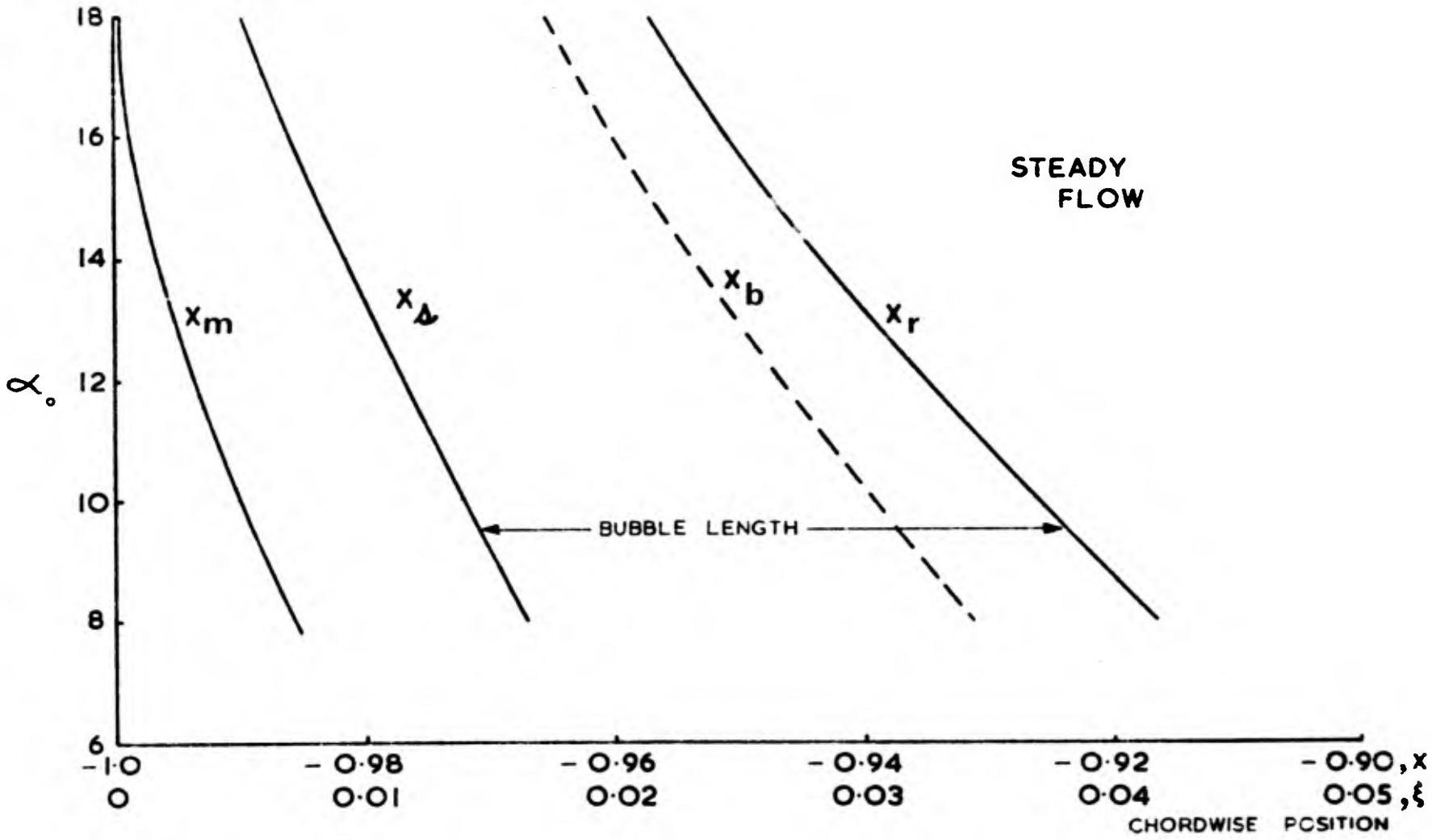

FIG. 19. NACA. 0012 BUBBLE LENGTH PARAMETERS.

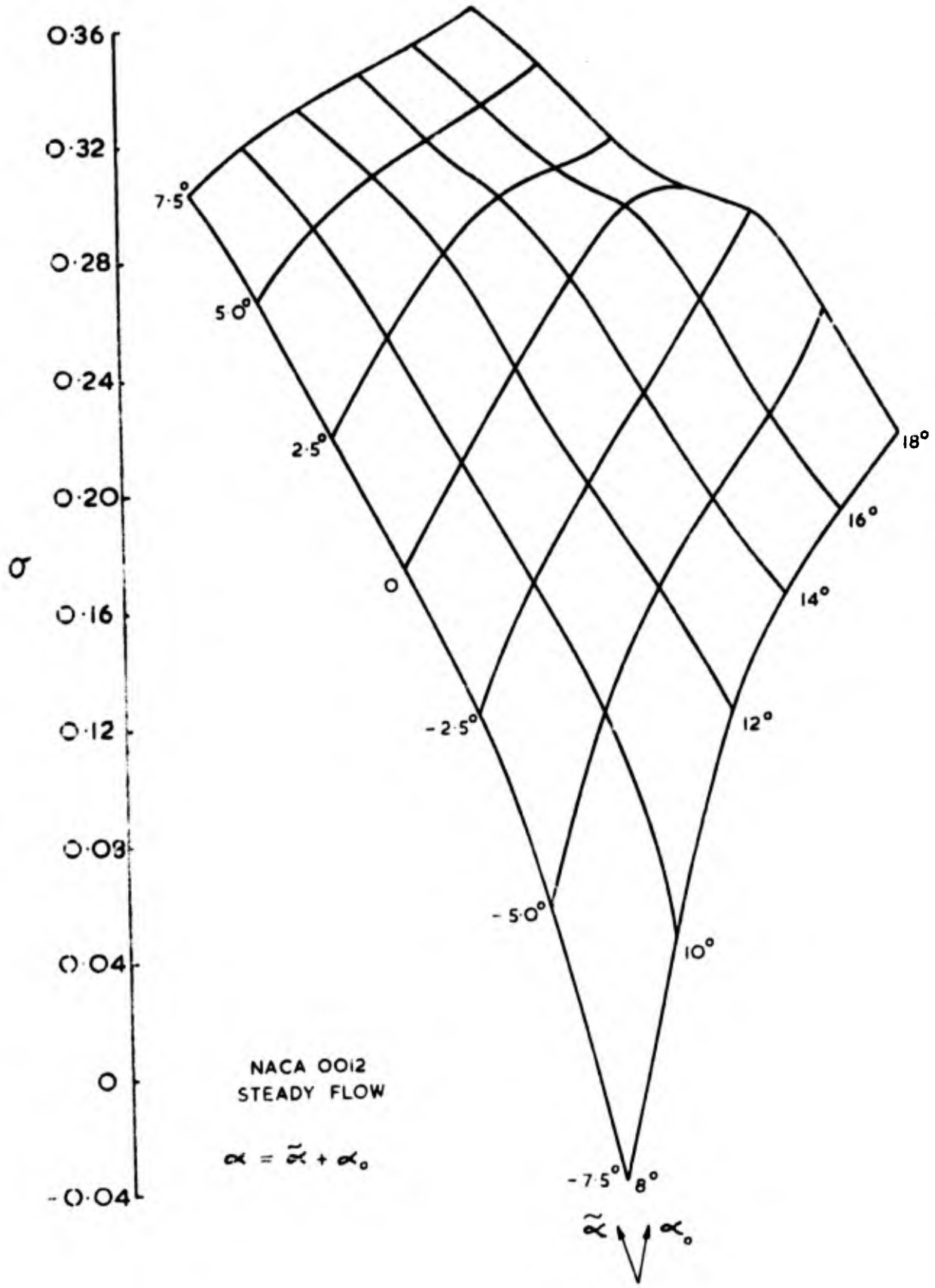

FIG. 20. CRABTREE'S PARAMETER FOR NACA 0012 INCIDENCE EFFECT.

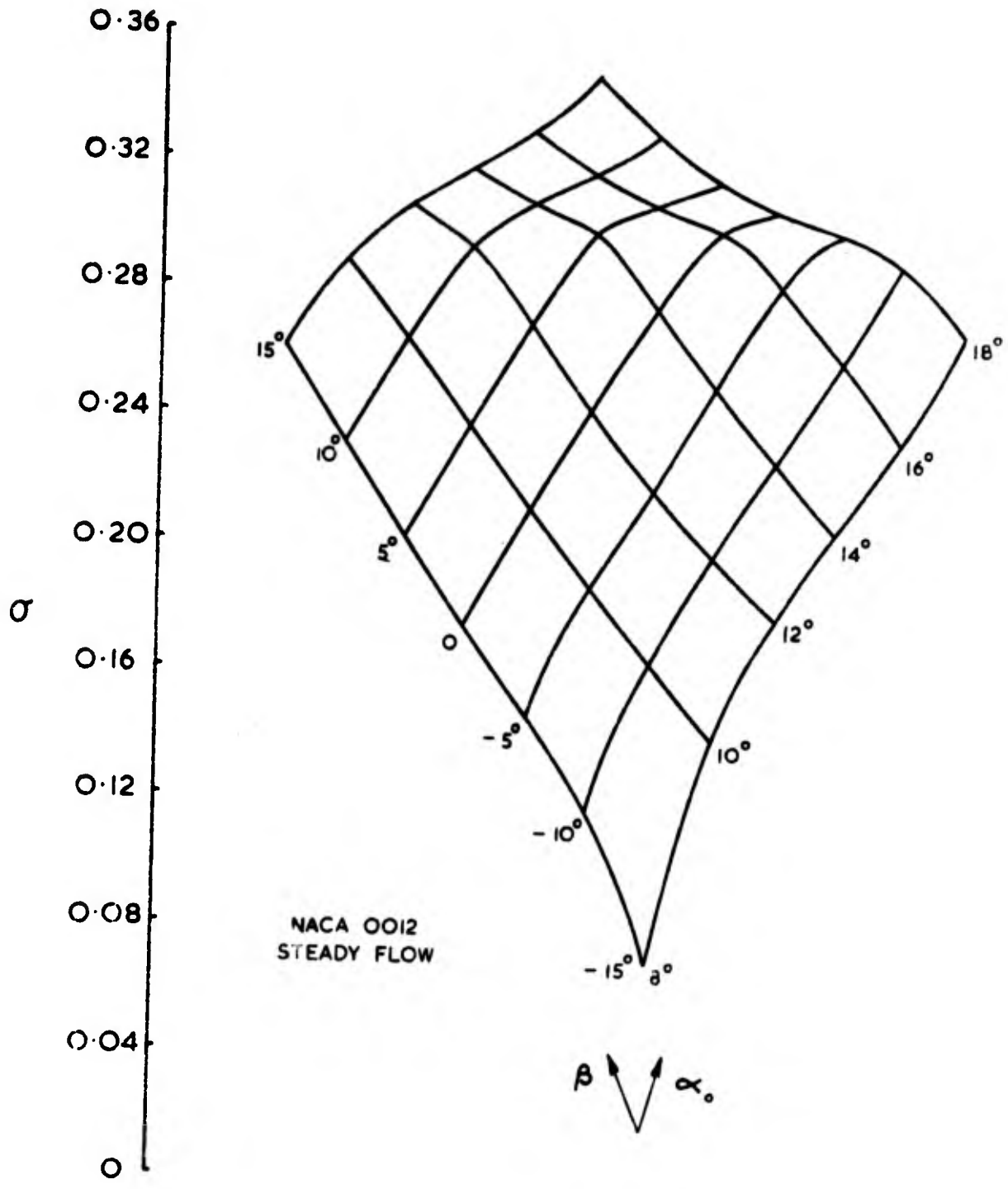

FIG. 21. CRABTREE'S PARAMETER FOR NACA 0012 FLAP EFFECT.

The present model was not derived in order to predict static stalling; however, it appears that the method does compare favorably with steady flow results concerning Crabtree's parameter.

A possible use of these results is best illustrated by considering Figure 21. It is suggested that a critical value of Crabtree's parameter can be found from rigid airfoil tests and applied to the prediction of airfoil stall which is induced by flap deflection. If pertinent parameters are not varied for the flap test (e.g., Re, free-stream turbulence, M, surface roughness) then it is suggested that stall will occur when $\sigma = \sigma_{CR}$. For example, if $\alpha_{stall} = 13^{o}$ then we take $\sigma_{CR} = .26$ and can find combinations of α_o and β that will cause bubble bursting and consequent airfoil stall. At present this is only a suggestion, and one that lacks complete experimental verification.

b. Prediction of Bubble Bursting

In reference 22 it was argued that a critical value of velocity drop across the bubble exists which relates to bubble bursting in unsteady flow. In steady flow, Crabtree's parameter is seen to be an appropriate measure of velocity drop since,

$$\sigma \equiv \frac{C_{p_r} - C_{p_s}}{1 - C_{p_s}} = 1 - \left(\frac{U_r}{U_s}\right)^2$$

Now define a parameter, Young and Horton's parameter,[15] which is:

$$\frac{\Delta U}{U_s} = \frac{U_r - U_s}{U_s}$$

Then in steady-flow:

$$\sigma = -\left[\frac{2\Delta U}{U_s} + \left(\frac{\Delta U}{U_s}\right)^2\right]$$

A typical variation of Young and Horton's parameter during a cycle of airfoil pitching is shown in Figure 22 for two cases. NACA 0012 pitching motion is considered with:

$$\alpha = 12^{o} + 5^{o} \cos \nu_a \tau_a \; ; \quad \nu_a = .04 \text{ and } .30$$

The steady-flow variation, represented by the dashed curve, follows from the related variation of Crabtree's parameter in Figure 20. The hysteresis effect due to unsteady motion is clearly evident in Figure 22. If we assume that a critical

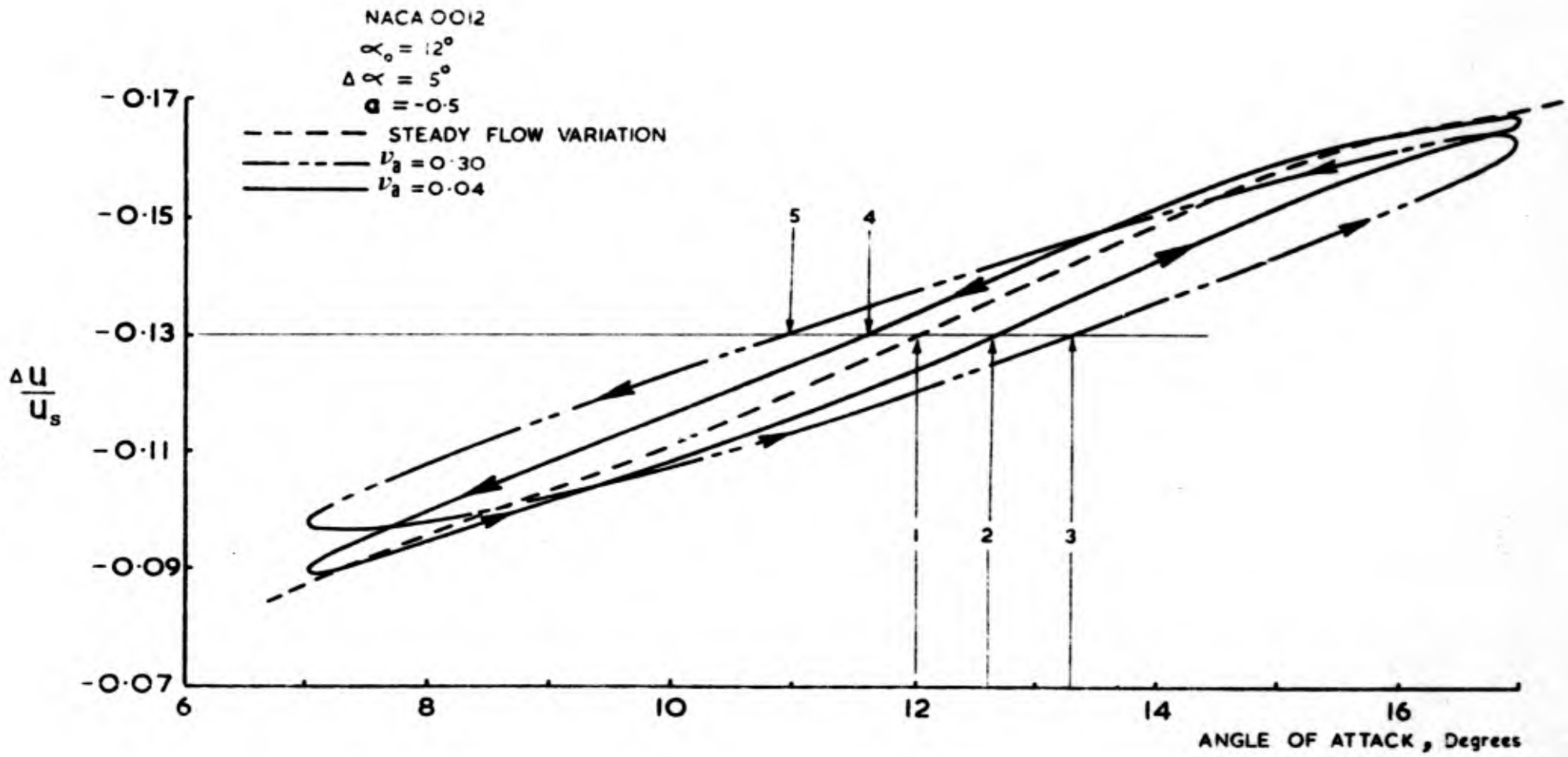

FIG. 22. TYPICAL VARIATION OF YOUNG & HORTON'S PARAMETER IN UNSTEADY FLOW.

value of $\Delta U/U_s$ exists and is not dependent on unsteady effects, then we could proceed as follows to evaluate static stall angle overshoot. We first find the value of

$$\left(\frac{\Delta U}{U_c}\right)_{CR}$$

where at present, it appears that static stall experiments must be relied upon to yield this value. For example, if

$$\alpha_{\substack{\text{static}\\ \text{stall}}} = 12.0^{\circ}$$

then the critical value of $\Delta U/U_s$ follows from point (1) on Figure 22 and we have:

$$\left(\frac{\Delta U}{U_s}\right)_{CR} = -.13 \text{ for } \alpha_{\substack{\text{static}\\ \text{stall}}} = 12.0^{\circ}$$

Then, in the unsteady case we assume that the bubble does not burst for:

$$\left(\frac{\Delta U}{U_s}\right) > -.13$$

Thus, on the upstroke, bubble bursting (and the initiation of dynamic stall) is assumed to occur at

$$\frac{\Delta U}{U_s} = \left(\frac{\Delta U}{U_s}\right)_{CR}$$

From Figure 22 we find that for

$$\nu_a = 0.04 \text{ (i.e., (2))}; \quad \alpha_{\substack{\text{dynamic}\\ \text{stall}}} = 12.6^{\circ}$$

or for

$$\nu_a = 0.30 \text{ (i.e., (3))}; \quad \alpha_{\substack{\text{dynamic}\\ \text{stall}}} = 13.2^{\circ}$$

If we define a stall angle overshoot, $\Delta\alpha_s$ where:

$$\Delta\alpha_s \equiv \alpha_{\substack{\text{dynamic}\\ \text{stall}}} - \alpha_{\substack{\text{static}\\ \text{stall}}}$$

then we have:

$$\Delta\alpha_s = \begin{cases} .6^\circ \text{ for } \nu_a = 0.04 \\ 1.2^\circ \text{ for } \nu_a = 0.30 \end{cases}$$

Points (4) and (5) on Figure 22 can be assumed to yield the reattachment angles as discussed previously.

The difference between using a velocity-based criterion $\Delta U/U_s$, and a pressure-based criterion σ, has been investigated over a range of pertinent parameters. It appears that the difference is mostly sensitive to frequency effects, and if we define an error parameter $\epsilon(\nu)$, where:

$$\epsilon(\nu) \equiv \frac{\Delta\alpha_{s_U} - \Delta\alpha_{s_p}}{\Delta\alpha_{s_U}}$$

and the U and p subscripts refer to unsteady overshoot predictions based on velocities and pressures respectively, we find that at $\nu_a = 0.30$ an error of 8% exists. The approximate relation shown below is characteristic of the frequency effect:

$$\epsilon(\nu) \sim .267\ \nu_a$$

Thus, at low frequencies, predictions based solely on pressures and Crabtree's criterion will yield reasonable results.

Results based on the velocity method of determining bubble bursting will now be presented as parameters are varied for the NACA 0012 and as airfoil and flap motion is considered. Computational procedures are discussed in reference 22.

Figure 23 contains results for the NACA 0012 pitching case where stall angle overshoot angle ($\Delta\alpha_s$) is plotted versus pitch rate at bubble burst (α'_s). The effect of frequency and amplitude of oscillation is clearly evident and we find that for a given frequency, $\Delta\alpha_s$ is roughly proportional to the amplitude of oscillation ($\Delta\alpha$) which is a more-or-less expected result since a linear unsteady flow model is used. Notice, however, that for a given value of $\Delta\alpha$ the effect of frequency is decidedly nonlinear. Vortical wake effects primarily account for this trend. Also, it must be mentioned that for Figure 23 a critical value of $(\Delta U/U_s)$ was determined from the somewhat arbitrary selection of steady flow stall angle where

$$\alpha_{\substack{\text{static} \\ \text{stall}}}$$

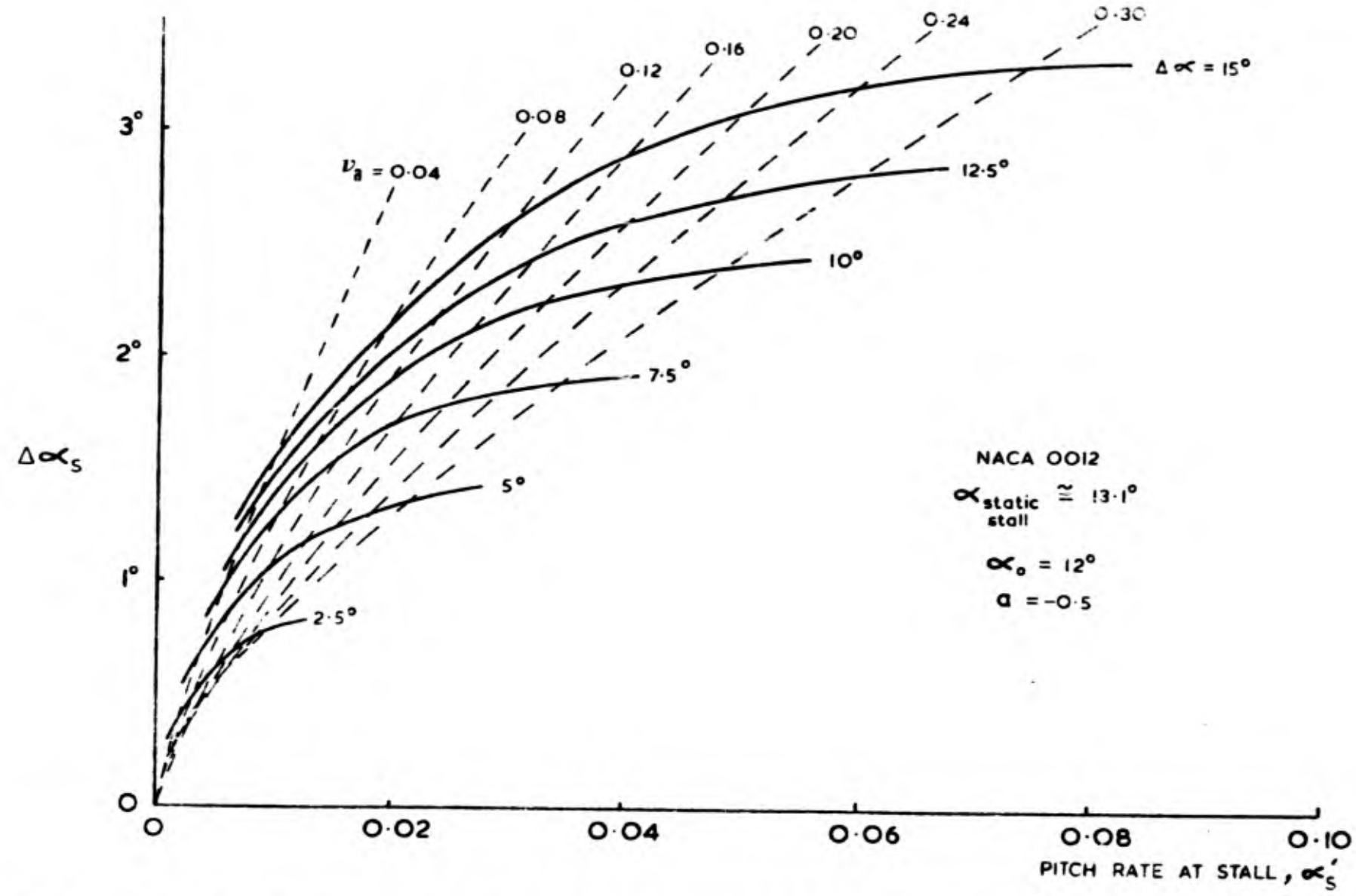

FIG. 23. PITCH RATES AT STALL AND OVERSHOOT ANGLES FOR NACA 0012

was assumed to be 13.1°. (This corresponds to $\alpha_{CR} = .26$ and

$$\left(\frac{\Delta U}{U_s}\right)_{CR} = - .14)$$

The results relate to airfoil pitching about the quarter-chord ($a = -.5$) at a mean incidence of 12°.

In Figure 24 we see a seemingly irregular result that can fortunately be explained. Flap motion effects on the NACA 0012 leading-edge bubble are considered where $\alpha_o = 12^o$ and

$$\left(\frac{\Delta U}{U_s}\right)_{CR} = - .14$$

which yields

$$\beta_{\substack{\text{static} \\ \text{stall}}} = 3.4^o$$

Also,

$$\Delta\beta_s \equiv \beta_{\substack{\text{dynamic} \\ \text{stall}}} - \beta_{\substack{\text{static} \\ \text{stall}}}$$

For the largest amplitude considered (i.e., $\Delta\beta = 20^o$) the effect of frequency on $\Delta\beta_s$ and β'_s generally follows trends which were seen previously; however, the lower amplitudes, $\Delta\beta = 10^o$, 15^o exhibit a different effect. Consider now the constant amplitude curve $\Delta\beta = 10^o$. At very high frequencies it appears that dynamic stall occurs at lower flap rates. This effect simply relates to the fact that at higher frequencies bubble bursting is delayed to such an extent that it occurs close to the maximum flap deflection angle, which for harmonic motion coincides with zero flap rate.

Notice also that bubble bursting does not occur during an oscillation for $\Delta\beta = 5^o$ (and for $\nu \geq .08$). This effect relates to the so called "stall-free regime" mentioned by McCroskey in reference 30.

Reference 22 contains further results of the application of the present theory to the cases of airfoil pitching and flap motion. Details are given of the effects of amplitude and frequency of oscillation, pitch axis location and mean incidence on the overshoot angle and interval (during a cycle) of overshoot. Furthermore, discussion is offered concerning the effects of wake vortical distribution and the speed of propagation of vortex elements into the wake. At high frequencies it appears that the assumption of constancy of circulation is justified when one considers loading due to growth of the separated region.[3]

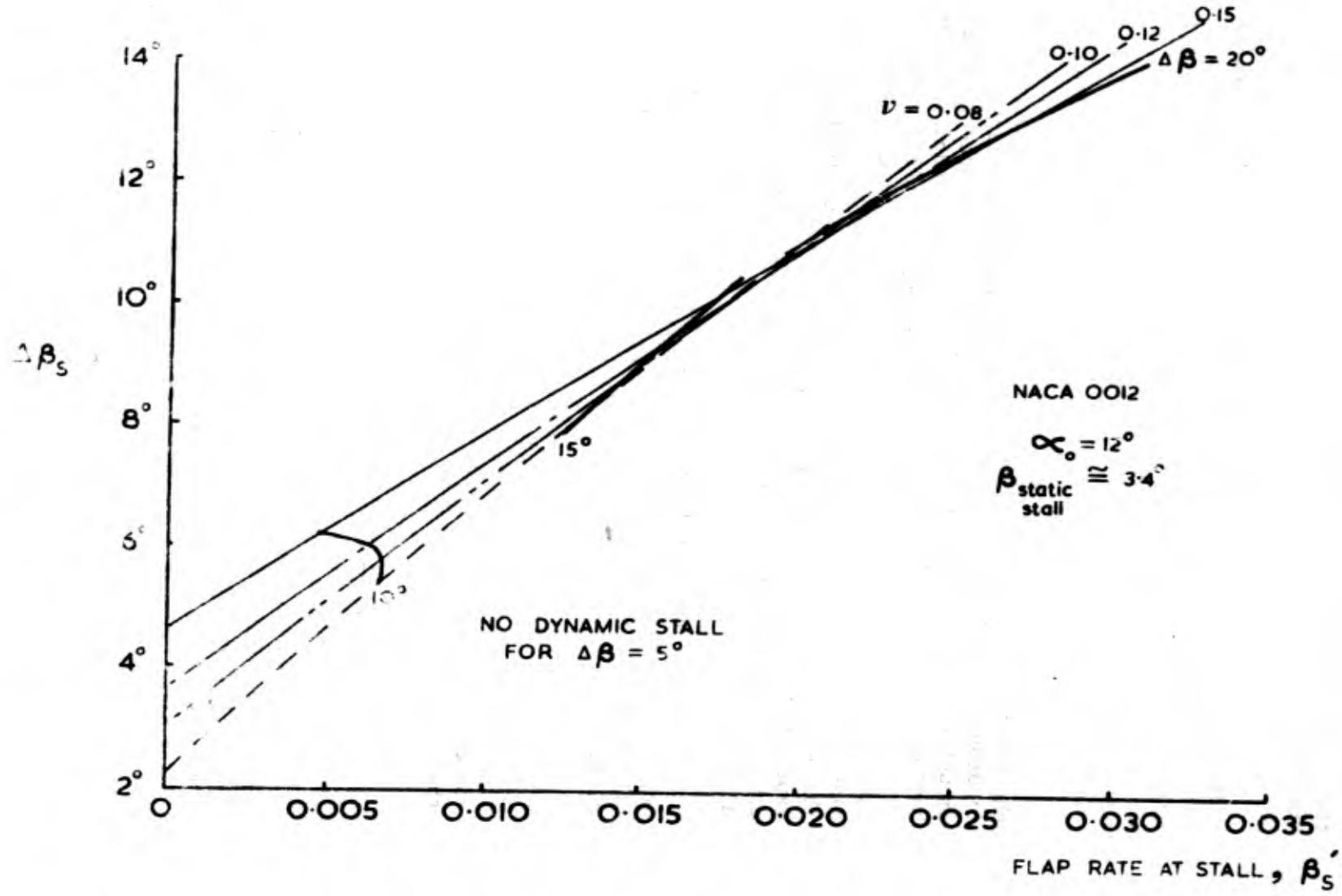

FIG 24. FLAP RATES AT STALL AND OVERSHOOT ANGLES FOR NACA 0012.

However, for low frequencies dissipation of energy in the growing bubble is significant as it moves across the airfoil surface, thus, the assumption of constancy of circulation does not appear justified.

Reference 22 also contains an approximate analysis of the effect of unsteady pressures on turbulent trailing-edge separation. Stratford's criterion[39] is used to show that on the airfoil upstroke (or flap downstroke) trailing-edge separation is likely to be supressed so that leading-edge separation and bubble bursting will occur in unsteady cases.

Finally, an additional element must be considered. The present analysis is expected to be useful in order to predict the onset of bubble instability. The term bursting, however, is probably misleading in the unsteady case since a finite amount of time is required for the bubble to grow once it does become unstable. Thus, the present quasi-steady model is limited in that it does not account for the dynamics of bubble growth once instability is achieved. McCroskey[30] has recently recognized this also and has compared a simple burst prediction (based on the instantaneous pressure gradient at 10% chord) to experimental observations which involve both the initial breakdown of the potential flow and data based on moment stall of an airfoil.

Consider now an extension of the previous quasi-steady model to allow for the dynamics of bubble growth. The model of separation bubble dynamics of section II serves as a starting point.

Crimi in Reference 40 has concluded that growth of the leading-edge separation bubble is dependent primarily on mass flux into the bubble from near the reattachment point. An incremental mass flux in the unsteady case is essential so that the bubble may grow, and we have:

$$\dot{m}_\epsilon \cong \rho \frac{d}{dt} (A_{bubble})$$

From the analysis of section II.2.b we find that the pressure rise near reattachment is expected to alter in proportion to the additional mass flux. So we have a change to the pressure drop across the bubble:

$$\Delta \tilde{C}_{p_{rb}} \equiv \frac{\Delta \tilde{p}_{rb}}{\frac{1}{2} \rho U_\infty^2} = \left[\frac{1}{3} \left(4 + \frac{1}{a} + \frac{1}{a^2}\right)\right] \frac{\dot{m}_\epsilon u_B}{\frac{1}{2} \rho U_\infty^2 \delta_r}$$

For quasi-steady bubble growth we have approximately:

$$A_{bubble} \cong k_1 l^2 (\alpha - \alpha_{stall})^2$$

or

$$\dot{m}_{\epsilon} \cong ? \rho k_1 b^2 (\alpha - \alpha_{stall}) \dot{\alpha}$$

and

$$\delta_r \cong k_2 b (\alpha - \alpha_{stall})$$

The above relations are appropriate for thin airfoil-type stall which involves the growth of a long bubble type. See also Wood's theory of bubble growth in reference 41.

The quasi-steady mass flux is assumed valid as for the bubble behind a spoiler. This appears well justified since the bubble is small and the shear layer is expected to have a small characteristic time. So we have for the pressure perturbation:

$$\Delta \tilde{C}_{p_{rb}} \cong \left[\tfrac{1}{3} \left(4 + \frac{1}{a} + \frac{1}{a^2}\right)\right] \frac{4k_1}{k_2} \frac{u_B b}{U_\infty^2} \dot{\alpha}$$

$$\cong k_3 \frac{u_B}{U_b} \left(\frac{U_b}{U_\infty}\right) \frac{\dot{\alpha} b}{U_\infty}$$

but

$$\frac{\dot{\alpha} b}{U_\infty} = - \nu_a \Delta\alpha \sin \omega t = \alpha'$$

for

$$\alpha = \alpha_o + \Delta\alpha \cos \omega t$$

and

$$\frac{U_b}{U_\infty} = (1 - C_{p_s})^{\frac{1}{2}}$$

Also, assume $\frac{u_B}{U_b}$ = constant so that

$$\Delta \tilde{C}_{p_{rb}} \cong k_4 (1 - C_{p_s})^{\frac{1}{2}} \alpha'$$

In the unsteady case then, the short leading-edge bubble will grow when sufficient mass is returned to the bubble. In effect, this means that the critical pressure recovery coefficient is modified in the unsteady case, so we have:

$$\sigma_{growth} = \sigma_{CR} + \Delta\sigma$$

where

$$\Delta\sigma = \frac{\Delta \tilde{C}_{p_{rb}}}{(i - C_{p_s})} \cong k_4 \frac{\alpha'}{(1 - C_{p_s})^{\frac{3}{2}}}$$

and

$$k_4 = \left[\frac{1}{3}\left(4 + \frac{1}{a} + \frac{1}{a^2}\right)\right] \frac{4k_1}{k_2} \frac{u_B}{U_B}$$

Computations were performed in order to find the overshoot angle-of-attack for a pitching airfoil. Overshoot angle in this case is defined to be:

$$\frac{\Delta\alpha_s}{\Delta\alpha} \equiv \frac{\alpha_{\substack{bubble \\ growth}} - \alpha_{\substack{static \\ stall}}}{\Delta\alpha}$$

A single case was chosen in order to compare with experimental data. Motion is of the form:

$$\alpha = 12^\circ + 5^\circ \cos \omega t$$

σ_{CR} was chosen so that $\alpha_{\substack{static \\ stall}} = 12^\circ$. In this case, a pressure criterion was used in order to predict overshoot angle, thus a small discrepancy is expected with overshoot angle being slightly underestimated.

Results are plotted in Figure 25, as curves for bubble growth. Two values of the shear layer parameter, k_4, were used (i.e., $k_4 = .25$ and $k_4 = .15$) and results show that overshoot is not strongly dependent on this parameter. Experimental data is taken from reference 30. Also shown in Figure 25 are results from the unmodified quasi-steady theory. The curve labeled "bubble burst based on pressures" is nearly coincident with results if either the pressure gradient at 1.25% chord or σ_{CR} is evaluated with bubble length fixed. The curve labeled "bubble burst based on velocities" follows directly from the original theory, which is based on Young and Horton's parameter, and is found to be nearly coincident with a prediction of McCroskey[30] based on his pressure gradient at 10% chord.

The onset of bubble growth, as predicted from the present theory, is seen to correspond well to observations of airfoil moment stall. Thus, it appears that the instant of dynamic stall initiation is associated not with bubble instability but

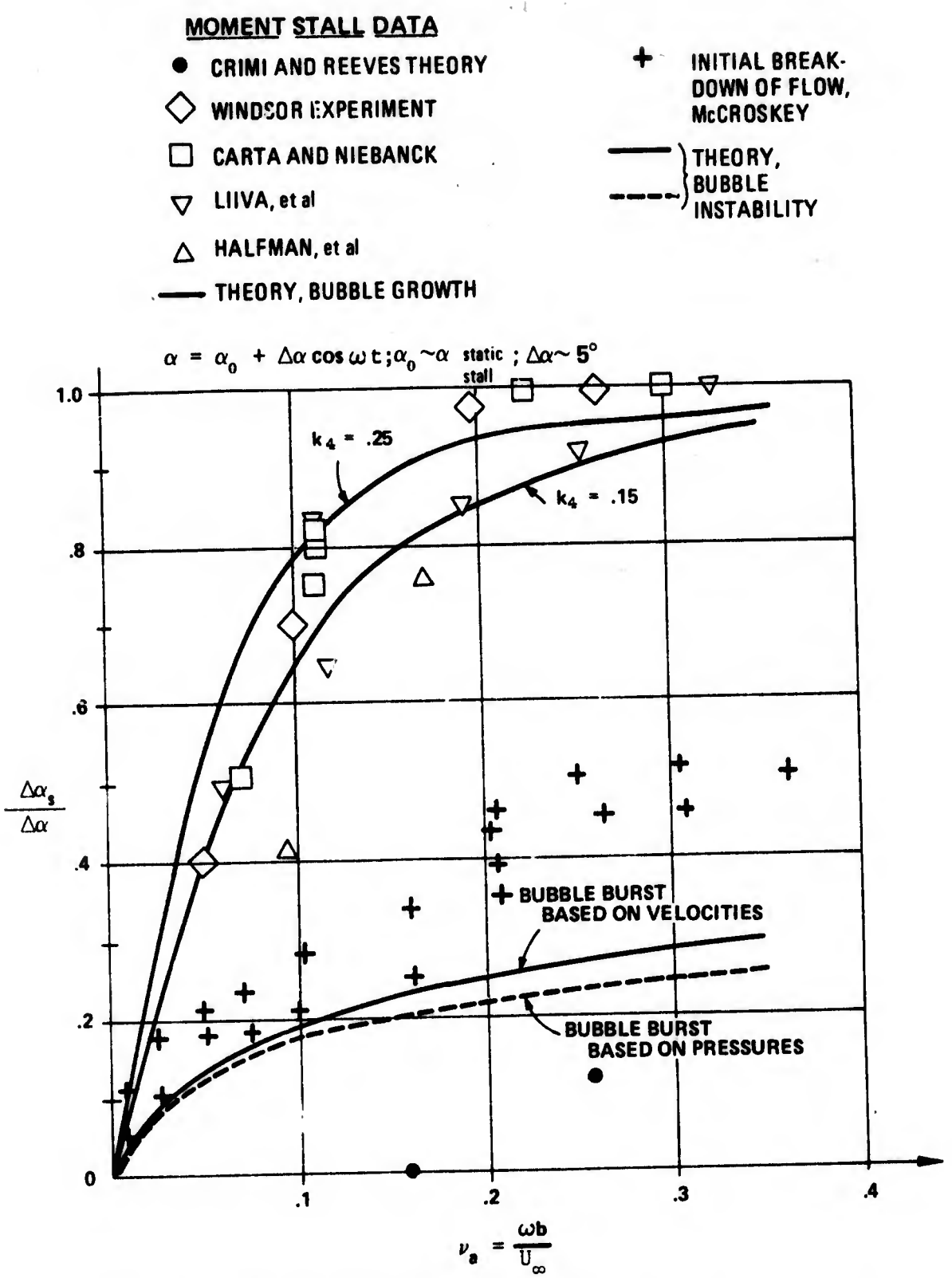

FIG. 25. THEORETICAL AND EXPERIMENTAL STALL DELAY ON OSCILLATING NACA 0012 AIRFOILS

with actual growth of the separation bubble. McCroskey's data for the initial breakdown of potential flow lies, as expected, between the instant for bubble bursting (or instability) and bubble growth.

In conclusion regarding dynamic stall, it is seen that the unsteady inviscid flowfield dominates bubble behavior and that a critical pressure or velocity drop across the bubble may be determined by considering that the small bubble reacts in a quasi-steady manner to changes in the external flowfield. Growth of the bubble, however, apparently depends on dynamic effects in that it does not begin until mass is forced into the bubble at a sufficient rate to cause growth.

2. A Type of Control-Surface-Buzz

The dynamics of a separating region are known to be an element in the problem of control-surface buzz. Lambourne in references 1,34 & 42 discusses this example of flutter in one degree-of-freedom which involves the interaction of a moving flap, shock wave(s) and a separating flow. A type of control-surface buzz (CSB), which is termed type A, involves shock wave(s) which lie on the airfoil surface ahead of the flap hinge-line. The flap is in subsonic flow and boundary-layer separation is induced by the shock wave(s).

Some conclusions concerning type A buzz are:[1]

1. The critical Mach number for buzz correlates with a criterion for the onset of shock-induced separation, e.g., trailing-edge pressure divergence.

2. The critical Mach number falls with increasing airfoil incidence.

3. The critical Mach number is not greatly altered by a change in the elastic hinge stiffness.

4. At constant Mach number, the buzz frequency is given approximately by:

$$\omega = \left[\frac{C - H_\beta}{A}\right]^{\frac{1}{2}}$$

The theoretical work of Eckhaus[43,44] included shock waves at the wing surface in an inviscid flow theory and has predicted the existence of a Mach number and frequency range in which the flap is negatively damped. Other analyses which included a time lag in the motion of the shock and subsequent lag in the aerodynamic hinge moment were offered.[45,46] At present, however, the exact mechanisms and interactions remain unknown.

Based on the results and theory for the oscillating spoiler case and some recent information concerning viscous-inviscid interactions at transonic speeds one can further speculate as to the mechanisms and interactions in type A control-surface buzz.

Consider now a typical type A flow which involves an airfoil at incidence, Mach number near critical, and a single shock-wave ahead of the flap on the upper surface. A separated region exists aft of the shock wave with reattachment occurring on the flap surface and no divergence in trailing edge pressure. The flap is fixed at a "steady flow equilibrium" angle with $C_H = 0$.

In this case, which borders between the so-called "weak" and "strong" interactions of the shock/shear-layer system and the overall flow[47] we expect that coupling (via shear layer displacement thickness effects) between the shear layer and pressure field is strong locally (in the region of the separation bubble) but relatively weak in the overall sense, since trailing-edge pressure has not diverged.

Now if the flap were to be oscillated harmonically with very small amplitude, as an assumption, we neglect a direct effect on the separation bubble and shear layer and instead consider that the outer inviscid flow responds as in the weak interaction, or attached flow, case. This assumption follows from results of the spoiler experiment where, for moderate spoiler heights, it was found that aerodynamic hinge-moment was approximately independent of spoiler height and bubble length.

As a result of flap motion, pressure perturbations are realized at the shock. If the region of supersonic flow ahead of the shock is sufficiently large, then propagation of pressure perturbations to the shock from upstream may be neglected. The flow may be considered "frozen" ahead of the shock. Tijdeman and Zwaan in reference 48 show that this type of pressure disturbance travels upstream as a receding wave and that the time taken to reach the aft face of the shock is as discussed in reference 46 and is approximately:

$$\Delta t = \frac{d}{\bar{a}_2 \ (1 - \bar{M}_2)}$$

where d is the distance between T.E. and shock location, $\bar{a}_2$ and $\bar{M}_2$ are the mean speed of sound and local Mach number along d. We can also write:

$$\Delta \tau \equiv \frac{\Delta t \ U_\infty}{c_f} = \frac{a_\infty \ M_\infty}{\bar{a}_2 \ (1 - \bar{M}_2)} \frac{d}{c_f}$$

A phase shift may be found:

$$\phi = 2\pi f \Delta t = \nu \Delta \tau$$

Thus, the pressure perturbations at the aft face of the shock, δp_2, result from flap motion and a time lag. Lambourne in reference 34 shows that this change in shock strength can be related to shock motion by means of the 1-D flow jump relations for a normal shock.

$$\frac{\delta p_2}{p_1} \cong \frac{4\gamma}{\gamma + 1} M_1 \left(\frac{U_s}{a_1}\right) \quad \text{for} \quad \left|\frac{U_s}{a_1}\right| \ll M_1$$

where U_s is shock velocity upstream relative to the airfoil surface and subscript 1 denotes conditions immediately upstream of the shock. Also, we have the pressure jump across the shock:

$$\frac{p_2 - p_1}{\frac{1}{2} \gamma p_1 M_1^2} = \frac{4}{\gamma + 1} \left(1 - \frac{1}{M_1^2}\right) + \frac{8}{\gamma + 1} \left(\frac{U_s}{U_1}\right)$$

For a normal shock, then, we find that the flap can "drive" the shock across the surface of the airfoil via unsteady pressure perturbations. This result is also found in Eckhaus' work[43,44] along with an equation that may be solved for the pressure perturbations due to flap motion.

Forced oscillation tests confirm that the flap/shock interaction as described above is qualitatively correct in the absence of significant separation. In reference 48 it is shown that for sufficiently large perturbations the shock does not exist during part of its downstream motion. We find in that case that $p_2 \approx p_1$. This is very strong evidence to support the hypothesis that prior to T.E. pressure divergence, flap motion serves to force the shock along the airfoil surface as described above, thus we expect that at the onset of buzz, coupling between the flap and shock motion may be represented by a parameter which is primarily a function of freestream Mach number, frequency and airfoil geometry. It is further probable, but remains to be verified, that for larger degrees of initial separation (for example those which involve recompression on the flap upper surface) the flap may also control the outer flow to a significant degree or may be able to force the shock by affecting mass flow in the separated region. It is expected, therefore, that the coupling relation between flap and shock depends on the amplitude of flap motion as well as on the initial degree of shock-induced separation. This non-linear effect is not simulated in the coupled spoiler/flap experiment of reference 22 where coupling parameters were held constant.

As the shock wave moves across the airfoil surface it affects the boundary layer. A forward moving shock causes severe separation; a rearward moving shock is weaker and leads to reduced separation. Measurements by Nakamura[49] and Lambourne, at both fixed chordwise positions and fixed distances aft of the moving shock, have shown that shear layer thickness is related to shock strength. In references 18 and 50 it is shown that the angle at which the boundary-layer is forced to separate from the airfoil surface is a function of shock strength. In the steady flow case for the region near the foot of a normal shock where an oblique shock emanates from the edge of the shear layer, we have an approximation from reference 51.

$$\frac{p_2 - p_1}{p_1} \cong \frac{\gamma M_1^2}{\sqrt{M_1^2 - 1}} \theta$$

where θ is the deflection angle of the outer flow and can be taken as equal to the angle at which the shear layer separates from the surface.

The above results show that shock strength corresponds to shear layer deflection angle at the foot of the shock. Trilling also shows this to be the case in unsteady flow, where the preceding equation yields approximately:

$$\frac{\delta p_2}{p_1} \cong \frac{\gamma M_1^2}{\sqrt{M_1^2 - 1}} \delta\theta \qquad \left(\text{for } \left|\frac{U_s}{a_1}\right| \ll M_1\right)$$

Entrainment of fluid from the "dead air" region under the shear-layer into the shear-layer (see reference 22 and section II) will result in a transverse pressure gradient and can cause shear layer curvature and reattachment.

Separation of the shear layer, as in the case of the oscillating spoiler, involves vorticity being convected into or past the separation "bubble." As the shock moves forward, vorticity is figuratively "peeled away" from the airfoil surface and may be convected downstream so that bubble circulation and size increase. Pressure in the region of the bubble is significantly reduced. Thus, in a manner analogous to spoiler induced effects, one would expect that shock motion induces alterations to separation bubble size and pressures.

As the shock moves forward, the shear layer (which has a small characteristic time) will separate at an angle which relates to shock strength (i.e., rate). The mechanism of bubble growth, however, involves mass flux and a time lag. In this case also, movement of the separation point and bubble is a factor. Bubble growth is expected to lag shock rate whereas pressure perturbations are assumed to depend on shock rate. (See section II for a discussion of possible integral effects.)

The net result is in a first harmonic component of incremental hinge-moment which depends on shock rate. For small perturbations the effect of shock and separation point location may be neglected as an approximation. The effect of shock position may also cancel the effect of lag in bubble growth. An incremental hinge-moment is nevertheless produced by shock motion. If the flap is free to respond, then we have the possibility of self-excited oscillations; that is, control-surface-buzz.

The preceding discussion involves a considerable amount of speculation concerning the exact interactions between flap motion, shock movement and incremental hinge-moment. For example, the displacement thickness effect of the shear-layer on the outer flow is neglected for small perturbations. The important assumptions, which are only appropriate at the onset of instability, are that the shock is primarily driven by flap motion through the outer flow and that shock strength, hence incremental hinge-moment, is altered due to shock motion. This scheme of interactions can be approximately modeled in order to study the onset of buzz.

As in the coupled spoiler/flap experiment, we take as the equation of motion:

$$\ddot{\beta} + \frac{(B - H_{\dot{\beta}})}{A}\dot{\beta} + \frac{(C - H_{\beta})}{A}\beta = \frac{\Delta H}{A} \qquad (24)$$

where $H_{\dot{\beta}}$ and H_{β} are aerodynamic terms which may be found from tests at moderate values of freestream Mach no. in the absence of significant shock-induced separation.

The incremental hinge-moment is related to the coefficient, ΔC_H, which can be determined in steady flow with the flap fixed by varying freestream Mach number, M_∞, over a range from that which involves the onset of shock-induced separation effects to that which corresponds to large-scale separation (e.g., when the shock wave(s) move onto the flap surface). Ideally ΔC_H should be evaluated by extrapolation with total hinge-moment on the flap equal to zero at a fixed Mach number. This will insure that ΔC_H is known near the steady-flow "equilibrium" flap position. The incremental hinge-moment coefficient as a function of M_∞ is expected to qualitatively resemble the corresponding term in the spoiler experiment as a function of spoiler height.

A solution for the coupling relation between flap and shock motion can possibly be found by extending Eckhaus' work. For flap motion of the form:

$$\beta = \beta_0 + \beta_1 \cos \omega t$$

shock position can be represented from the linear theory of Eckhaus as:

$$x_{sh} \equiv \frac{X_{sh}}{c} = x_{sh_o} + x_1 \cos(\omega t - \gamma)$$

where $x_1 = \frac{\partial x_1}{\partial \beta_1} \beta_1$. $\frac{\partial x_1}{\partial \beta_1}$ and γ (the lag angle) are functions of x_{sh_o}, M_1, ν and $\frac{c_f}{c}$. x_{sh_o} can be found as a function of M_∞ from flap fixed experiments with $\beta = \beta_o$. β_o should be the steady flow equilibrium value for a given M_∞. It will be expected in the present asymmetric flow example (i.e., a single shock exists at the onset) that a "rectification effect" will exist so that $\beta_o = \beta_o(t)$ as in the spoiler/flap experiment; therefore, x_{sh_o} will vary during the transient growth of oscillations in a buzz situation. We may take:

$$x_{sh_o} \cong (x_{sh_o})_{\beta=0} + \frac{dx_{sh}}{d\beta} \beta_o$$

where $\frac{dx_{sh}}{d\beta}$ is found from experiment or theory, or as an approximation:

$$x_{sh_o} \cong (x_{sh_o})_{\beta=0} + \frac{\partial x_1}{\partial \beta_1} \beta_o$$

The ratio $\frac{M_\infty}{M_1}$ should also be found as M_∞ is varied. Experimental results found by Nakamura (Ref 49) indicate that $\gamma = 0$ for $\nu \cong .09$, however, other tests and the time lag theory previously discussed indicate that γ may be nearer 80^o or so.[48] γ is found to be primarily a function of frequency, ν.

The effect of shock motion on ΔC_H is complex. An equivalent change to the freestream Mach number is approximately:

$$\tilde{M}_\infty = \frac{M_\infty}{M_1} \tilde{M}_1 = \frac{M_\infty}{M_1 a_1} U_s$$

where $U_s = -\frac{dX_{sh}}{dt} = -c\,\dot{x}_{sh}$ and for transient motion:

$$U_s \cong -c \left[\dot{x}_{sh_o} + \frac{\partial x_1}{\partial \beta_1} \dot{\beta}_1 \cos(\omega t - \gamma) - \omega \frac{\partial x_1}{\partial \beta_1} \beta_1 \sin(\omega t - \gamma)\right]$$

where Eckhaus' theory could be used to find values of $\frac{\partial x_1}{\partial \beta_1}$ and γ which are based on average values of ν and x_{sh_o} over a cycle of motion.

We then have:

$$\tilde{M}_\infty \cong - \frac{M_\infty c}{M_1 a_1} \left[\dot{x}_{sh_o} + \frac{\partial x_1}{\partial \beta_1} \dot{\beta}_1 \cos (\omega t - \gamma) - \omega \frac{\partial x_1}{\partial \beta_1} \beta_1 \sin (\omega t - \gamma)\right]$$

or with the approximation $\dot{x}_{sh_o} \cong \frac{\partial x_1}{\partial \beta_1} \dot{\beta}_o$ we have:

$$\tilde{M}_\infty \cong - \frac{M_\infty c}{M_1 a_1} \frac{\partial x_1}{\partial \beta_1} \left[\dot{\beta}_o + \dot{\beta}_1 \cos (\omega t - \gamma) - \omega \beta_1 \sin (\omega t - \gamma)\right]$$

In an actual buzz case the coupling terms $\frac{\partial x_1}{\partial \beta_1}$ and γ are expected to be functions of flap amplitude as well as shear-layer displacement thickness. The present relation can be written for the limit-cycle case as:

$$\tilde{M}_\infty \cong \frac{M_\infty c}{M_1 a_1} \frac{\partial x_1}{\partial \beta_1} \left[\omega \beta_1 \sin (\omega t - \gamma)\right]$$

or as:

$$\tilde{M}_\infty \cong k_1 \beta_1 \cos (\omega t - \frac{\pi}{2} - \gamma)$$

which shows that the equivalent Mach number perturbation lags flap motion by $90^\circ + \gamma$, where k_1 and γ depend on frequency and M_1. This relation may be compared to the spoiler height perturbation in the coupled spoiler/flap experiment.

$$\tilde{h} = k \beta_1 \cos \omega t$$

where

$$h = h_o + \tilde{h}$$

The Mach number perturbation may be modified, as in the spoiler case, to account for a lag in bubble growth which is also expected in the compressible flow behind a moving shock. A modified theory would yield an "effective" Mach number perturbation:

$$\tilde{M}_{\infty_{eff}} \cong Ak_1 \beta_1 \cos\left(\omega t - \frac{\pi}{2} - \gamma - \alpha\right)$$

For a critical range of γ it is probable that effects due to lag in bubble growth are countered by the effect of instantaneous shock location; that is, the shear-layer reattachment point may not move significantly across the flap surface. Also, a correction to bubble dead air pressure is required due to unsteady momentum flux to the bubble and alterations to bubble circulation. These corrections would involve evaluation of shear layer parameters and a steady-flow bubble growth law. The correction would be applied to steady-flow ΔC_H results as in the spoiler case.

The net result is that unsteady incremental hinge moment may be approximately found as a function of β_o, β_1, $\hat{\beta}_1$, ν and M_∞. Under the apparently reasonable assumption that flap motion is approximately of the form:

$$\beta = \beta_o + \beta_1 \cos \omega t$$

We can proceed to find ΔC_H in describing function form:

$$\Delta C_H \cong \Delta C_{H_o} + N_1 k_1 \beta_1 \cos \omega t + \frac{N_2 k_1}{\omega} (-\omega \beta_1 \sin \omega t)$$

and for transient motion we have:

$$\Delta C_H \cong \Delta \hat{C}_{H_o} + \left[\hat{N}_1 + \frac{\hat{N}_2}{\omega} \lambda\right] k_1 \beta_1 \cos \omega t$$

$$+ \frac{\hat{N}_2 k_1}{\omega} (-\omega \beta_1 \sin \omega t)$$

where $\lambda \equiv \frac{\dot{\beta}_1}{\beta_1}$ and terms in the series are found in the obvious way, with $\frac{\Delta C_{H_1}}{\Delta M_\infty} = N_1 + i N_2$ and $\frac{\Delta \hat{C}_{H_1}}{\Delta M_\infty} = \hat{N}_1 + i \hat{N}_2$.

Consider now a qualitative discussion of transient and limit cycle behavior for the buzz problem based on results for the coupled spoiler/flap problem and other experimental data.

In the experiment with spoiler and flap coupled we have the coupling relation:

$$h = h_{o_1} + k \beta = (h_{o_1} + k \beta_o) + k \beta_1 \cos \omega t$$

$$= h_o + \Delta h \cos \omega t$$

for flap motion of the form:

$$\beta = \beta_o + \beta_1 \cos \omega t$$

Thus, the mean spoiler height is $h_o = h_{o_1} + k\,\beta_o$ and spoiler amplitude is $\Delta h = k\,\beta_1$. The spoiler oscillates in phase with the flap.

In the buzz problem for flap motion of the form $\beta = \beta_o + \beta_1 \cos \omega t$ we have an approximate mean effective freestream Mach number.

$$(M_\infty)_{eff} \cong M_\infty + \frac{\beta_o}{\frac{d\,\beta_o}{d\,M_\infty}}$$

where $\frac{d\,\beta_o}{d\,M_\infty}$ may be found from experiment or we may use as an approximation:

$$\frac{d\,\beta_o}{d\,M_\infty} \cong \frac{M_1 \frac{dx_{sh}}{dM_1}}{M_\infty \frac{dx_{sh}}{d\beta}}$$

with the derivatives on the RHS found by a suitable transonic flow theory. The mean effective freestream Mach number is analogous to mean spoiler height.

We also have a shock relation:

$$x_{sh} = x_{sh_o} + x_1 \cos(\omega t - \gamma)$$

$$= x_{sh_o} + \frac{\partial x_1}{\partial \beta_1} \beta_1 \cos(\omega t - \gamma)$$

and an effective freestream Mach number perturbation that is approximately:

$$(\tilde{M}_\infty)_{eff} \cong A\, k_1 \beta_1 \cos\left[\omega t - \left(\frac{\pi}{2} + \gamma + \alpha\right)\right]$$

$$= (\Delta M_\infty)_{eff} \cos\left[\omega t - \left(\frac{\pi}{2} + \gamma + \alpha\right)\right]$$

with

$$A \approx 1.0; \quad k_1 \equiv \frac{M_\infty c}{M_1 a_1} \frac{\partial x_1}{\partial \beta_1} \omega$$

This relation is valid for $|\dot{\beta}_o| \ll |\dot{\beta}_1|$ and $|\lambda| \ll 1$.

We may tentatively assume that the lag in bubble growth is negligible and we have:

$$(\tilde{M}_\infty)_{eff} \cong k_1 \beta_1 \cos [\omega t - (\frac{\pi}{2} + \gamma)]$$

The above result is essentially a quasi-steady model of shock effects.

At the onset of instability we find from Nakamura's results[49] that the perturbations act nearly in quadrature with flap motion for $\nu \cong .09$. Results based on the time lag theory and flap forced testing indicate that the perturbations would lag flap motion by a greater amount. Perhaps this anomaly relates to the increasing shear layer displacement thickness effect as oscillations build in amplitude. In order to qualitatively study the stability of a coupled system, therefore, it appears appropriate to tentatively take $\gamma \cong 0$. In this case, perturbations are in-quadrature with flap deflection and we have a result which also includes the pressure perturbations to the separated region, which are assumed to act in phase with $(\tilde{M}_\infty)_{eff}$:

$$\Delta C_H \cong \Delta \hat{C}_{H_o} + \frac{\hat{N}_2}{\omega} \lambda k_1 \beta_1 \cos \omega t + \frac{\hat{N}_2 k_1}{\omega} (-\omega \beta_1 \sin \omega t)$$

When the above expression is substituted into the equation of motion (24) we find as in section II:

$$\beta_o \cong \frac{\Delta \hat{C}_{H_o}}{(\frac{C}{q_\infty b_f c_f^2} - C_{H_\beta})}$$

$$\lambda \cong \frac{1}{2A} [(\frac{c_f}{U_\infty} C_{H_{\dot{\beta}}} + \frac{\hat{N}_2 k_1}{\omega}) q_\infty b_f c_f^2 - B]$$

$$\omega^2 \cong -\lambda^2 + [\frac{C - C_{H_\beta} q_\infty b_f c_f^2}{A}]$$

Since the effect of freestream Mach number on ΔC_H in steady flow is expected to be qualitatively similar to the spoiler height effect, it follows that the describing function $\frac{\Delta \hat{C}_{H_1}}{\Delta M_\infty}$ will be of similar form. Refer to Figure 4 and note that a maximum value of $\left|\frac{\Delta C_{H_1}}{\Delta h}\right|$ occurs at about h = .065. In the buzz case we expect a similar dependence on M_∞. The effect of Δh on $\frac{\Delta C_{H_1}}{\Delta h}$ is expected to reflect the dependence of $\frac{\Delta C_{H_1}}{\Delta M_\infty}$ on $(\Delta M_\infty)_{eff}$ where $(\Delta M_\infty)_{eff} \cong A\, k_1 \beta_1 \cong \frac{M_\infty c}{M_1 a_1} \frac{\partial x_1}{\partial \beta_1} \omega \beta_1$. Thus, we can study system stability with the notion that M_∞ relates to h_{o_1} and k_1 relates to k for the spoiler and flap system.

Unlike the spoiler and flap system, however, k_1 is a function of M_∞, β_o, β_1, $\frac{c_f}{c}$ and ν. As M_∞ and ν increase we expect $\frac{\partial x_1}{\partial \beta_1}$ to decrease. This follows because in transonic flow as $\frac{\frac{\omega b}{U_\infty}}{|1 - M_\infty|}$ increases, receding waves which are propagated upstream tend to cancel and for $\frac{\frac{\omega b}{U_\infty}}{|1 - M_\infty|} \gg 1$ upstream effects can be neglected. The parameter $\frac{k_1}{\omega}$ then will decrease as ν or M_∞ increase, and $\frac{\hat{N}_2 k_1}{\omega}$ will decrease as ν increases.

The solution for stability parameters in the buzz case may be represented as in the sketch below:

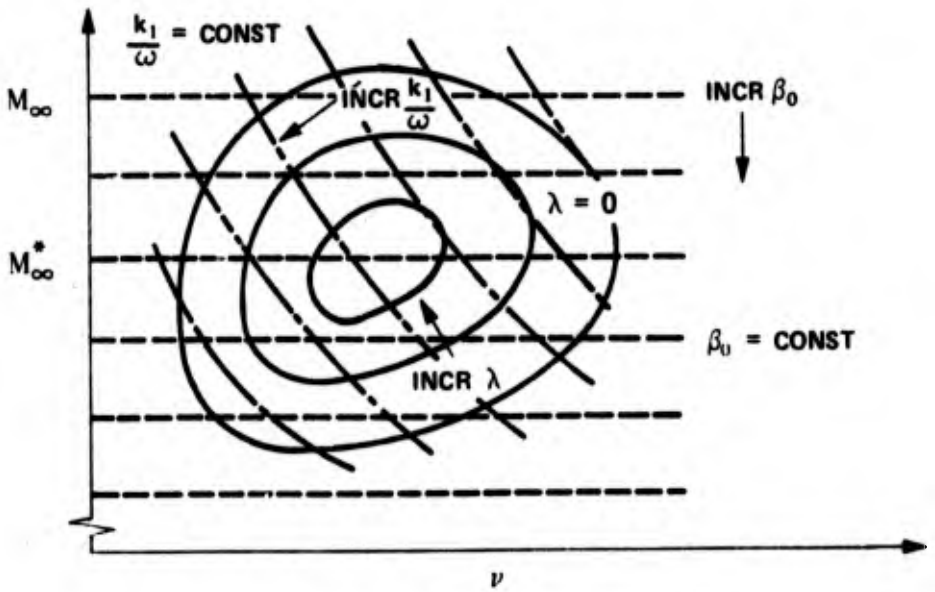

SYSTEM STABILITY PARAMETERS

The $\lambda = 0$ curve is a closed curve due to the effect of γ at low and high frequencies and because $\frac{N_2 k_1}{\omega} \rightarrow 0$ at high frequencies. The horizontal line labeled $M_\infty{}^*$ relates to the M_∞ value for $\left|\frac{\Delta \hat{C}_{H_1}}{\Delta M_\infty}\right|_{max}$. The horizontal lines labeled β_0 = const represent "steady flow equilibrium" flap angles. The coupling parameter $\frac{k_1}{\omega}$, being a function of M_∞ and ν, acts to distort the curves of constant λ. A point within the $\lambda = 0$ contour would relate to a self-excited oscillation.

Limit-cycle behavior may also be predicted even in the absence of amplitude effects on $\frac{\partial x_1}{\partial \beta_1}$ and γ since $\frac{\Delta C_{H_1}}{\Delta M_\infty} \rightarrow 0$ as $(\Delta M_\infty)_{eff}$ increases as in the spoiler/flap case.

A sketch of limit cycle parameters, as in Figure 7, would likely appear as follows:

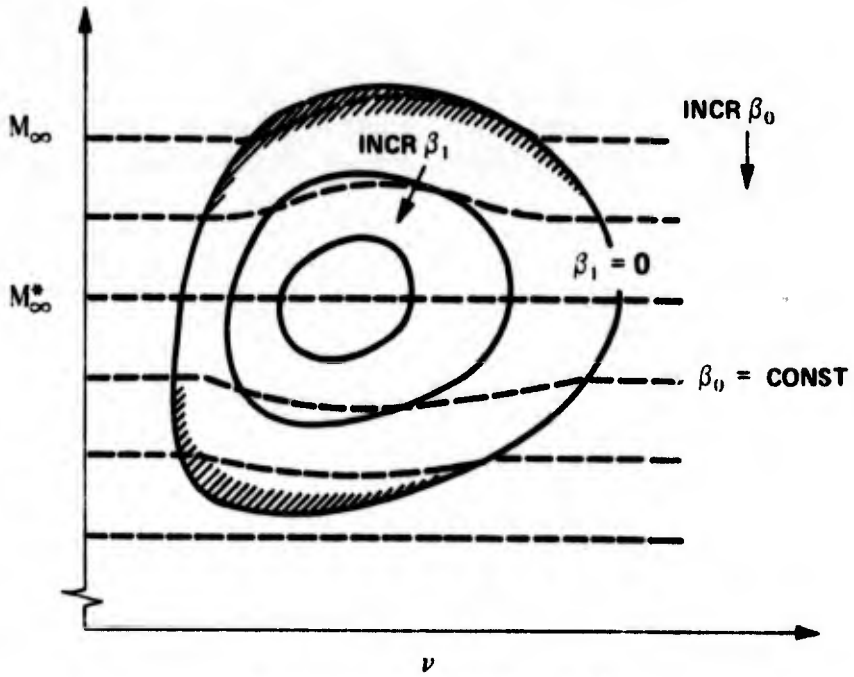

LIMIT-CYCLE PARAMETERS

Maximum amplitude limit-cycle oscillations relate to $M_\infty{}^*$ and a critical value of ν (somewhere around $\nu = .10$). For lower frequencies the coupling parameter $\frac{k_1}{\omega}$ is increased and in the actual case γ, the shock lag angle, would increase as β_1 increases, thus allowing for large amplitude limit cycles at low frequencies. Curves of constant amplitude, β_1, are therefore skewed to the left. At high frequencies the coupling

parameter $\frac{k_1}{\omega}$ decreases. At $M_\infty = M_\infty^*$ the $\beta_1 = 0$ locations will likely correspond to the $\lambda = 0$ points in the preceding sketch. For values of M_∞ above or below M_∞^* we expect that a "rectification effect" (as in the spoiler experiment) would serve to modify β_0, with the degree of rectification depending on amplitude, β_1.

The shaded regions in the sketch lie outside the previous $\lambda = 0$ curve, and result primarily from the rectification effect. These regions would relate to "hard oscillator" behavior.

In conclusion, it can be stated that some similarities appear to exist between the coupled spoiler/flap problem and control-surface-buzz. Significant additional effects, such as the lag in shock motion, exist and of course mechanisms of the shock/shear layer interaction are not well understood. It appears, however, that the clue to Mach number effect on stability can be found by study of the steady flow hinge-moment dependence on Mach number. Frequency effect relates primarily to coupling strength and a phase relation that is associated with shock motion. It is obvious that further tests are necessary in order to gain insight into the many unknown aspects of this problem. Also, the effect of three-dimensional flow needs to be studied since it is likely that it is significant. It is probably very important in other related cases of shock/shear-layer/body interactions such as the problem of wing rock, for example.

IV. CONCLUSIONS

It has been shown in the experiments with an oscillating spoiler that significant dynamic effects modify the behavior of an unsteady separating flow.[22] Quasi-steady models are not appropriate even at low frequencies of oscillation. It appears, however, that a useful analytical model can be derived if mass flow in a separated region is considered. A quasi-steady model for mass flux in the reattachment region of a separated bubble and the assumption of propagation of mass upstream at a mean backflow velocity is used in order to predict the experimentally observed lag in bubble growth. The quasi-steady assumption can be used in conjunction with the momentum equation in order to find the perturbation to "dead air" pressure that accompanies unsteady mass flux. The resultant analytical model of bubble behavior is then used to predict experimental results with good qualitative and fair quantitative agreement.

In the study of a laminar leading-edge separation bubble on an airfoil, it is shown that a model based on an unsteady inviscid flowfield acting on a small quasi-steady bubble is useful in order to predict bubble instability. Instability is taken to occur when the turbulent mixing and reattachment process can not take place due to an extreme pressure rise or velocity drop across the bubble. In order for the bubble to grow, mass must be forced into the bubble at a sufficient rate to cause growth. In unsteady flow then we find that an overshoot of static stall angle may occur. This may be due to airfoil or flap motion. As the static stall angle is overshot, bubble instability first occurs and is followed by a larger rate dependent overshoot which is necessary in order for the bubble to grow. As the bubble continues to grow, consideration must be given to the effect of viscosity on energy dissipation within the bubble. At very high frequencies it may be reasonable to assume (as Ham did in Ref 38) constancy of circulation over the flowfield.

In the case of control-surface-buzz (or other cases which involve shock-induced separation), it is argued that prior to trailing-edge pressure divergence the motion of an airfoil or flap will control the inviscid flowfield (as in attached flow) so that unsteady pressure perturbations are realized at the shock. These perturbations can be related to shock motion across the airfoil surface and subsequent unsteady boundary-layer separation. Dynamics of the separated region are expected to follow the predictions of the separation bubble model when compressibility corrections are made. The assumption of quasi-steady shear layer behavior also appears justified (where the shear-layer above is taken to be external to a separation bubble).

The phenomenon of self-excited oscillations and subsequent limit-cycle motion was investigated for the coupled spoiler/flap configuration and discussed in the case of control-surface-buzz. It appears that the nonlinear nature of these problems is strongly related to the steady-flow functional dependence of incremental hinge-moment coefficient on either spoiler height or freestream Mach number. Additional nonlinear effects in unsteady flow, such as amplitude dependent phase lags and coupling, may not be necessary additions to an analytical model which is used to describe the coupled system motion.

More information is needed in order to better model the fluid dynamics of unsteady separating flows. In particular, it is desirable to study dissipation of energy in separation bubbles in the unsteady case, also the character and role of convection, diffusion and creation of vorticity needs to be studied, and perhaps most important are the effects of spanwise flow in the bubble interior, end plates, and other three-dimensional flow considerations.

The most significant results of the present study relate to better understanding of and a useful analytical model for the dynamics of an unsteady separation bubble. It is expected that these results are appropriate when considering most, if not all, of the aerodynamic problem areas mentioned in the introduction.

REFERENCES

1. Lambourne, N.C. "Flutter in One Degree of Freedom," AGARD Manual on Aeroelasticity, Part V, Ch. 5, 1968.

2. Ormiston, R.A. "Experimental Investigation of Stability and Stall Flutter of a Free-Floating Wing V/STOL Model," NASA TN D-6831, June 1972.

3. Goldman, R.L. and Obremski, H.J. "Experimental Investigation of Hypersonic Buzz on a High Cross-Range Shuttle Configuration," AIAA Paper No. 73-157, January 1973.

4. Jones, J.C. "The Dynamic Analysis of Buffeting and Related Phenomena," RAE Tech. Memo Aero 1401, March 1972.

5. Lang, J.D. "Experiments on an Airfoil with Oscillating Spoiler and Flap," FJSRL-TR-74-0011, June 1974.

6. Chang, P.K. Separation of Flow, Pergamon Press, 1970.

7. Crimi, P. and Reeves, B.L. "A Method for Analyzing Dynamic Stall of Helicopter Rotor Blades," NASA CR-2009, May 1972.

8. Barnes, C.S. "Two-Dimensional Normal Fences on a Flat Plate," ARC Current Paper 863, February 1965.

9. Newman, B.G. "The Re-Attachment of a Turbulent Boundary-Layer Behind a Spoiler," Aeronautical Research Labs, Report A64, Melbourne, Austrailia, 1949.

10. Debroderode, V. and Bradshaw, P. "Three-Dimensional Flow in Nominally Two-Dimensional Separation Bubbles, I. Flow Behind a Rearward-Facing Step," Imperial College of Science and Technology, I.C. Aero Rpt. 72-19, August 1972.

11. Bradshaw, P. and Wong, F.Y.F. "The Reattachment and Relaxation of a Turbulent Shear Layer," Journal of Fluid Mechanics, Vol. 52, Part 1, pp. 113-135, 1972.

12. Norbury, J.F. and Crabtree, L.F. "A Simplified Model of the Incompressible Flow Past Two-Dimensional Aerofoils with a Long Bubble Type of Flow Separation," RAE Tech. Note Aero 2352, June 1955.

13. McGregor, I. "Regions of Localized Boundary Layer Separation and Their Role in the Nose-Stalling of Aerofoils," Ph.D. Thesis, Queen Mary College, Univ. of London, 1954.

14. Gaster, M. "The Structure and Behavior of Laminar Separation Bubbles," Separated Flows, Part 2, AGARD Conference Proceedings No. 4, pp. 813-854, May 1966.

15. Young, A.D. and Horton, H.P. "Some Results of Investigations of Separation Bubbles," Separated Flows, Part 2, AGARD Conference Proceedings No. 4, pp. 779-812, May 1966.

16. Horton, H.P. "A Semi-Empirical Theory for the Growth and Bursting of Laminar Separation Bubbles," ARC Current Paper 1073, June 1967.

17. Woodward, D.S. "An Investigation of the Flow in Separation Bubbles," Ph.D. Thesis, Univ. of London, 1970.

18. Trilling, L. "Oscillating Shock Boundary-Layer Interaction," Journal of the Aeronautical Sciences, Vol. 25, No. 5, May 1958.

19. East, R.A. and Wilkinson, P.R. "A Study of the Oscillating Laminar Separated Flow Ahead of a Forward Facing Step Oscillating Transversely to a Hypersonic Free Stream," Separated Flows, Part 2, AGARD Conference Proceedings No. 4, pp. 509-530, May 1966.

20. Theisen, J.G. "Vortex Periodicity in Wakes," AIAA Paper No. 67-34, January 1967.

21. Lang, J.D. "The Interaction of an Oscillating Airfoil and/or Flap with a Separating Flow," Ph.D. Thesis, Cranfield Institute of Technology, England, January 1975.

22. Lang, J.D. "On Predicting Leading-Edge Bubble Bursting on an Airfoil in Unsteady Incompressible Flow," Cranfield Memo 109, Cranfield Institute of Technology, England, April 1973.

23. Barnes, C.S. "A Developed Theory of Spoilers on Aerofoils," ARC Current Paper 887, July 1965.

24. Jones, A.L., Lamb, O.P. and Cronk, A.E. "A Method for Predicting Lift Effectiveness of Spoilers at Subsonic Speeds," Journal of the Aeronautical Sciences, April 1956.

25. Woods, L.C. "Theory of Aerofoil Spoilers," ARC R&M 2969, 1953.

26. Siljak, D.D. Nonlinear Systems, John Wiley & Sons, 1969.

27. Beecham, L.J. and Titchener, I.M. "Some Notes on an Approximate Solution for the Free Oscillation Characteristics of Non-linear Systems Typified by $\ddot{x} + F(x,\dot{x}) = 0$," ARC R&M 3651, 1971.

28. Titchener, I.M. "Development of a Technique for the Analysis of Non-linear Dynamic Characteristics of a Flight Vehicle," Paper No. A.1, Symposium on Non-linear Dynamics, Loughborough, England, 1972.

29. Carta, F.O. "Effect of Unsteady Pressure Gradient Reduction on Dynamic Stall Delay," Journal of Aircraft, Vol. 8, No. 10, pp. 839-841, October 1971.

30. McCroskey, W.J. "Inviscid Flowfield of an Unsteady Airfoil," AIAA Journal, Vol. 11, No. 8, pp. 1130-1137, August 1973.

31. Liiva, J., Davenport, F.J., et. al. "Two-Dimensional Tests of Airfoils Oscillating Near Stall," Volume I, Summary and Evaluation of Results, USAAVLABS, Technical Report 68-13A, April 1968.

32. Gray, L. and Liiva, J. "Wind Tunnel Tests of Thin Airfoils Oscillating Near Stall," Volume I, Summary and Evaluation of Results, USAAVLABS Technical Report 68-89A, January 1969.

33. Drescher, H. "Untersuchungen an einem symmetrischen Tragflügel mit spaltlos angeschlossenem Ruder bei Raschen Aenderungen des Ruderausschlags (ebene Strömung)," Mitt. Max-Planck-Inst. Strömungs-Forsch. No. 6, 1952.

34. Lambourne, N.C. "Some Instabilities Arising from the Interactions Between Shock Waves and Boundary Layers," ARC Current Paper 473, 1958.

35. Ericsson, L.E. and Reding, J.P. "Stall-Flutter Analysis," Journal of Aircraft, Vol. 10, No. 1, pp. 5-13, January 1973.

36. Gault, D.E. "An Experimental Investigation of Regions of Separated Laminar Flow," NACA TN 3505, September 1955.

37. Wortmann, F.K. "A Critical Review of the Physical Aspects of Airfoil Design at Low Mach Numbers," M.I.T. Symposium, 1972, Technology and Science of Motorless Flight, Cambridge, Mass.

38. Ham, N.D. "Aerodynamic Loading on a Two-Dimensional Airfoil during Dynamic Stall," AIAA Journal, Vol. 6, No. 10, pp. 1927-1934, October 1968.

39. Stratford, B.S. "The Prediction of Separation of the Turbulent Boundary-Layer," Journal of Fluid Mechanics, Vol. 5, No. 17, pp. 1-16, 1959.

40. Crimi, P. "Investigation of Nonlinear Inviscid and Viscous Flow Effects in the Analysis of Dynamic Stall," NASA CR-2335, February 1974.

41. Woods, L.C. "Theory of Aerofoils on Which Occur Bubbles of Stationary Air," ARC R&M 3049, 1957.

42. Lambourne, N.C. "On Certain Types of Self-Excited Oscillation Occurring with Aircraft Control Surfaces in Transonic Flow," NPL Aero Report 1191, 1966.

43. Eckhaus, W. "Two-Dimensional Transonic Unsteady Flow with Shock Waves," OSR Tech. Note No. 59-491, 1959.

44. Eckhaus, W. "On the Theory of Transonic Aileron Buzz," AFOSR Report No. 229, December 1960.

45. Smilg, B. "The Prevention of Aileron Oscillations at Transonic Airspeeds," Army Air Force Tech. Rpt. No. 5530, 1946.

46. Erickson, A.L. and Stephenson, J.D. "A Suggested Method of Analyzing for Transonic Flutter of Control Surfaces Based on Available Experimental Evidence," NACA R&M A7F30, 1947.

47. Green, J.E. "A Discussion of Viscous-Inviscid Interactions at Transonic Speeds," RAE Tech. Rpt. 72050, May 1972.

48. Tijdeman, H. and Zwaan, R.J. "On the Prediction of Aerodynamic Loads on Oscillating Wings in Transonic Flow," AGARD Rpt. No. 612, January 1974.

49. Nakamura, Y. "Some Contributions on a Control-Surface Buzz at High Subsonic Speeds," Journal of Aircraft, Vol. 5, No. 2, pp. 118-125, March 1968.

50. Mager, A. "On the Model of the Free, Shock-Separated, Turbulent Boundary Layer," Journal of Aeronautical Sciences, pp. 181-184, February 1956.

51. Liepmann, H.W. and Roshko, A. Elements of Gasdynamics, John Wiley & Sons, 1967.